skb.se

SKB P-25-07

ISSN 1651-4416

ID 2088069

December 2025

Forsmark site investigation - Boreholes KFM06C and KFM08C

Uniaxial compression, triaxial compression and indirect tensile strength tests of intact rock

Lars Jacobsson
RISE Research Institutes of Sweden

Abel Sánchez Juncal
Svensk Kärnbränslehantering AB

Keywords: Rock mechanics, Indirect tensile test, Uniaxial compression test, Triaxial compression test, Elasticity parameters, Stress-strain curve, Post-failure behaviour, AP SFK-25-016

Summary

The density and mechanical properties were determined on water saturated specimens from boreholes KFM06C and KFM08C in rock domain RFM045 at the Forsmark site investigation area. The rock types in the selected sections were aplitic granite (101058) with none, faint or weak albitization deformation. Previous investigations in this area were focussed on aplitic granite samples with strong or high intensity of albitization, rock type code 101058_104 (with the additional code 104 for albitization).

The specimens were water saturated using tap water and all subsequent measurements were conducted at this moisture condition. The density was first determined on 32 specimens. The testing continued with 12 indirect tensile tests yielding the indirect tensile strength and 11 uniaxial compression tests, respectively, 8 triaxial compression tests including the post-peak response yielding the Young's modulus, Poisson ratio and the uniaxial compressive strength.

The density at a water saturated condition was 2 624–2 649 kg/m^3. The specimens had an isotropic structure. The indirect tensile strength was 13.3–17.6 MPa. The Young's modulus obtained from the compression tests was 75.0 –84.2 GPa and the Poisson ratio was 0.243 – 0.380. The peak values of the axial compressive stress were in the range 263.6–433.9 MPa. The triaxial compression tests were conducted at 5, 10, 15 and 20 MPa confining pressure yielding compressive strength values in the range 392.8–738.1 MPa. Two specimens were tested at 20 MPa. One specimen failed at an axial stress of 674.6 MPa. The other specimen was loaded under 15 minutes with a continuously increasing load up to the maximum load of the equipment, corresponding to an axial stress of 738.1 MPa, without going to failure. The load was kept at this level and failure occurred after totally 49 minutes. Hence, the strength of the specimen was higher than the recorded stress and could have been determined if higher load had been applied.

Sammanfattning

Densiteten och de mekaniska egenskaperna bestämdes på vattenmättade prover från borrhålen KFM06C och KFM08C i bergartsdomänen RFM045 vid Forsmarksplatsundersökningsområde. Bergarterna i de utvalda sektionerna var aplitisk granit (101058) utan någon eller svag albitiseringsdeformation. Tidigare undersökningar i detta område fokuserade på aplitiska granitprover med stark eller hög intensitet av albitisering, bergartskod 101058_104 (med tilläggskod 104 för albitisering).

Proverna vattenmättades med kranvatten och alla efterföljande mätningar gjordes vid denna fukthalt. Densiteten mättes först på samtliga 32 prover. Testerna fortsatte med 12 indirekta dragförsök som gav indirekt draghållfasthet och 11 enaxiella kompressionförsök, respektive, 8 triaxialförsök inkluderat efterbrottsbeteende som gav värden på elasticitetsmodul, Poissons tal och tryckhållfasthet.

Densiteten vid vattenmättat tillstånd var 2 624–2 649 kg/m^3. Proverna hade en isotrop struktur. Den indirekta draghållfastheten var 13,3–17,6 MPa. Elasticitetsmoduluen som erhölls från kompressionstesterna var 75,0–84,2 GPa och Poissons tal var 0,243–0,380. Toppvärdena för den axiella tryckspänningen låg i intervallet 263,6–433,9 MPa. De triaxiella kompressionsförsöken utfördes vid 5, 10, 15 och 20 MPa omslutningstryck, vilket gav tryckhållfasthetsvärden i intervallet 392,8–738,1 MPa. Två prover genomfördes vid 20 MPa. Ett prov gick till brott vid en axialspänning på 674,6 MPa. Det andra provet lastades på under 15 minuter med en kontinuerligt ökande belastning upp till utrustningens maximala kraft, motsvarande en axiell spänning på 738,1 MPa, utan att gå till brott. Lasten hölls på denna nivå och brott inträffade efter totalt 49 minuter. Därför var provets styrka högre än den registrerade spänningen och hade kunnat bestämmas om högre belastning hade applicerats.

Content

1 Introduction

This document reports performance and results of measurements of density, indirect tensile strength tests and uniaxial and triaxial compression tests, with loading beyond the failure point into the post-failure regime, on water-saturated drill core specimens. The drill cores originate from the boreholes KFM06C and KFM08C which are located within the site investigation area in Forsmark, see map in Figure 1-1.

Borehole KFM06C is a core drilled borehole with a total length of 1 000.91 m and an inclination of 60.12° from the horizontal plane at its starting point and plunging towards NNE, reaching a horizontal extension of about 500 m. KFM06C is drilled from the tectonic lens in rock domain RFM029 into a wide belt of aplitic metagranite located in the rock domain RFM045. The aplitic metagranite predominates below the approximate borehole length of 410 metres, where some intervals show an intense degree of albitization (Petersson et al. 2006a).

Borehole KFM08C is also a core drilled borehole with a total length of 951.08 m and it is inclined 60.46° from the horizontal plane plunging towards NE. This borehole is drilled in the northeastern margin of rock domain RFM029, crossing a belt of mainly aplitic material in the rock domain RFM045 which occurs approximately between 340–550 metres length. These subordinate occurrences of aplitic metagranite are variably affected by intense albitization (Petersson et al. 2006b).

Figure 1-1. *Geological map showing the location of boreholes KFM06C and KFM08C within or close to the Forsmark candidate area. The projection of each borehole on the horizontal plane at top of casing is also shown in the figure.*

The testing has been concentrated to the rock type aplitic granite (rock type code 101058) occurring at depth intervals between borehole lengths 500–720 m in KFM06C and 400–425 m in KFM08C. The selected samples for testing are characterized with none, faint or weak intensity albitization. Aplitic granite samples with high albitization, rock type code 101058_104 (with the additional code 104 for albitization), were disregarded and not included in this report.

The tests were carried out in the material and rock mechanics laboratories at the Department of Chemistry and Applied Mechanics and Department of Infrastructure and Concrete at RISE Research Institutes of Sweden in Borås.

SKB sent rock cores to RISE which arrived in Borås in June 2025 and were tested during August to November 2025. SKB provided an extraction plan for all specimens. Cylindrical specimens were cut from the cores based on the plan. The end surfaces of the specimens were grinded in order to comply with the required shape tolerances. The specimens were water saturated and stored in water with a minimum of 7 days, up to testing. This yields a water saturation which is intended to resemble the in-situ moisture condition. All tests were carried out at this moisture condition. The density was first determined on each specimen followed by mechanical tests.

The method description SKB MD 160.002e was followed for the water saturation and density measurements. The method description SKB MD 190.004e was followed for the sampling and for the indirect tensile strength tests and the method description SKB MD 190.001e was followed for the uniaxial compression tests. For the triaxial compression tests, the method description SKB MD 190.003 was followed.

The controlling documents for the activity are listed in Table 1-1. Both Activity Plan and Method Descriptions are SKB's internal controlling documents, whereas the Quality Plan referred to in the table is a RISE internal controlling document.

Table 1-1 Controlling documents for performance of the activity.

Table head		
Activity plan	**Number**	**Version**
Laboratorieprovning hållfasthet aplitisk granit	AP SFK-25-016	1.0
Method descriptions	**Number**	**Version**
Determining density and porosity of intact rock	SKB MD 160.002e	3.0
Uniaxial compression test for intact rock	SKB MD 190.001e	4.0
Triaxial compression test for intact rock	SKB MD 190.003	3.0
Indirect test of tensile strength	SKB MD 190.004e	3.0
Quality plan		
Activity specific quality plan	RISE document	

2 Objective

The spent nuclear fuel from the Swedish nuclear power program is planned to be finally disposed of through geological deposition in the Swedish bedrock. The Swedish Nuclear Fuel and Waste Management Company, SKB, has the main task of building a deep geological repository at the Forsmark site for the long-term safety of people and the environment. This requires a proper site-descriptive model of the Forsmark bedrock.

Previous descriptions of the intact rock mechanical behaviour of the aplitic metagranite present in the rock domain RFM045 are based on results only from aplitic granite samples with strong or high intensity of albitization, rock type code 101058_104 (with the additional code 104 for albitization). The presence of the aplitic granite with none, faint or weak albitization deformation is significant and common in the rock domain RFM045. This supplementary investigation carried out and reported here is necessary to provide a correct and independent description of the aplitic granite (101058), as a separate rock type from its counterpart rock type (101058_104) with high albitization, to improve the Forsmark site descriptive model and to complete the intact rock parameters in the Sicada database.

3 Specimens

Several specimens of aplitic granite (101058) with weak or lower intensity of albitization have been selected from five depths (elevation in meters below sea level), 300 m, 400 m, 450 m, 500 m and 600 m at boreholes KFM06C and KFM08C. These specimens were taken to obtain the required samples to perform 10 uniaxial compressive strength (UCS), 12 indirect tensile strength (ITS) and 8 triaxial compressive strength (TCS).

The rock type characterisation was made according to Stråhle (2001) using the SKB mapping system (Boremap). An overview of the core mapping for the two boreholes containing rock units and domains and deformation zones are found in Appendix A.

3.1 Extraction plan

A total of 20 core parts were selected for this investigation, eighteen parts from KFM06C and two from KFM08C. SKB provided a plan showing section depths and the designated specimen types for each core section. RISE followed the plan and marked the specimen positions on the cores and named all the specimens and documented their exact borehole length levels (adj sec up and adj sec low) based on the supplied information. Photos of all core sections with the original label attached to the core sections are shown in Figure 3-1 to Figure 3-2.

Figure 3-1. *Specimen layout for cutting the test specimens on core sections from KFM06C (borehole length 510–520 m).*

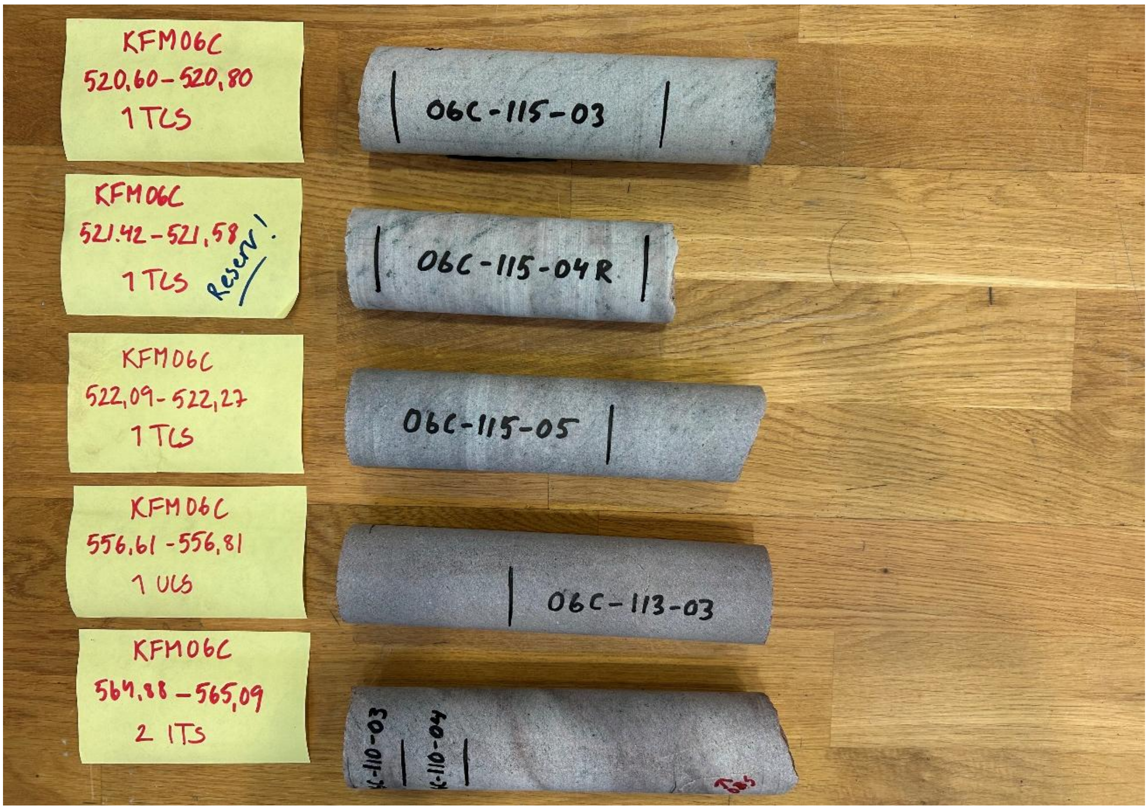

Figure 3-2. Specimen layout for cutting the test specimens on core sections from KFM06C (borehole length 520–565 m).

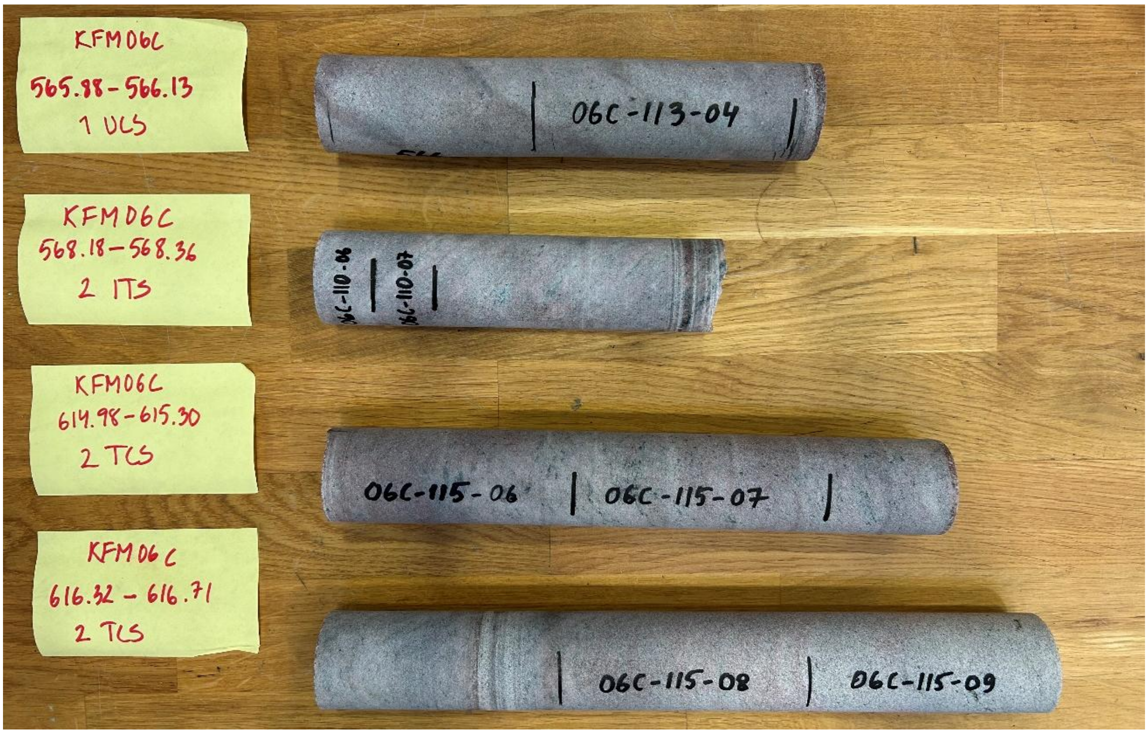

Figure 3-3. Specimen layout for cutting the test specimens on core sections from KFM06C (borehole length 565–617 m).

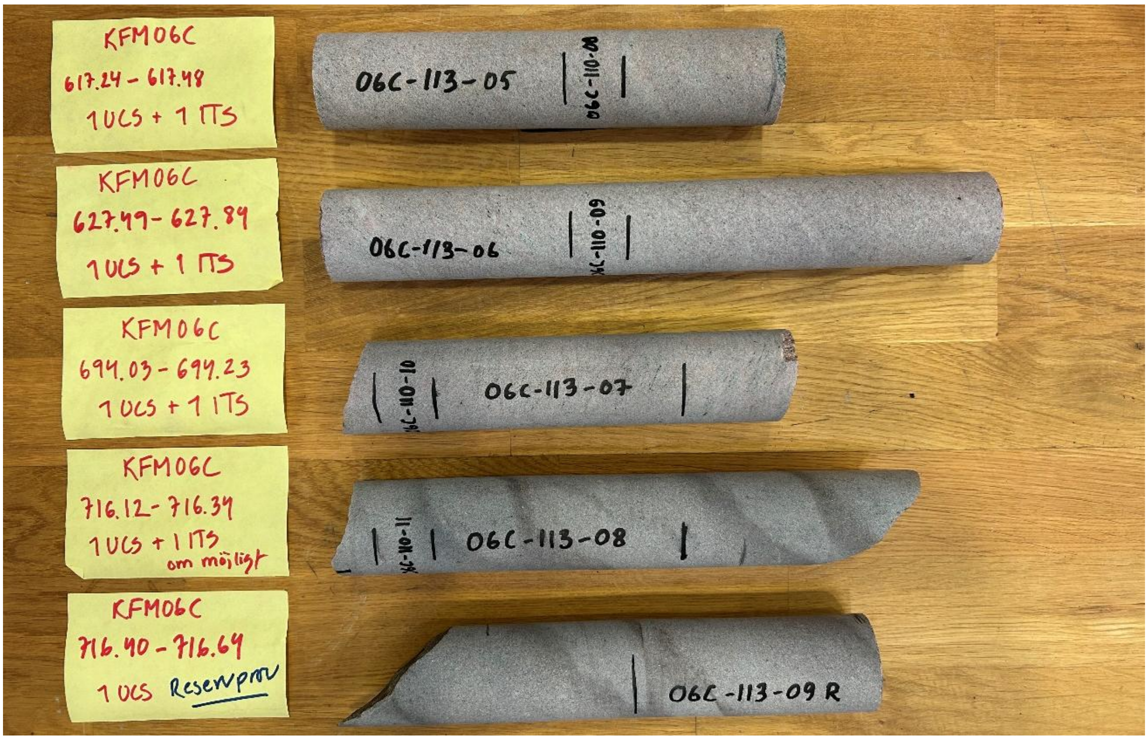

Figure 3-4. *Specimen layout for cutting the test specimens on core sections from KFM06C (borehole length 617–717 m).*

Figure 3-5. *Specimen layout for cutting the test specimens on core sections from KFM08C (borehole length 412–413 m).*

3.2 Specimens for indirect tensile tests

A list of 12 specimens for the indirect tensile tests is shown in Table 3-1.

Table 3-1. Core and specimen identification, sampling level (borehole length), degree of albitization intensity and rock type for all specimens (based on the Boremap overview mapping).

Identification	Adj Secup (m)	Adj Seclow (m)	Albitization intensity	Rock type/occurrence
KFM06C-110-01	510.54	510.57	weak	Aplitic granite (101058)
KFM06C-110-02	511.03	511.06	none	Aplitic granite (101058)
KFM06C-110-03	564.88	564.91	weak/faint	Aplitic granite (101058)
KFM06C-110-04	564.91	564.94	weak/faint	Aplitic granite (101058)
KFM06C-110-06	568.18	568.21	faint	Aplitic granite (101058)
KFM06C-110-07	568.21	568.24	faint	Aplitic granite (101058)
KFM06C-110-08	617.37	617.40	none	Aplitic granite (101058)
KFM06C-110-09	627.62	627.65	none	Aplitic granite (101058)
KFM06C-110-10	694.05	694.08	none	Aplitic granite (101058)
KFM06C-110-11	716.14	716.17	none	Aplitic granite (101058)
KFM08C-110-01	413.48	413.51	faint	Aplitic granite (101058)
KFM08C-110-02	413.51	413.54	faint	Aplitic granite (101058)

3.3 Specimens for uniaxial compression tests

A list of 11 specimens for the uniaxial compression tests is shown in Table 3-2.

Table 3-2. Specimen identification, sampling level (borehole length), degree of albitization intensity and rock type for all specimens (based on the Boremap overview mapping).

Identification	Adj Secup (m)	Adj Seclow (m)	Albitization intensity	Rock type/occurrence
KFM06C-113-01	510.41	510.54	weak	Aplitic granite (101058)
KFM06C-113-02	511.25	511.38	none	Aplitic granite (101058)
KFM06C-113-03	556.68	556.81	none	Aplitic granite (101058)
KFM06C-113-04	565.98	566.11	none	Aplitic granite (101058)
KFM06C-113-05	617.24	617.37	none	Aplitic granite (101058)
KFM06C-113-06	627.49	627.62	none	Aplitic granite (101058)
KFM06C-113-07	694.08	694.21	none	Aplitic granite (101058)
KFM06C-113-08	716.17	716.30	none	Aplitic granite (101058)
KFM06C-113-09 R	716.51	716.64	none	Aplitic granite (101058)
KFM08C-113-01	412.38	412.51	weak	Aplitic granite (101058)
KFM08C-113-02	413.35	413.48	faint	Aplitic granite (101058)

3.4 Specimens for triaxial compression tests

A list of 9 specimens for the triaxial compression tests is shown in Table 3-3.

Table 3-3. Specimen identification, sampling level (borehole length), degree of albitization intensity and rock type for all specimens (based on the Boremap overview mapping).

Identification	Adj Secup (m)	Adj Seclow (m)	Albitization intensity	Rock type/occurrence
KFM06C-115-01	519.66	519.79	weak	Aplitic granite (101058)
KFM06C-115-02	519.79	519.92	weak	Aplitic granite (101058)
KFM06C-115-03	520.62	520.75	weak	Aplitic granite (101058)
KFM06C-115-04 R	521.44	521.57	weak	Aplitic granite (101058)
KFM06C-115-05	522.09	522.22	weak	Aplitic granite (101058)
KFM06C-115-06	614.98	615.11	faint	Aplitic granite (101058)
KFM06C-115-07	615.11	615.24	faint	Aplitic granite (101058)
KFM06C-115-08	616.45	616.58	weak	Aplitic granite (101058)
KFM06C-115-09	616.58	616.71	weak	Aplitic granite (101058)

4 Equipment

4.1 Specimen preparation and density measurement

A circular saw with a diamond blade was used to cut the specimens to their final lengths. The surfaces were then grinded after cutting in a grinding machine in order to achieve a high-quality surface for the axial loading that complies with the required tolerances. The measurements of the specimen dimensions were made with a sliding calliper. Furthermore, the tolerances were checked by means of a dial indicator and a stone face plate. The specimen preparation is carried out in accordance with ASTM (2001).

The following equipment was used for the density determinations:

- scale for weight measurement after water saturation (scale routinely checked with reference weight). Measurement accuracy ± 0.002 g,
- scale for weight measurement after water saturation in surface dry condition (scale routinely checked with reference weight). Measurement accuracy ± 0.02 g

4.2 Indirect tensile strength test

The mechanical testing was carried out in a load frame where the crossbar is mechanically driven by screws and has a maximum load capacity of 100 kN in compression. The axial compressive load was measured by an external 100 kN load cell. The uncertainty of the load measurement is less than 1%.

The frame was equipped with a pair of curved bearing blocks, radius 39 mm and width 29 mm, with pins for guiding the vertical deformation, see Figure 4-1. The top platen includes a spherical seating in order to have a fully centred loading position. The specimens were photographed with a digital camera and the photographs were stored in a jpeg-format.

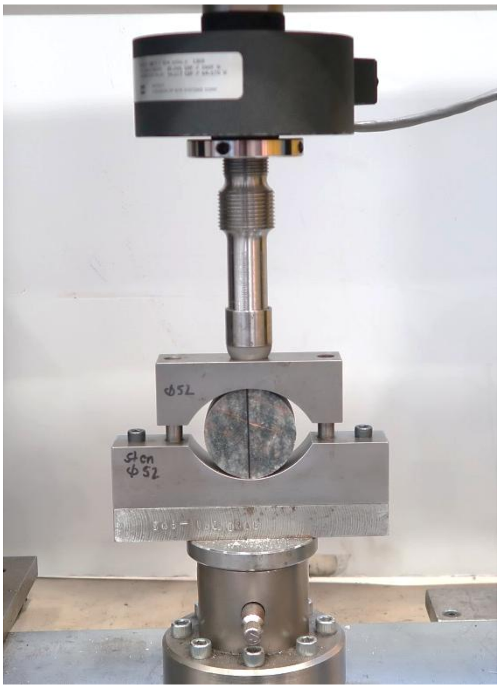

Figure 4-1. *Test-set up for the indirect tensile strength test. The load cell is visible in the top and the curved bearing blocks are seen below that.*

4.3 Uniaxial compression test

The mechanical tests were carried out in a servo-controlled testing machine specially designed for rock tests, see Figure 4-2. The system consists of a load frame, a hydraulic pump unit, a controller unit and various sensors. The communication with the controller unit is accomplished by means of special testing software run on a PC connected to the controller. The load frame is characterized by a high stiffness and is supplied with a fast-responding actuator, cf. the ISRM suggested method (ISRM 1999).

Figure 4-2. *Rock testing system. From left: Digital controller unit, pressure cabinet (used for triaxial tests) and load frame. The PC with the test software (not shown in the picture) is placed on the left hand side of the controller unit.*

The stiffness of the various components of the loading chain in the load frame has been optimized in order to obtain a high total stiffness. This includes the load frame, load cell, load platens and piston, as well as having a minimum amount of hydraulic oil in the cylinder. Furthermore, the sensors, the controller and the servo valve are rapidly responding components. The axial load is determined using a load cell, which has a maximum capacity of 1.5 MN. The uncertainty of the load measurement is less than 1%.

The axial and circumferential (radial) deformations of the rock specimens were measured. The rock deformation measurement systems are based on miniature LVDTs with a measurement range of ± 2.5 mm. The relative error for the LVDTs is less than 0.6% within a 1 mm range for the axial deformation measurements and less than 1.3% within a 3 mm range for the circumferential deformation measurement. The LVDTs have been calibrated by means of a micrometre.

Two independent systems were used for the axial deformation measurement in order to obtain two comparative results. The first system (S1), see Figure 4-3, comprises two aluminium rings attached on the specimen, placed at ¼ and ¾ of the specimen height. Two LVDTs mounted on the rings are used to measure the distance change between the rings on opposite sides of the specimen. As to the attachment, two rubber bands made of a thin rubber hose with a total thickness of 1 mm thickness are first mounted on the specimen right under where the two rings are to be positioned. The rings are supplied with three adjustable spring-loaded screws, each with a rounded tip pointing on the specimen with 120 degrees division. The screw tips are thus pressing on the rubber band, when the rings are mounted. The second system (S2), see Figure 4-3, consists of two aluminium plates clamped around the circular loading platens of steel on top and on bottom of the specimen. Two LVDTs, mounted on the plates, measure the distance change between these plates at opposite sides of the specimen at corresponding positions as for the first measurement system (S1).

The radial deformation was obtained by using a chain mounted around the specimen at mid-height, see Figure 4-3 and Appendix B. The change of the chain-opening gap was measured by means of one LVDT and the circumferential, and thereby also the radial deformation could be obtained. See Appendix B.

The specimens were photographed with a digital camera and the photographs were stored in a jpeg-format.

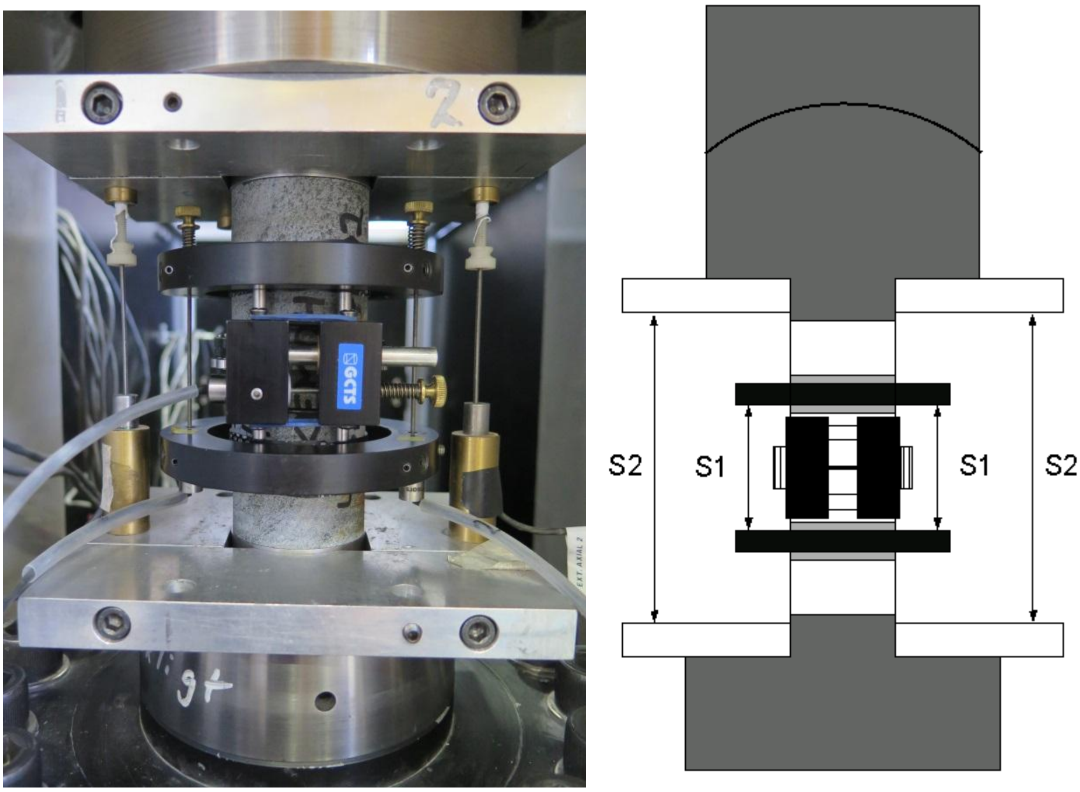

Figure 4-3. *Left: Specimen inserted between the loading platens. The two separate axial deformation measurement devices can be seen: system (S1) that measures the local axial deformation (rings), and system (S2) that measures the deformation between the aluminium plates (total deformation). Right: Principal sketch showing the two systems used for the axial deformation measurements.*

4.4 Triaxial compression test

The mechanical tests were carried out in a servo controlled testing machine specially designed for rock tests, see Figure 4-4. The system consists of a load frame, a hydraulic pump unit, a controller unit and various sensors. The communication with the controller unit is accomplished by special testing software run on a PC connected to the controller. The load frame is characterized by a high stiffness and is supplied with a fast responding actuator, cf. the ISRM suggested ISRM (1999). Furthermore, the sensors, the controller and the servo valves are rapidly responding components. The machine is equipped with a pressure vessel in which the specimens are tested under a confinement pressure. A thin rubber membrane is mounted on the specimen in order to seal the specimen from the oil that is used as the confinement medium, cf. Figure 4-5. The axial load is determined using a load cell, which is located inside the pressure vessel and has a maximum capacity of 1.5 MN. The uncertainty of the load measurement is less than 1%.

The axial and circumferential (radial) deformation of the rock specimen was measured. The rock deformation measurement systems are based on miniature LVDTs, which have a measurement range of +/- 2.5 mm. The LVDTs were calibrated by means of a micrometer and they displayed an accuracy of +/- 2.5% within a +/- 2 mm range. The axial deformation measurement system comprises two aluminium rings attached on the specimen, placed approximately at ¼ and ¾ of the specimen height, cf. Figures 4-4 and 4-5. Two LVDTs mounted on the rings are used to measure the distance change between the rings on opposite sides of the specimen. The rings are supplied with three adjustable spring-loaded screws, each with a rounded tip, pointing towards the specimen with 120 degrees division. The rings are mounted directly on the rubber membrane. The pre-load of the screws fixates the rings. The position of the frame piston was also stored during the test in order to permit a possibility for comparison with the measurements made with the measurement system that was based on the displacement of the rings.

The radial deformation was obtained by using a chain mounted around the specimen at mid-height, see Figure 4-5. The change of the chain-opening gap was measured by means of one LVDT and the circumferential and thereby also the radial deformation could be obtained. See Appendix B.

The specimens were photographed with a digital camera and the photographs were stored in a jpeg-format.

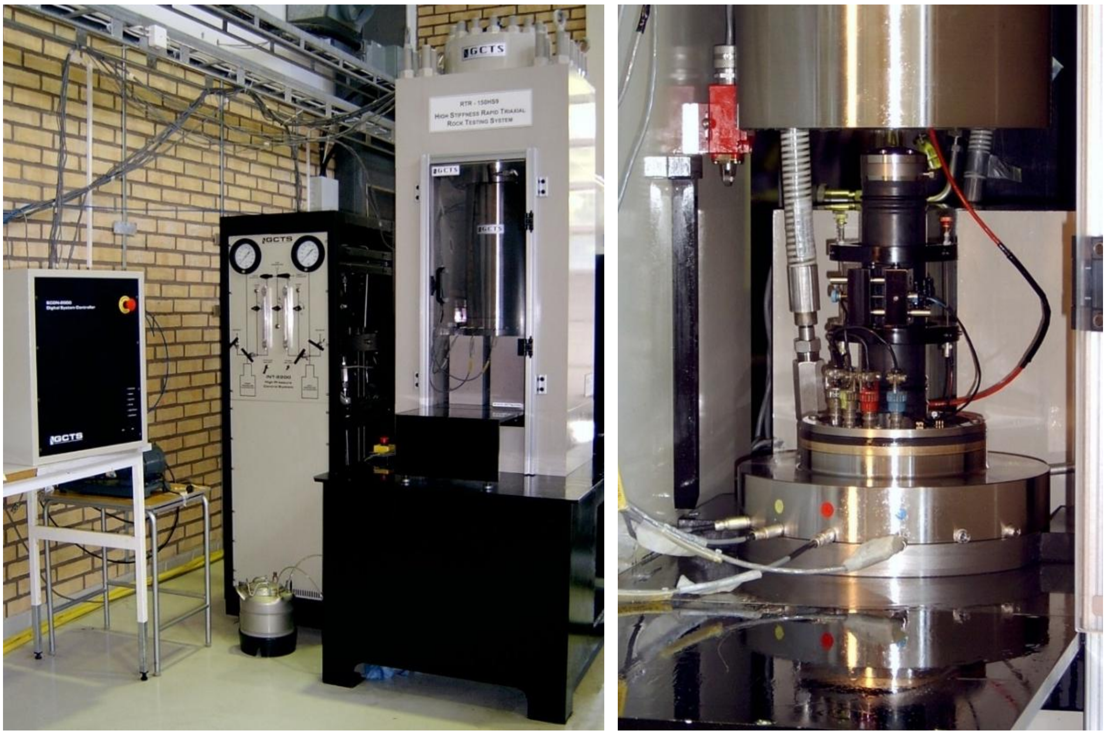

Figure 4-4. *Left: Digital controller unit, pressure cabinet with cell pressure intensifier and oil reservoir inside, and the load frame with closed cell (pressure vessel). Right: Bottom of the cell is lowered. The specimen is instrumented and ready for inserting in the cell.*

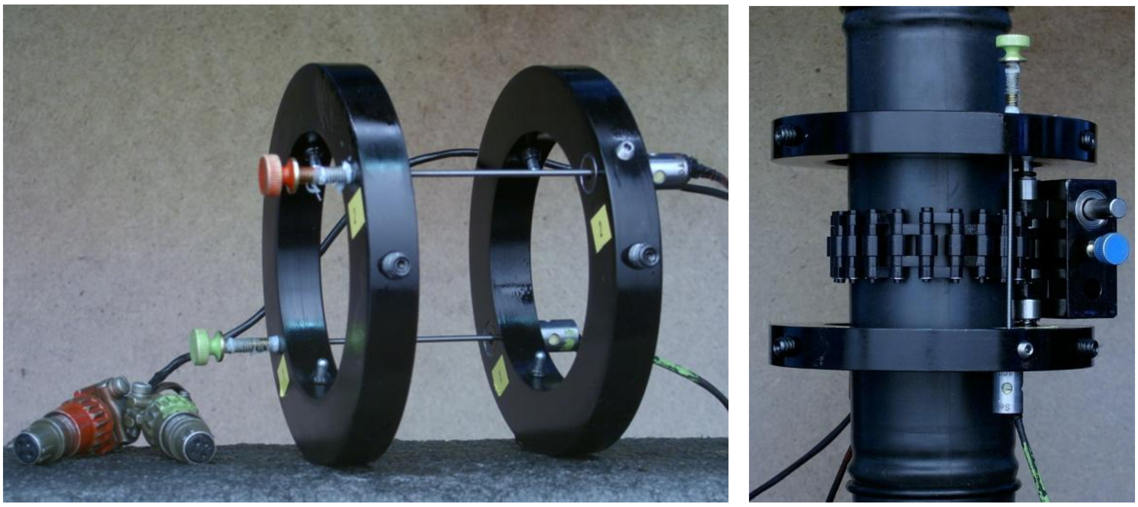

Figure 4-5. *Left: Rings and LVDTs for axial deformation measurement. Right: Specimen and loading platens sealed with a rubber membrane. Devices for axial and circumferential deformation measurements are attached.*

5 Execution

5.1 Specimen preparation

The steps for the specimen preparation are shown in Table 5-1.

Table 5-1. Activities during the specimen preparation.

Step	Activity
1	The drill cores were marked where the specimens are to be taken.
2	The specimens were cut to the specified length according to markings.
3	The cutting surfaces were grinded (only uniaxial and triaxial compression test specimens)
4	The tolerances were checked: parallel and perpendicular end surfaces, smooth and straight circumferential surface.
5	The diameter and height were measured three times each. The respective mean value determines the dimensions that are reported.

5.2 Water saturation and density measurement

The water saturation and determination of the density of the wet specimens were made in accordance with the method description SKB MD 160.002e (SKB internal controlling document). This includes determination of density in accordance to ISRM (1979) and water saturation by EN 13755 (CEN 2008).

The specimens had been stored during 7 days in water when the density was determined. The density of the water at the time for the measurements was 998 kg/m^3. The execution procedure followed the prescription in SKB MD 160.002e, see Table 5-2.

Table 5-2. Activities during the water saturation and density measurements.

Step	Activity
1	The specimens were water saturated using tap water in normal air pressure for at least seven days.
2	The specimens were weighed in tap water. The temperature of the water was measured and the water density was determined from a table.
3	The specimens were surface dried with a towel and weighed.
4	The density at a water saturated condition was determined.

5.3 Indirect tensile strength test

The specimens had been stored 22 days in water when the indirect tensile strength was determined.

An auto-calibration of the load frame was run prior to the mechanical test in order to check the system. Further, an individual check-list was filled in and checked for every specimen during all the steps in the execution.

The diameter and thickness were entered into the test software which computed the indirect tensile strength together with the mean value and standard deviation for the whole test series. The results were then exported as text-files and stored in a file server on the RISE computer network

A list of the activities conducted during the indirect tensile strength tests is shown in Table 5-3.

Table 5-3. Activities during the indirect tensile strength tests.

Step	Activity
1	The direction of compressive loading was marked as a line on one of the plane surfaces with a marker pen.
2	Digital photos were taken on each specimen before the mechanical testing.
3	The wet specimens were inserted into the loading device one by one, with the correct orientation given by the marked line. The strain gauges were connected to the sampling device and the signals were checked. The specimens were loaded up to failure during deformation control. The displacement rate was set to 0.3 mm/min during loading. The maximum compressive load, which also defines the failure load, was registered.
4	Digital photos were taken on each specimen after the mechanical testing.

5.4 Uniaxial compression tests

5.4.1 Test procedure

The specimens had been stored 32–33 days in water when the uniaxial compression tests were carried out. The functionality of the testing system was checked before starting the tests.

An overview of the activities during the mechanical testing is shown in the step-by step description in Table 5-4.

Table 5-4. Activities during the uniaxial compression tests.

Step	Activity
1	Digital photos were taken on each specimen before the mechanical testing.
2	Devices for measuring axial and circumferential deformations were attached to the specimen.
3	The specimen was put in place and centred between the frame loading platens.
4	The core on each LVDT was adjusted by means of a set screw to the right initial position. This was done so that the optimal range of the LVDTs can be used for the deformation measurement.
5	The frame piston was brought down into contact with the specimen with a force corresponding to 1.0 MPa axial stress.

Step	Activity
6	A load cycle with loading up to 5 MPa and unloading to 1.0 MPa was conducted in order to settle possible contact gaps in the spherical seat in the piston and between the rock specimen and the loading platens.
7	The centring was checked again.
8	The deformation measurement channels were zeroed in the test software.
9	The loading was started and the initial loading rate was set to a radial strain rate of -0.025%/min. The loading rate was increased after reaching the post-failure region. This was done in order to prevent the total time for the test to become too long.
10	The test was stopped either manually when the test had proceeded long enough to reveal the post-failure behaviour, or after severe cracking had occurred and it was judged that very little residual axial loading capacity was left in the specimen.
11	Digital photos were taken on each specimen after the mechanical testing.

5.4.2 Analyses and interpretation

As to the definition of the different results parameters we begin with the axial stress σ_a, which is defined as

$$\sigma_a = \frac{F}{A}$$

where F is the axial force acting on the specimen, and A is the specimen cross section area. The peak value of the axial stress during a test is representing the uniaxial compressive strength σ_c in the results presentation.

The average value of the two axial displacement measurements on opposite sides of the specimen is used for the axial strain calculation, cf. Figure 4-5. In the first measurement system (S1), the recorded deformation represents a local axial deformation δ_{local} between the points at ¼ and ¾ height. A local axial strain is defined as

$$\varepsilon_{a,local} = \delta_{local}/L_{local}$$

where L_{local} is the centre to centre distance between the rings before loading.

In the second measurement system (S2), the recorded displacement corresponds to a total deformation that, in addition to total rock deformation, also contains the local deformations that occur in the contact between the rock and the loading platens, and further it also contains the deformation of the steel loading platens at each side of the specimen ends. The average value of the two total deformation measurements on opposite sides of the specimen is defined as the total deformation δ_{total}. An axial strain based on the total of the deformation is defined as

$$\varepsilon_{a,total} = \delta_{total}/L_{total}$$

where L_{total} is the height of the rock specimen.

The radial deformation is measured by means of a chain mounted around the specimen at mid-height, cf. Figure 4-5. The change of chain opening gap is measured by means of one LVDT. This measurement is used to compute the radial strain ε_r, see Appendix B. Moreover, the volumetric strain ε_{vol} is defined as

$$\varepsilon_{vol} = \varepsilon_a + 2\varepsilon_r$$

The stresses and the strains are defined as positive in compressive loading and deformation. The elasticity parameters are defined by the tangent Young's modulus E and tangent Poisson ratio ν as

$$E = \frac{\sigma_\mathrm{a}(0.60\sigma_\mathrm{c}) - \sigma_\mathrm{a}(0.40\sigma_\mathrm{c})}{\varepsilon_\mathrm{a}(0.60\sigma_\mathrm{c}) - \varepsilon_\mathrm{a}(0.40\sigma_\mathrm{c})}$$

$$\nu = -\frac{\varepsilon_\mathrm{r}(0.60\sigma_\mathrm{c}) - \varepsilon_\mathrm{r}(0.40\sigma_\mathrm{c})}{\varepsilon_\mathrm{a}(0.60\sigma_\mathrm{c}) - \varepsilon_\mathrm{a}(0.40\sigma_\mathrm{c})}$$

The tangents were evaluated with values corresponding to an axial load between 40% and 60% of the axial peak stress σ_c.

Two important observations can be made from the results:

(i) The results based on the total axial deformation measurement (S2) display a lower axial stiffness, i.e. a lower value on Young's modulus, than in the case when the results are based on the local axial deformation measurement (S1). This is due to the additional deformations from the contact interface between the rock specimen and the steel loading platens and also due to the deformation of the loading platens themselves.

(ii) It can be seen that the response differs qualitatively between the results obtained with the local axial deformation measurement system (S1) and the system that measures total axial deformation (S2). In some cases the post-peak response obtained with the local deformation measurement system seems not to be physically correct. This can be due to a number of reasons, e.g. that a crack caused a localized deformation, see Figure 5-1. Another explanation could be that the rings attached to the specimens have slightly slipped or moved, for example if a crack was formed nearby one of the attachment points.

It is reasonable to assume that results based on the local axial deformation measurement (S1) are fairly accurate up to the formation of the first macro-cracks or up to the peak load, but not thereafter. However, the results obtained with the total axial deformation measurement (S2) seem to be qualitatively correct after failure. We will therefore report the results based on the total axial deformation measurement, but carry out a correction of those results as described below in order to obtain overall good results.

The total axial deformation δ_total measured by (S2) is a summation of several deformations

$$\delta_\mathrm{total} = \delta_\mathrm{rock} + \delta_\mathrm{system} \qquad (1)$$

where

$$\delta_\mathrm{system} = \delta_\mathrm{interface} + \delta_\mathrm{loading\ platens}$$

and δ_rock is the axial deformation of the whole rock specimen. Assume that the system deformation is proportional to the applied axial force F in the loading chain, i.e.

$$\delta_\mathrm{system} = F/K_\mathrm{system} \qquad (2)$$

where K_system is the axial stiffness in the system (containing the interface between the rock and loading platens and the deformation of the loading platens). Combining (1) and (2) leads to

$$\delta_\mathrm{rock} = \delta_\mathrm{total} - F/K_\mathrm{system} \qquad (3)$$

where an expression of the axial deformation in the whole specimen is obtained. This can be viewed as a correction of the measurements made by system (S2). By using δ_rock to represent the axial deformation of the specimen that is based on a correction of the results of the total axial deformation will yield good results both in the loading range up to failure and at loading after failure. However, it is noticed that K_system is not known and has to be determined.

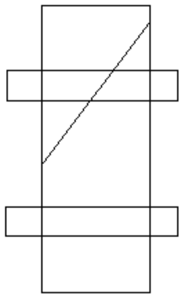

Figure 5-1. *Example of cracking that may cause results that are difficult to interpret with a local deformation measurement*

It was previously suggested that the local axial deformation measurement (S1) represents the real rock deformation well up to the load where the macro-cracks form. Further, it is fair to assume that the axial deformation is homogenous at this part of the loading. Hence, we get

$$\delta_{\text{rock}} = \delta_{\text{local}} \cdot L_{\text{total}}/L_{\text{local}} \qquad (4)$$

This yields representative values of the total rock deformation for the first part of the loading up to the point where macro-cracking is taking place. It is now possible to determine δ_{system} up to the threshold of macro-cracking by combining (1) and (4) which yields

$$\delta_{\text{system}} = \delta_{\text{total}} - \delta_{\text{local}} \cdot L_{\text{total}}/L_{\text{local}} \qquad (5)$$

Finally, we need to compute K_{system}. By rewriting (2) we get

$$K_{\text{system}} = \frac{F}{\delta_{\text{system}}}$$

We will compute the system stiffness based on the results between 40% and 60% of the axial peak stress σ_{c}. This means that the Young's modulus and the Poisson ratio will take the same values both when the data from the local axial deformation measurement (S1) and when the data from corrected total axial deformation are used. Thus, we have

$$K_{\text{system}} = \frac{F(0.60\sigma_{\text{c}}) - F(0.40\sigma_{\text{c}})}{\delta_{\text{system}}(0.60\sigma_{\text{c}}) - \delta_{\text{system}}(0.40\sigma_{\text{c}})} \qquad (6)$$

The results based on the correction according to (3) and (6) are presented in Section 6.2, whereas the original measured unprocessed data are reported in Appendix C.

A closure of present micro-cracks will take place initially during axial loading. Development of new micro-cracks will start when the load is further increased and axial stress reaches the crack initiation stress σ_{i}. The crack growth at this stage is as stable as increased loading is required for further cracking. A transition from a development of micro-cracks to macro-cracks will occur when the axial load is further increased. At a certain stress level the crack growth becomes unstable. The stress level when this happens is denoted the crack damage stress σ_{d}, cf. Martin and Chandler (1994). In order to determine the stress levels, we look at the volumetric strain.

By subtracting the elastic volumetric strain $\varepsilon_{\text{vol}}^{\text{e}}$ from the total volumetric strain, a volumetric strain corresponding to the crack volume $\varepsilon_{\text{vol}}^{\text{cr}}$ is obtained. This has been denoted calculated crack volumetric strain in the literature, cf. Martin and Chandler (1994) and Eberhardt et al. (1998). We thus have

$$\varepsilon_{\text{vol}}^{\text{cr}} = \varepsilon_{\text{vol}} - \varepsilon_{\text{vol}}^{\text{e}}$$

Assuming linear elasticity leads to

$$\varepsilon_{\text{vol}}^{\text{cr}} = \varepsilon_{\text{vol}} - \frac{1-2\upsilon}{E}\sigma_{\text{a}}$$

Experimental investigations have shown that the crack initiation stress σ_i coincides with the onset of increase of the calculated crack volume, cf. Martin and Chandler (1994) and Eberhardt et al. (1998). The same investigations also indicate that the crack damage stress σ_d can be defined as the axial stress at which the total volume starts to increase, i.e. when a dilatant behaviour is observed.

Another method to assess the crack initiation stress based on strain measurements is to use the Inverse Tangent Lateral Stiffness, cf. Ghazvinian et al. (2012), which was used in e.g. Jacobsson et al. (2016).

5.5 Triaxial compression tests

5.5.1 Test procedure

The specimens had been stored 47–49 days in water when the triaxial compression tests were carried out. The functionality of the testing system was checked before starting the tests.

An overview of the activities during the mechanical testing is shown in the step-by step description in Table 5-5.

Table 5-5. Activities during the triaxial compression tests.

Step	Activity
1	Digital photos were taken on each specimen before the mechanical testing.
2	The specimen was put in testing position and centred between the loading platens.
3	A rubber membrane was mounted on the specimen and the devices for measuring axial and circumferential deformations were attached to the specimen on top of the rubber membrane.
4	The core on each LVDT was adjusted by means of a set screw to the right initial position. This was done so that the optimal range of the LVDTs can be used for the deformation measurement.
5	The triaxial cell was closed and filled with oil whereby a cell pressure of 0.6 MPa is applied.
6	The frame piston was brought down into contact with the specimen with a force corresponding to a deviator stress (stress difference) of 1.0 MPa. The cell pressure was then raised to the specified level and at the same time keeping the deviator stress constant.
7	The deformation measurement channels were zeroed in the test software.
8	The loading was started and the initial loading rate was set to a radial strain rate of –0.025%/min. The loading rate was increased after reaching the post-failure region. This was done in order to prevent the total time for the test to become too long.
9	The test was stopped either manually, when the test had proceeded long enough to reveal the post-failure behaviour, or after severe cracking had occurred and it was judged that very little residual axial loading capacity was left in the specimen.
10	The oil pressure was brought down to zero and the oil was poured out of the cell. The cell was opened and the specimen removed.
11	Digital photos were taken on each specimen after the mechanical testing.

5.5.2 Analyses and interpretation

Analogous to the uniaxial compressive tests, we begin the definition of the different results parameters with the axial stress σ_a, which is defined as

$$\sigma_a = \frac{F}{A}$$

where F is the axial force acting on the specimen, and A is the specimen cross section area. The pressure vessel (triaxial cell) filled with oil is pressurized with a cell (confining) pressure p. This implies that the specimen, located inside the pressure vessel, becomes confined and attains a radial stress σ_r equal to the confining pressure p. The (effective) deviator stress is defined as

$$\sigma_{dev} = \sigma_a - \sigma_r$$

The peak value of the axial stress during a test is representing the triaxial compressive strength σ_c, for the actual confining pressure used in the test, see the results presentation.

The average value of the two axial displacement measurements on opposite sides of the specimen is used for the axial strain calculation. The recorded deformation δ_{local} represents a local axial displacement between the points approximately at ¼ and ¾ of the specimen height, cf. Figure 5-2. The axial strain is defined as

$$\varepsilon_{a,local} = \delta_{local}/L_{local}$$

where L_{local} is tthe distance between the rings before loading.

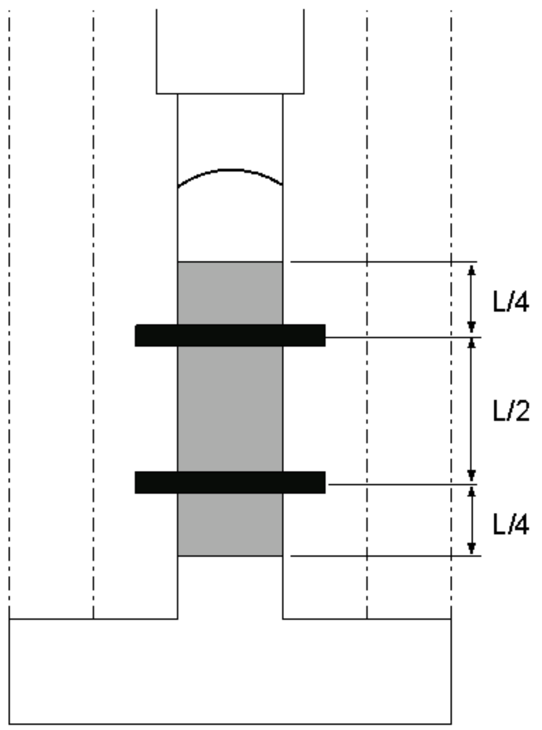

Figure 5-2. *Sketch showing the triaxial cell with the rock specimen (grey) with height L and the position of the rings (black) used for the axial deformation measurements. The membrane is omitted in the figure for simplicity.*

The radial deformation is measured by means of a chain mounted around the specimen at mid-height, see Figure 4-5. The change of chain opening gap is measured by means of one LVDT. This measurement is used to compute the radial strain ε_{r}, see Appendix B. Moreover, the volumetric strain $\varepsilon_{\mathrm{vol}}$ is defined as

$$\varepsilon_{\mathrm{vol}} = \varepsilon_{\mathrm{a}} + 2\varepsilon_{\mathrm{r}}$$

The stresses and the strains are defined as positive in compressive loading and deformation. The elasticity parameters are defined by the tangent Young's modulus E and tangent Poisson ratio ν as

$$E = \frac{\sigma_{\mathrm{a}}(0.60\sigma_{\mathrm{c}}) - \sigma_{\mathrm{a}}(0.40\sigma_{\mathrm{c}})}{\varepsilon_{\mathrm{a}}(0.60\sigma_{\mathrm{c}}) - \varepsilon_{\mathrm{a}}(0.40\sigma_{\mathrm{c}})}$$

$$\nu = -\frac{\varepsilon_{\mathrm{r}}(0.60\sigma_{\mathrm{c}}) - \varepsilon_{\mathrm{r}}(0.40\sigma_{\mathrm{c}})}{\varepsilon_{\mathrm{a}}(0.60\sigma_{\mathrm{c}}) - \varepsilon_{\mathrm{a}}(0.40\sigma_{\mathrm{c}})}$$

The tangents were evaluated with values corresponding to an axial load between 40% and 60% of the axial peak stress σ_{c}.

A closure of present micro-cracks will take place initially during axial loading. Development of new micro-cracks will start when the load is further increased and axial stress reaches the crack initiation stress σ_{i}. The crack growth at this stage is as stable as increased loading is required for further cracking. A transition from a development of micro-cracks to macro-cracks will occur when the axial load is further increased. At a certain stress level the crack growth becomes unstable. The stress level when this happens is denoted the crack damage stress σ_{d}, cf. Martin and Chandler (1994). In order to determine the stress levels, we look at the volumetric strain.

By subtracting the elastic volumetric strain $\varepsilon_{\mathrm{vol}}^{\mathrm{e}}$ from the total volumetric strain, a volumetric strain corresponding to the crack volume $\varepsilon_{\mathrm{vol}}^{\mathrm{cr}}$ is obtained. This has been denoted calculated crack volumetric strain in the literature, cf. Martin and Chandler (1994) and Eberhardt et al. (1998). We thus have

$$\varepsilon_{\mathrm{vol}}^{\mathrm{cr}} = \varepsilon_{\mathrm{vol}} - \varepsilon_{\mathrm{vol}}^{\mathrm{e}}$$

Assuming linear elasticity leads to

$$\varepsilon_{\mathrm{vol}}^{\mathrm{cr}} = \varepsilon_{\mathrm{vol}} - \frac{1-2\upsilon}{E}(\sigma_{\mathrm{a}} - \sigma_{\mathrm{r}})$$

where $\sigma_{\mathrm{r}} = p$ was used. Experimental investigations have shown that the crack initiation stress σ_{i} coincides with the onset of increase of the calculated crack volume, cf. Martin and Chandler (1994) and Eberhardt et al. (1998). The same investigations also indicate that the crack damage stress σ_{d} can be defined as the axial stress at which the total volume starts to increase, i.e. when a dilatant behaviour is observed.

Another method to assess the crack initiation stress based on strain measurements is to use the Inverse Tangent Lateral Stiffness, cf. Ghazvinian et al. (2012), which was used in e.g. Jacobsson et al. (2016).

5.6 Data handling

The test results were transferred to and stored in a file server on the RISE computer network after completed tests. The main data processing, in which the elastic moduli were computed and the peak stress was determined, has been carried out using the program MATLAB, MathWorks (2025). Moreover, MATLAB was used to produce the diagrams shown in Sections 6.3 and 6.4 and in Appendix C. MS Excel (version 2604) was used to produce the other diagrams and for reporting data to the SICADA database.

5.7 Nonconformities

The testing was conducted according to the method description with some deviations. The circumferential strains have been determined within a relative error of 1.5%, which is larger than what is specified in the ISRM-standard for (ISRM 1999). Further, double systems for measuring the axial deformation have been used, which is beyond the specifications in the method description. This was conducted as development of the test method specially aimed for high-strength brittle rock.

The activity plan was followed with following departures:

KFM06C-113-09 R was tested in addition to the activity plan.

KFM06C-115-03 was not loaded immediately to failure due to the load limitation in the testing equipment. A creep failure was obtained (see results of KFM06C-115-03 in section 6.4.1).

6 Results

The reported parameters are based both on unprocessed raw data obtained from the testing and processed data and were reported to the Sicada database, where they are traceable by the activity plan number. These data together with the digital photographs of the individual specimens were handed over to SKB. The handling of the results follows SDP-508 (SKB internal controlling document) in general.

6.1 Density

The density of the specimens at a water saturated condition is shown in the results tables for the mechanical tests in Sections 6.2 to 6.4. An overview of the results for all specimens is shown in Figure 6-1.

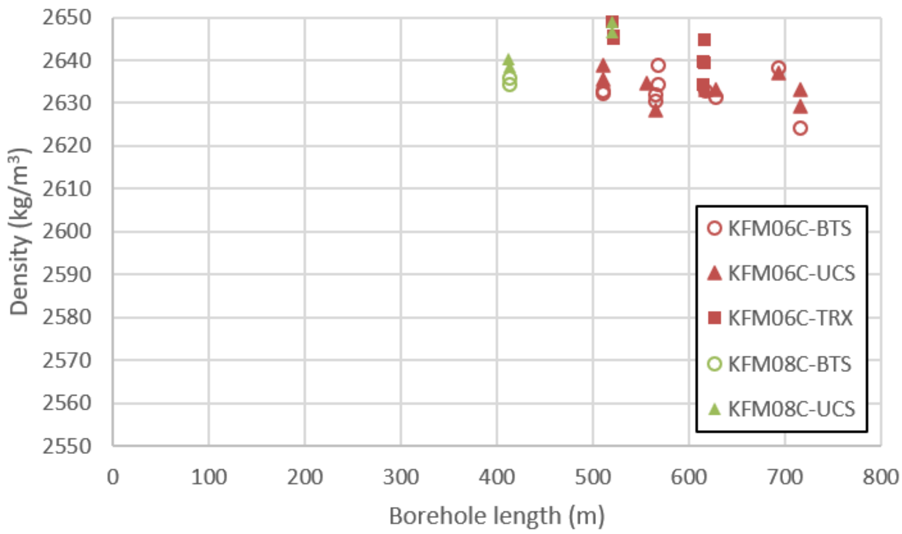

Figure 6-1. *Density as a function of borehole length for the two rock types in the study.*

6.2 Indirect tensile strength test

6.2.1 Results for each individual specimen

The results and photographs for the individual specimen are presented below.

Specimen ID: KFM06C-110-01			
Before mechanical test			After mechanical test
			
			
Diameter (mm)	**Height (mm)**	**Density (kg/m^3)**	**Tensile strength (MPa)**
50.6	26.1	2 632	16.5
Comments:	None		

Specimen ID: KFM06C-110-02			
Before mechanical test			After mechanical test
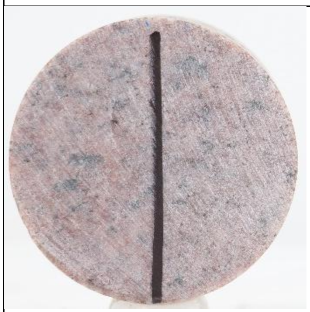			
			
Diameter (mm)	**Height (mm)**	**Density (kg/m^3)**	**Tensile strength (MPa)**
50.5	28.2	2 633	16.6
Comments:	None		

Specimen ID: KFM06C-110-03			
Before mechanical test			After mechanical test
			
			
Diameter (mm)	**Height (mm)**	**Density (kg/m^3)**	**Tensile strength (MPa)**
50.4	29.0	2 630	16.2
Comments:	None		

Specimen ID: KFM06C-110-04			
Before mechanical test			After mechanical test
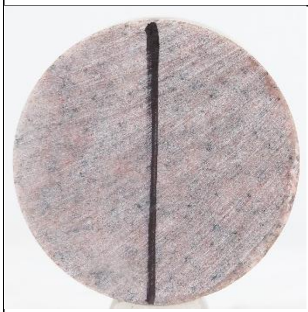			
			
Diameter (mm)	**Height (mm)**	**Density (kg/m^3)**	**Tensile strength (MPa)**
50.4	28.2	2 632	13.3
Comments:	None		

Specimen ID: KFM06C-110-06			
Before mechanical test			After mechanical test
 			 
Diameter (mm)	**Height (mm)**	**Density (kg/m^3)**	**Tensile strength (MPa)**
50.6	29.3	2 639	14.8
Comments:	None		

Specimen ID: KFM06C-110-07			
Before mechanical test			After mechanical test
 			 
Diameter (mm)	**Height (mm)**	**Density (kg/m^3)**	**Tensile strength (MPa)**
50.6	27.8	2 634	15.7
Comments:	None		

Specimen ID: KFM06C-110-08			
Before mechanical test			After mechanical test
 			 
Diameter (mm)	**Height (mm)**	**Density (kg/m^3)**	**Tensile strength (MPa)**
50.9	27.5	2 633	17.6
Comments:	None		

Specimen ID: KFM06C-110-09			
Before mechanical test			After mechanical test
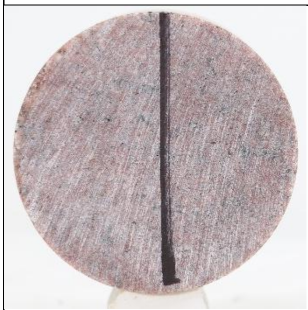 			 
Diameter (mm)	**Height (mm)**	**Density (kg/m^3)**	**Tensile strength (MPa)**
50.3	27.1	2 631	16.9
Comments:	None		

Specimen ID: KFM06C-110-10			
Before mechanical test			After mechanical test
 			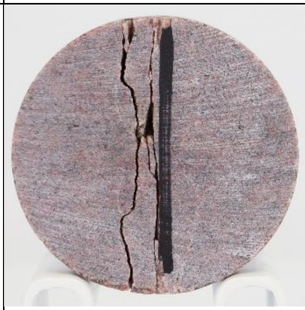 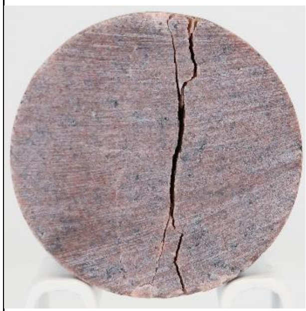
Diameter (mm)	**Height (mm)**	**Density (kg/m^3)**	**Tensile strength (MPa)**
50.6	27.3	2 638	17.6
Comments:	None		

Specimen ID: KFM06C-110-11			
Before mechanical test			After mechanical test
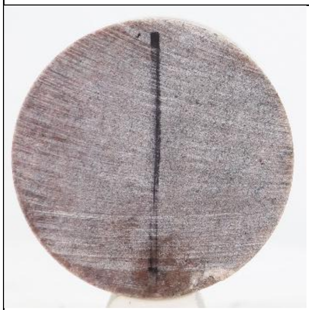 			 
Diameter (mm)	**Height (mm)**	**Density (kg/m^3)**	**Tensile strength (MPa)**
50.7	26.9	2 624	15.6
Comments:	None		

Specimen ID: KFM08C-110-01			
Before mechanical test			After mechanical test
 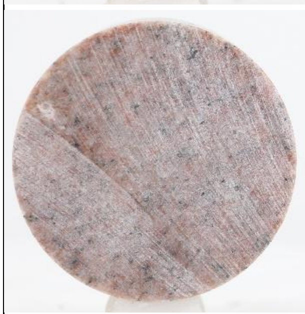			 
Diameter (mm)	**Height (mm)**	**Density (kg/m^3)**	**Tensile strength (MPa)**
50.6	29.0	2 636	14.8
Comments:	None		

Specimen ID: KFM08C-110-02			
Before mechanical test			After mechanical test
 			 
Diameter (mm)	**Height (mm)**	**Density (kg/m^3)**	**Tensile strength (MPa)**
50.6	27.7	2 634	14.7
Comments:	None		

6.2.2 Results for the entire test series

The test results for all indirect tensile strength tests are shown in Table 6-1 and the mean values and standard deviations are shown in Table 6-2. The indirect tensile strength versus borehole length (secup) are shown in in Figure 6-2.

Table 6-1. Results from density measurements and direct tensile tests.

Identification	Density (kg/m^3)	Tensile strength (MPa)	Comments
KFM06C-110-01	2 632	16.5	I (I = Isotropic)
KFM06C-110-02	2 633	16.6	I
KFM06C-110-03	2 630	16.2	I
KFM06C-110-04	2 632	13.3	I
KFM06C-110-06	2 639	14.8	I
KFM06C-110-07	2 634	15.7	I
KFM06C-110-08	2 633	17.6	I
KFM06C-110-09	2 631	16.9	I
KFM06C-110-10	2 638	17.6	I
KFM06C-110-11	2 624	15.6	I
KFM08C-110-01	2 636	14.8	I
KFM08C-110-02	2 634	14.7	I

Table 6-2. Calculated mean values and standard deviations.

Identification	Density (kg/m^3)	Tensile strength (MPa)
Mean value	2 633	15.9
Std dev	3.8	1.3

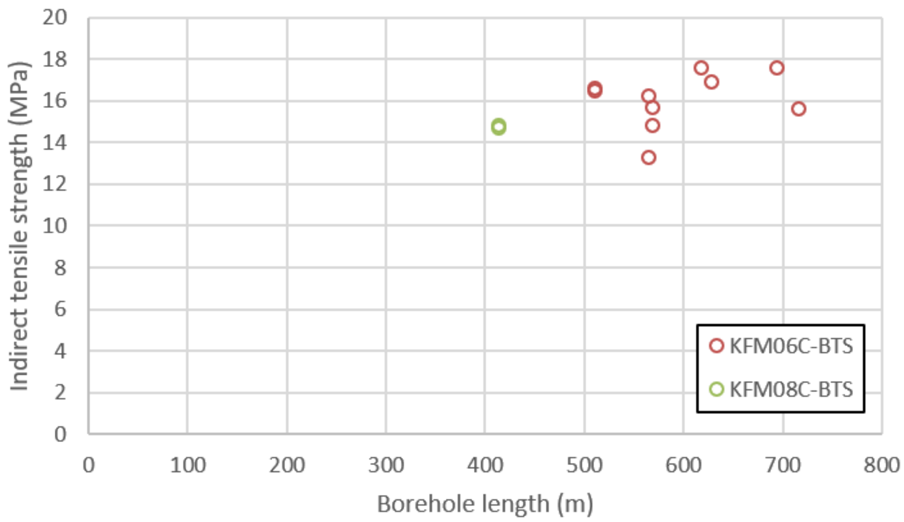

Figure 6-2. Indirect tensile strength as a function of borehole length for the two rock types in the study.

6.3 Uniaxial compression test

6.3.1 Results for each individual specimen

The cracking is shown in photos of the specimens, and comments on observations made during the testing are reported. The elasticity parameters have been evaluated by using the results from the local axial deformation measurements. The data from the adjusted total axial deformation measurements, cf. Section 5.4.2, are shown in this section.

Diagrams showing the data from both the local and the total axial deformation measurements, system (S1) and (S2) in Figure 4-3, and the computed individual values of K_{system} used at the data corrections are shown in Appendix C. Diagrams displaying actual radial strain rates versus the test time are also presented in Appendix C. The results for the individual specimens are as follows:

Specimen ID: KFM06C-113-01			
Before mechanical test		After mechanical test	
			
Diameter (mm)	**Height (mm)**	**Density (kg/m^3)**	
50.6	126.0	2 639	
Comments:			

Specimen ID: KFM06C-113-01

Youngs Modulus (E):	82.8	[GPa]
Poisson Ratio (ν):	0.345	[-]
Axial peak stress (σ_c):	372.9	[MPa]

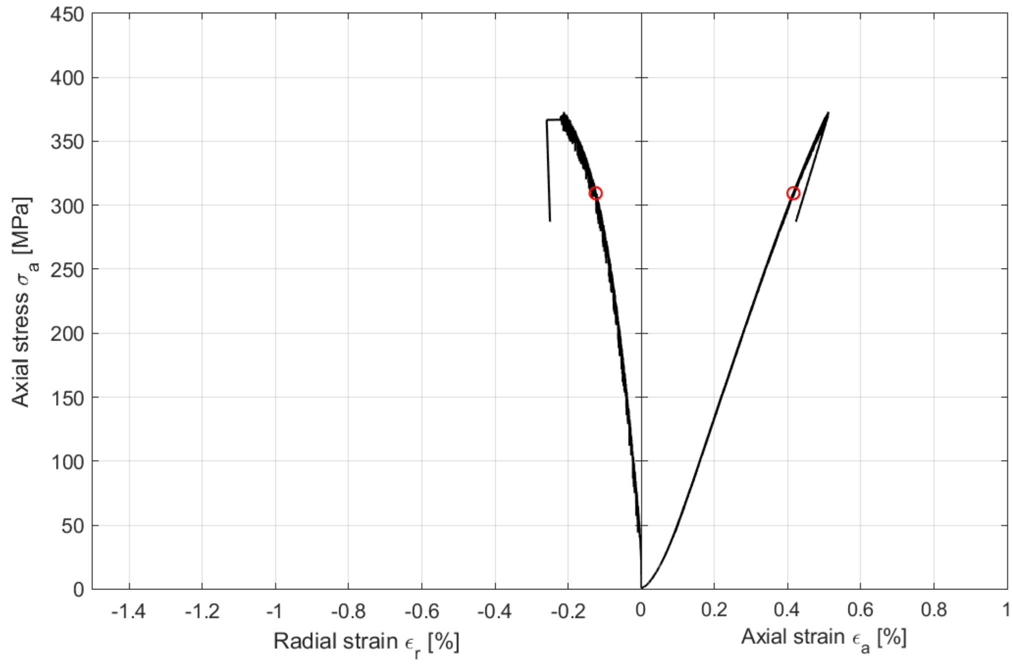

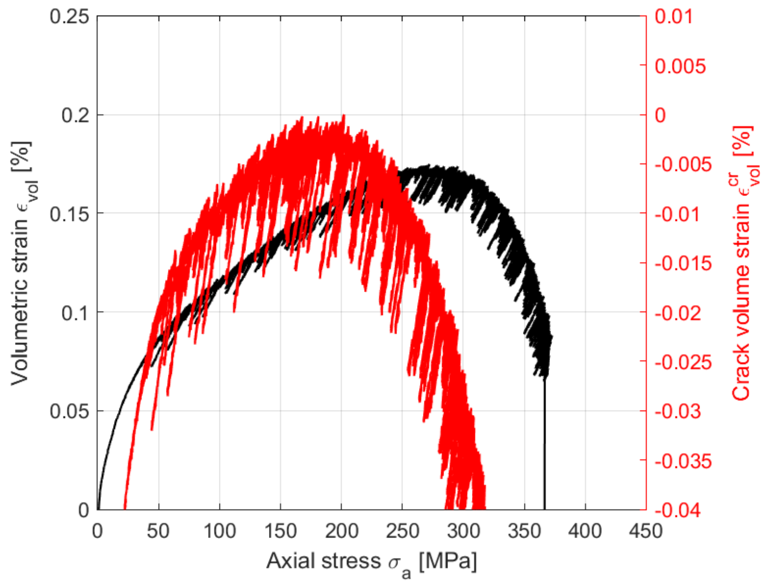

Specimen ID: KFM06C-113-02			
Before mechanical test		After mechanical test	
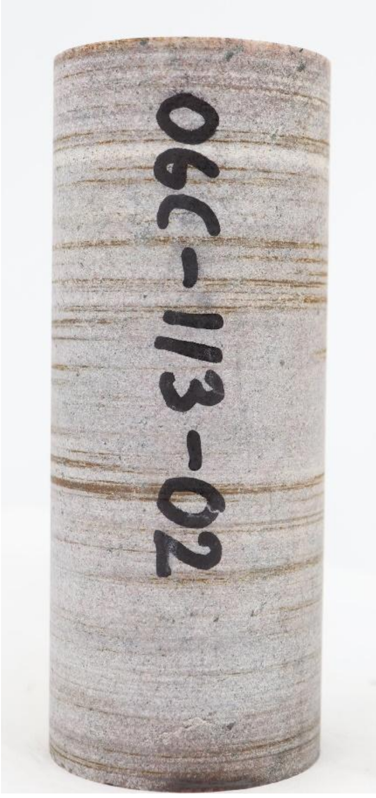			
Diameter (mm)	**Height (mm)**	**Density (kg/m^3)**	
50.5	126.5	2 636	
Comments:			

Specimen ID: KFM06C-113-02

Youngs Modulus (E):	80.1	[GPa]
Poisson Ratio (ν):	0.337	[-]
Axial peak stress (σ_c):	324.9	[MPa]

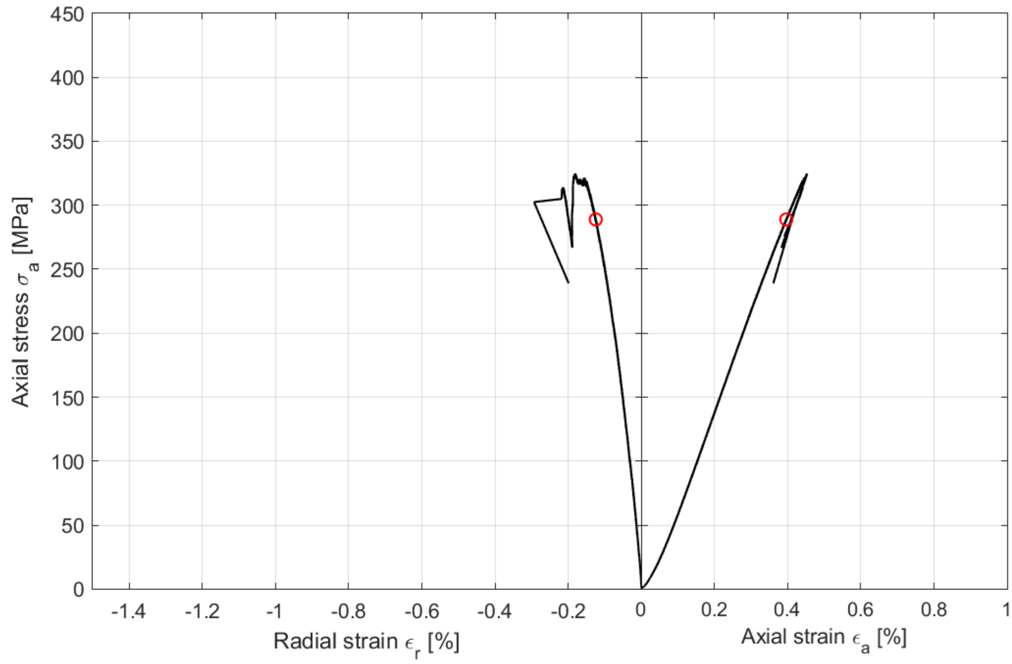

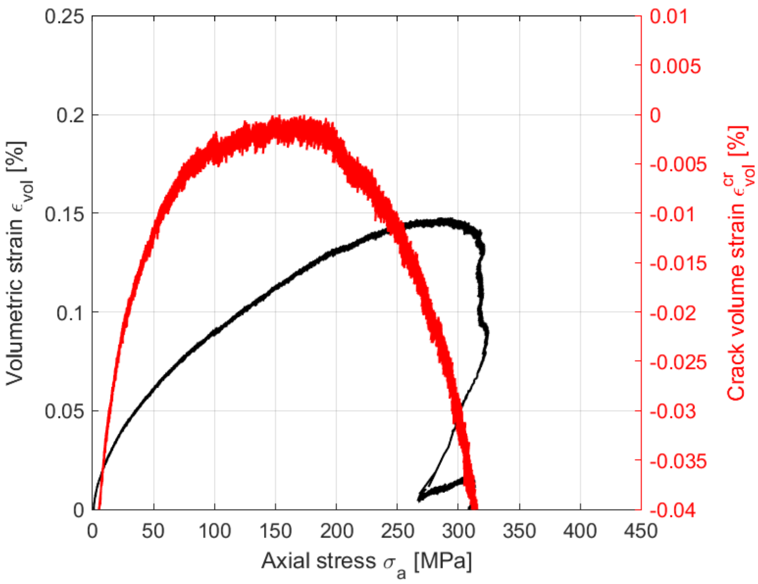

Specimen ID: KFM06C-113-03			
Before mechanical test		After mechanical test	
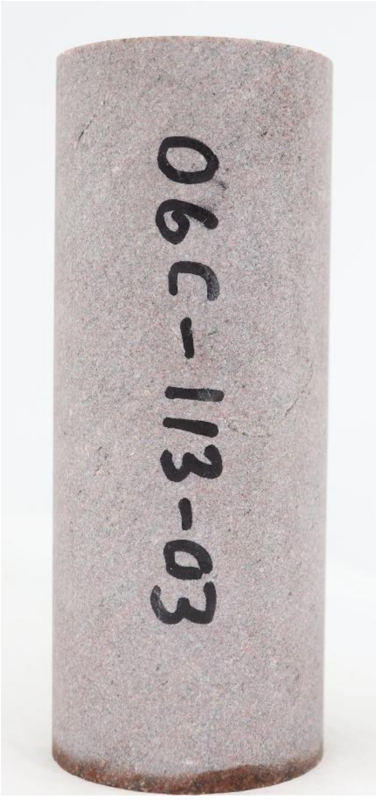			
Diameter (mm)	**Height (mm)**	**Density (kg/m^3)**	
50.7	127.3	2 635	
Comments:	A surface instability occurred and a chip ws formed that pushed the circumferential gauge and caused an unloading.		

Specimen ID: KFM06C-113-03

Youngs Modulus (E):	79.0	[GPa]
Poisson Ratio (ν):	0.267	[-]
Axial peak stress (σ_c):	263.6	[MPa]

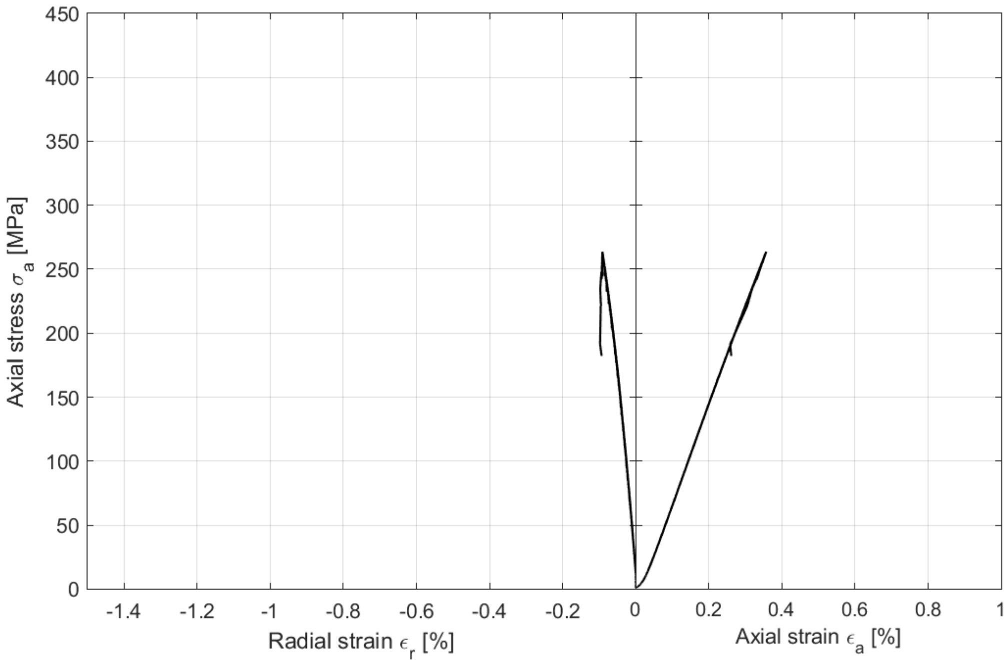

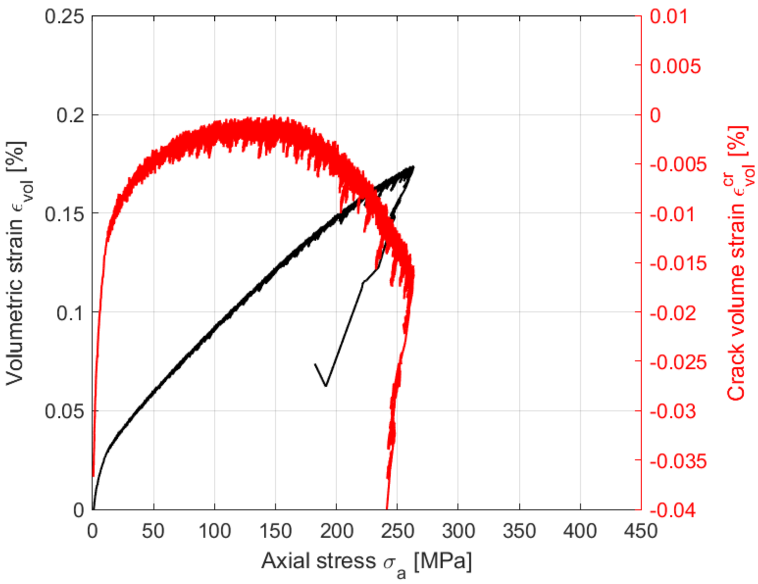

Specimen ID: KFM06C-113-04			
Before mechanical test		After mechanical test	
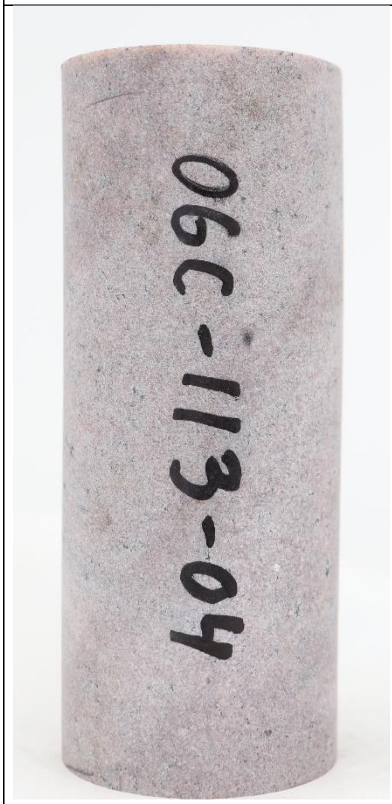			
Diameter (mm)	**Height (mm)**	**Density (kg/m^3)**	
50.6	125.0	2 628	
Comments:			

Specimen ID: KFM06C-113-04

Youngs Modulus (E):	76.5	[GPa]
Poisson Ratio (ν):	0.326	[-]
Axial peak stress (σ_c):	345.4	[MPa]

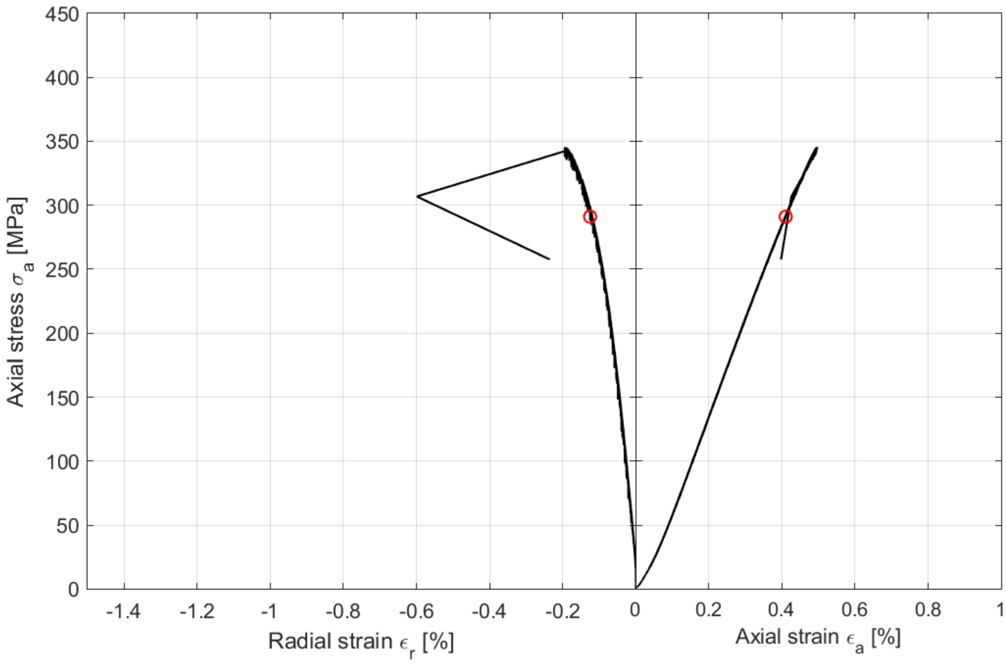

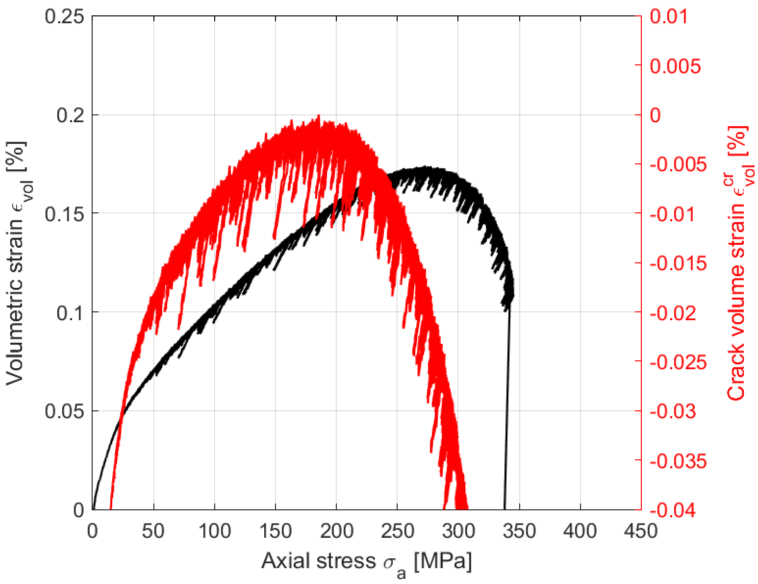

Specimen ID: KFM06C-113-05			
Before mechanical test		After mechanical test	
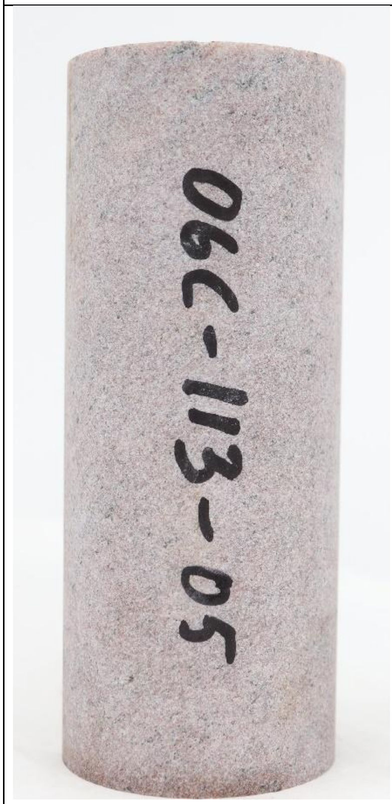			
Diameter (mm)	**Height (mm)**	**Density (kg/m^3)**	
50.9	127.3	2 633	
Comments:			

Specimen ID: KFM06C-113-05

Youngs Modulus (E):	80.5	[GPa]
Poisson Ratio (ν):	0.343	[-]
Axial peak stress (σ_c):	386.9	[MPa]

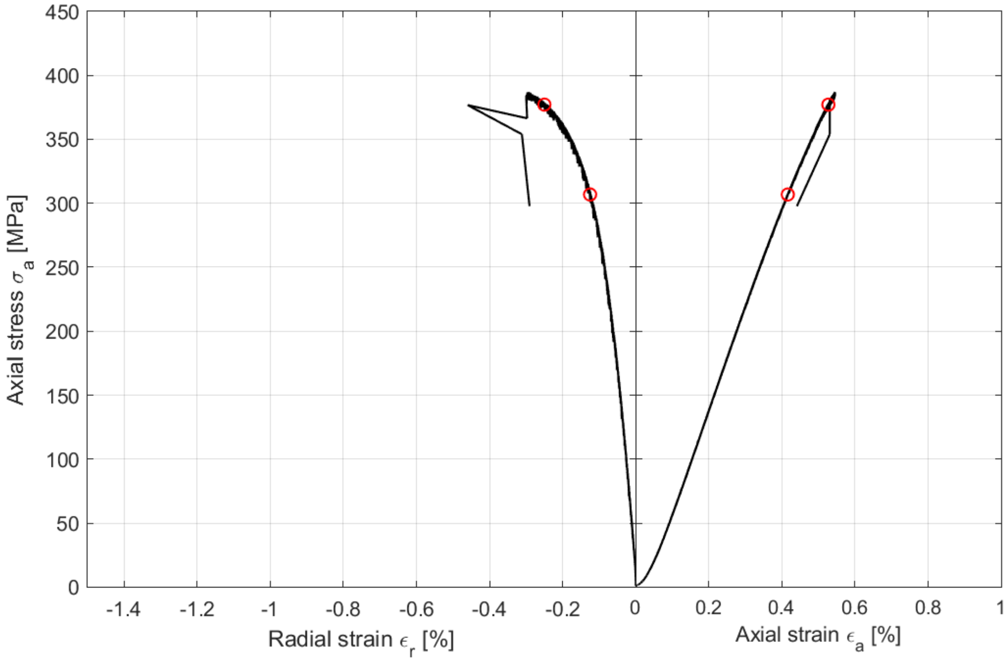

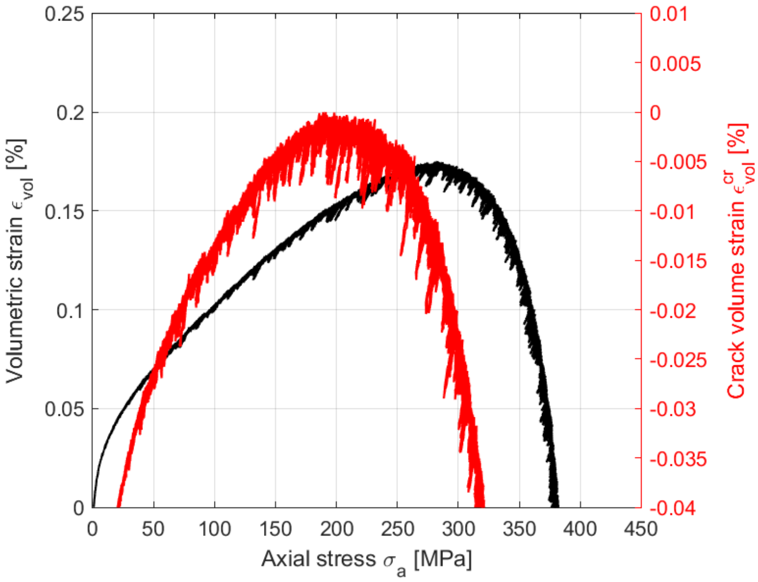

Specimen ID: KFM06C-113-06			
Before mechanical test		After mechanical test	
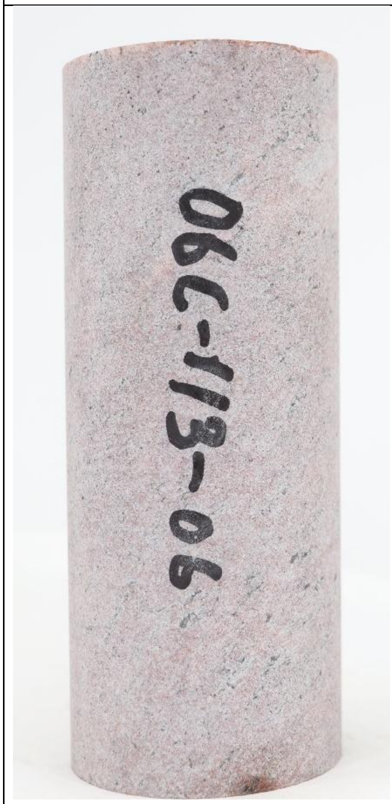			
Diameter (mm)	**Height (mm)**	**Density (kg/m^3)**	
50.3	127.3	2 633	
Comments:			

Specimen ID: KFM06C-113-06

Youngs Modulus (E):	79.8	[GPa]
Poisson Ratio (ν):	0.306	[-]
Axial peak stress (σ_c):	328.1	[MPa]

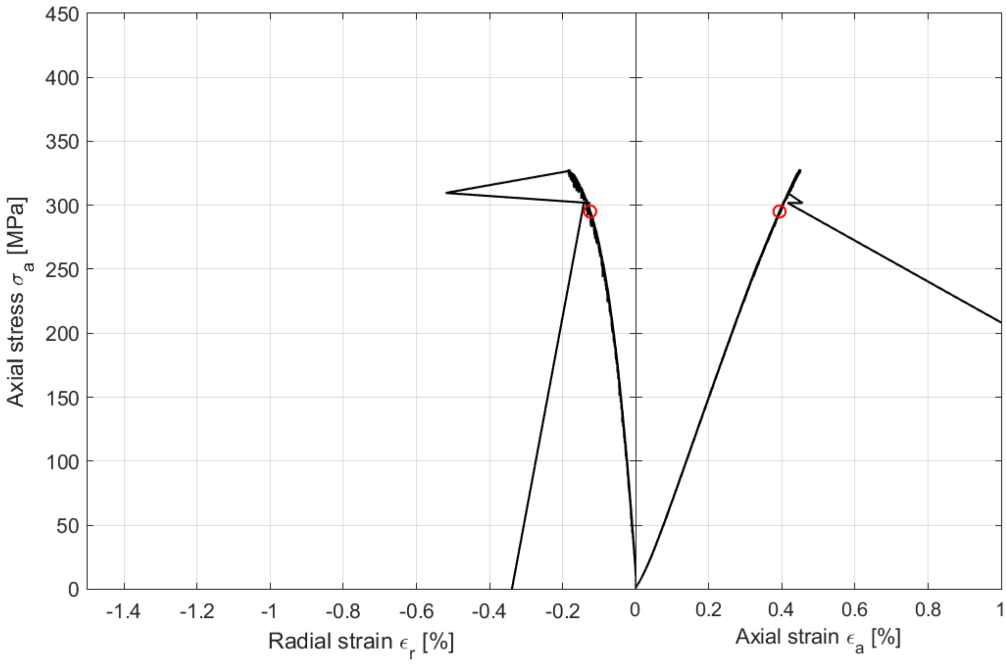

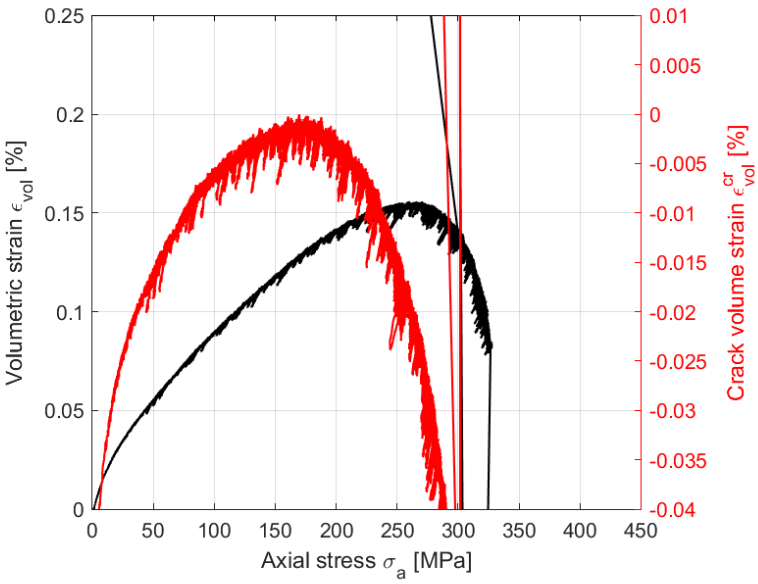

<table>
<tr><td colspan="2">Specimen ID: KFM06C-113-07</td><td colspan="2"></td></tr>
<tr><td colspan="2">Before mechanical test</td><td colspan="2">After mechanical test</td></tr>
<tr><td colspan="2">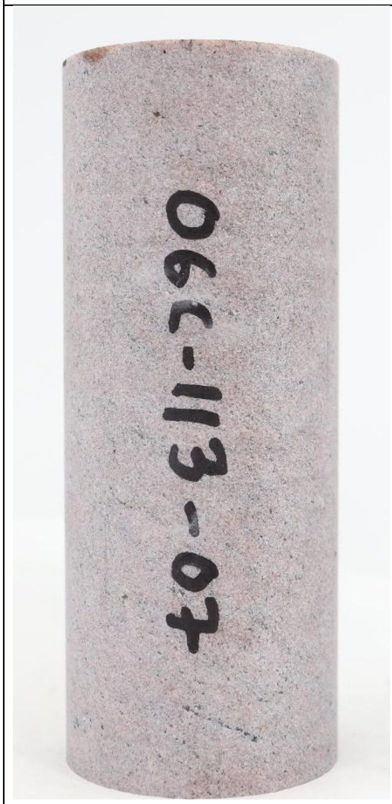
</td><td>
</td><td></td></tr>
<tr><td>Diameter (mm)</td><td>Height (mm)</td><td>Density (kg/m^3)</td><td></td></tr>
<tr><td>50.6</td><td>127.6</td><td>2 637</td><td></td></tr>
<tr><td>Comments:</td><td colspan="3"></td></tr>
</table>

Specimen ID: KFM06C-113-07

Youngs Modulus (E):	78.4	[GPa]
Poisson Ratio (ν):	0.333	[-]
Axial peak stress (σ_c):	342.4	[MPa]

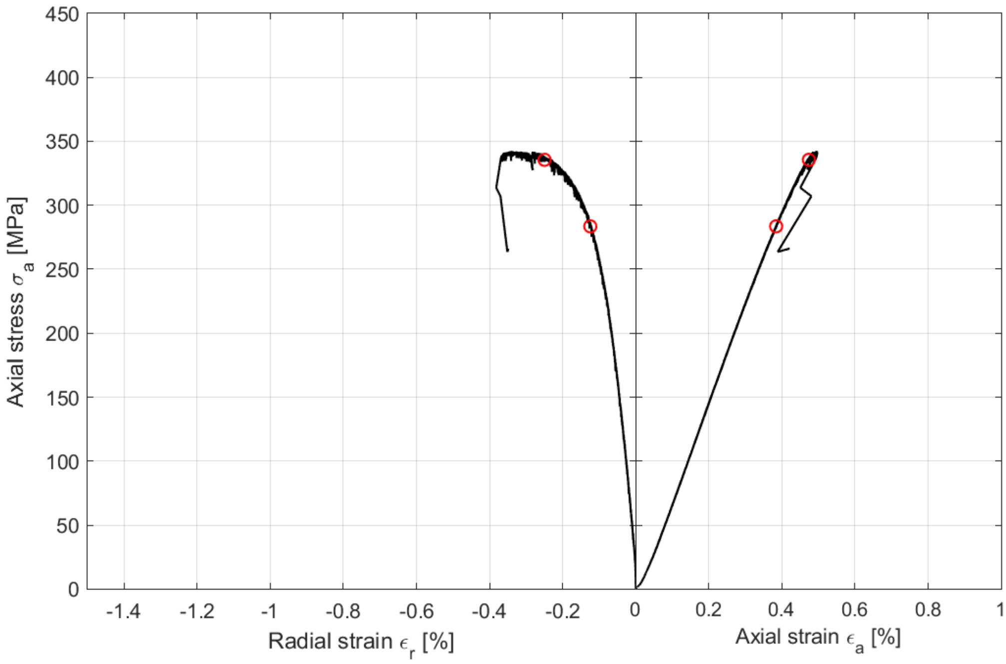

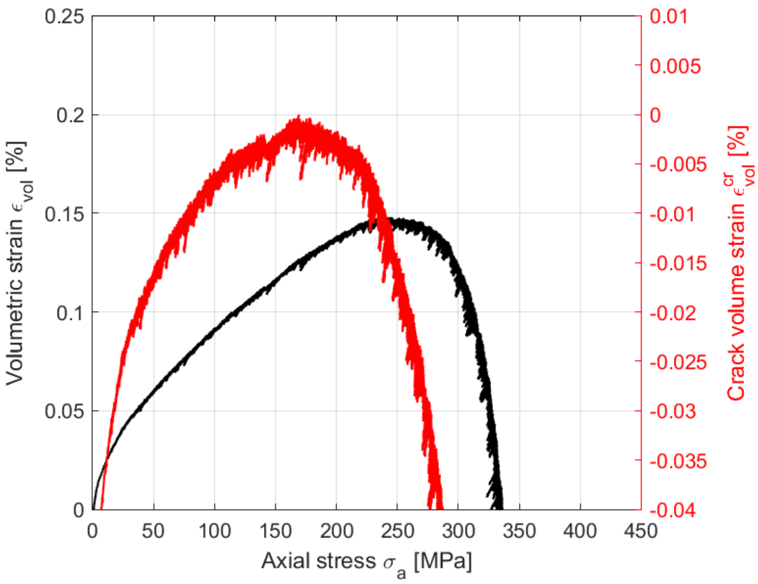

Specimen ID: KFM06C-113-08			
Before mechanical test		After mechanical test	
			
Diameter (mm)	**Height (mm)**	**Density (kg/m^3)**	
50.7	127.0	2 629	
Comments:	A small surface instability seems to have occurred at ca. 160 MPa which yielded small instant increase of the recorded radial strain.		

Specimen ID: KFM06C-113-08

Youngs Modulus (E):	82.3	[GPa]
Poisson Ratio (ν):	0.323	[-]
Axial peak stress (σ_c):	433.9	[MPa]

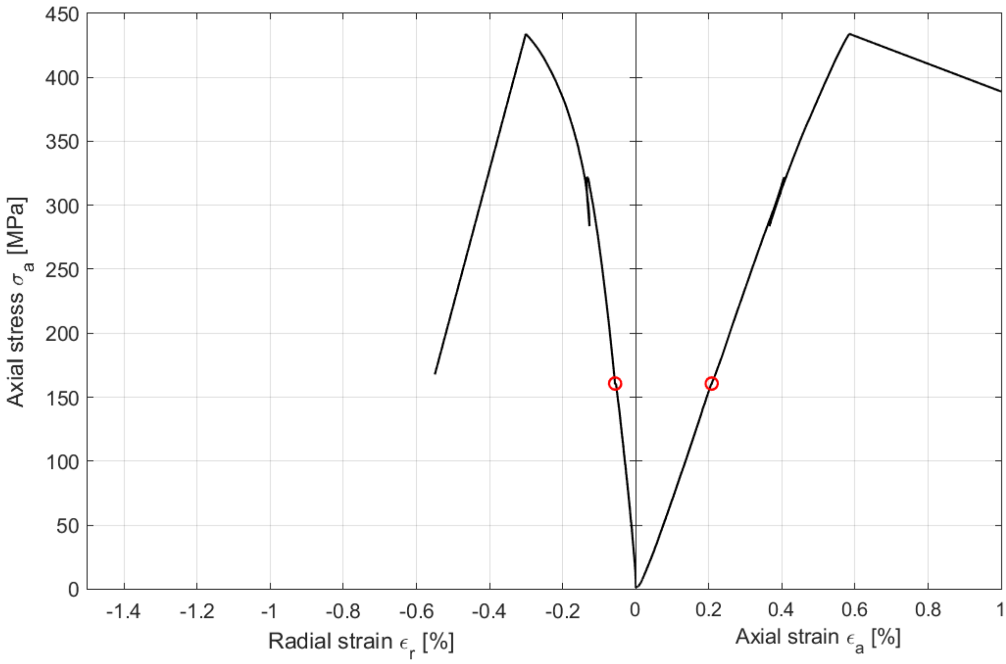

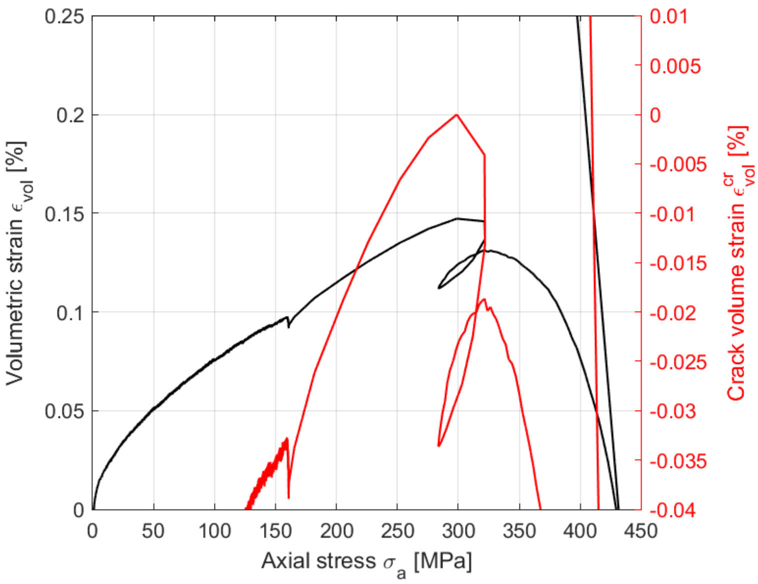

Specimen ID: KFM06C-113-09R			
Before mechanical test		After mechanical test	
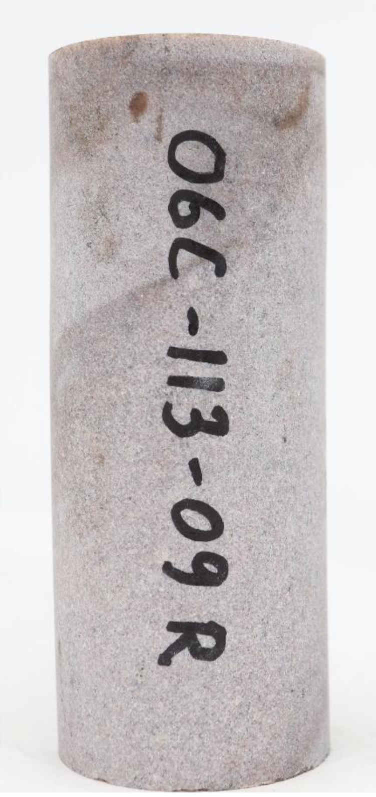			
Diameter (mm)	**Height (mm)**	**Density (kg/m^3)**	
50.7	127.55	2 633	
Comments:			

Specimen ID: KFM06C-113-09R

Youngs Modulus (E):	77.1	[GPa]
Poisson Ratio (ν):	0.365	[-]
Axial peak stress (σ_c):	371.2	[MPa]

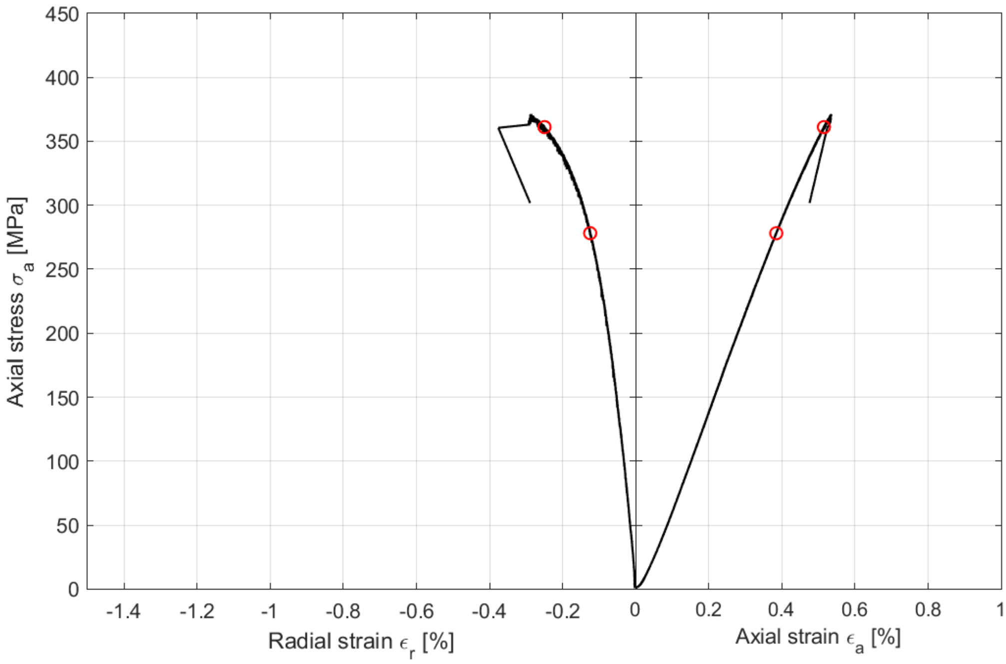

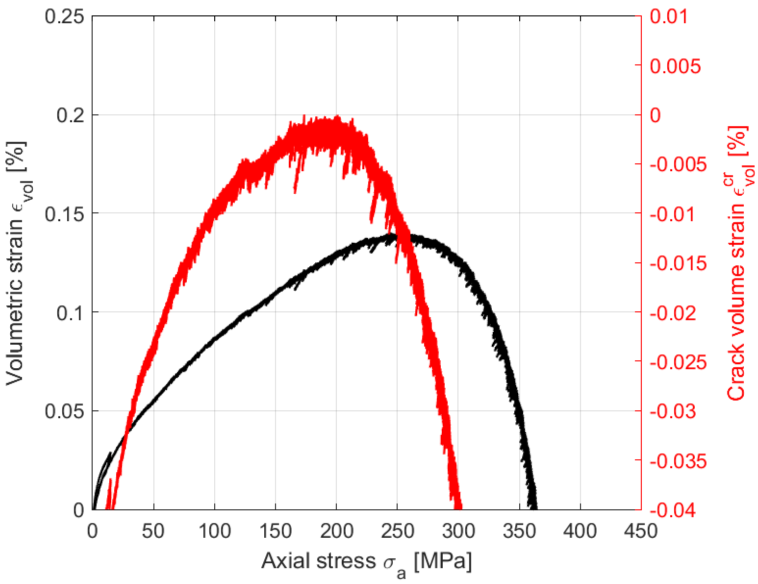

Specimen ID: KFM08C-113-01			
Before mechanical test		After mechanical test	
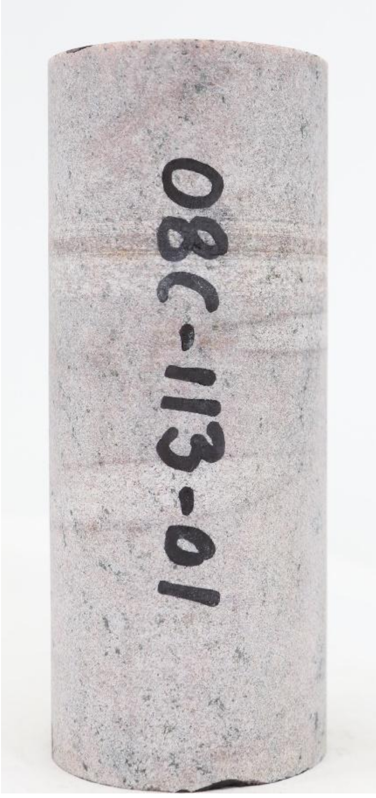		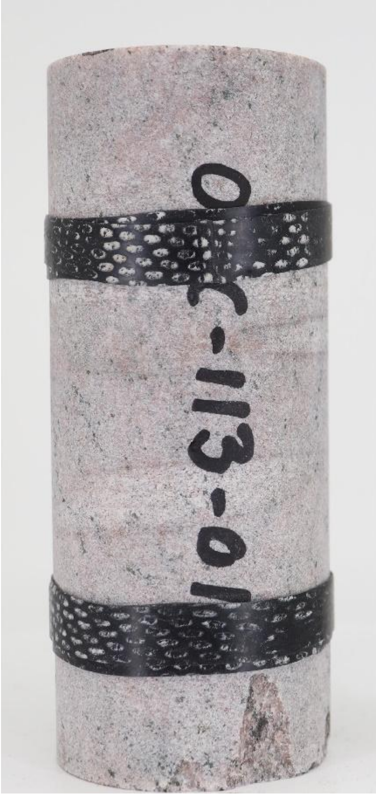	
Diameter (mm)	**Height (mm)**	**Density (kg/m^3)**	
50.6	124.9	2 640	
Comments:			

Specimen ID: KFM08C-113-01

Youngs Modulus (E):	84.2	[GPa]
Poisson Ratio (ν):	0.366	[-]
Axial peak stress (σ_c):	330.5	[MPa]

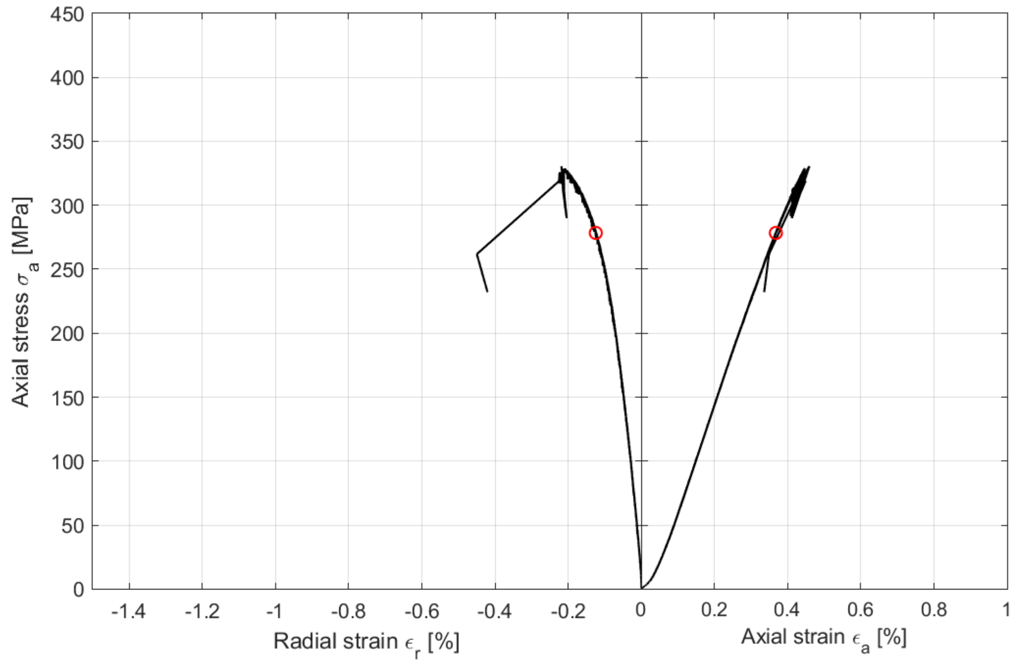

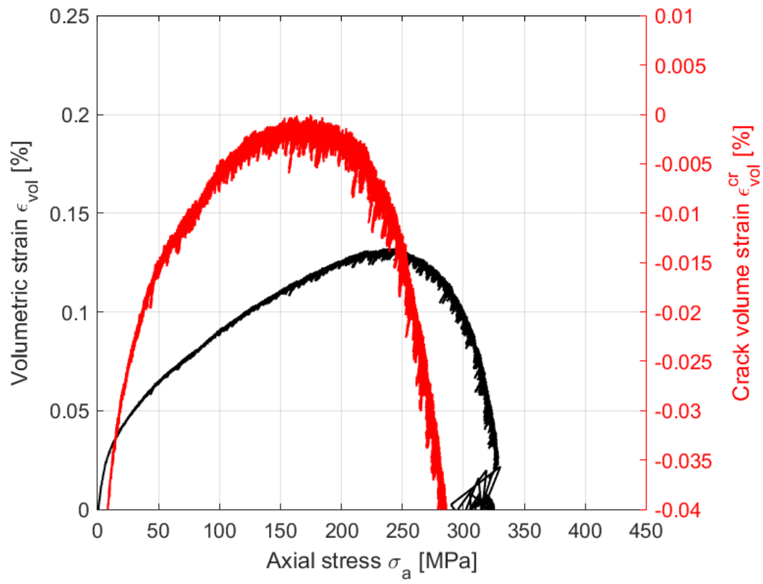

Specimen ID: KFM08C-113-02			
Before mechanical test		After mechanical test	
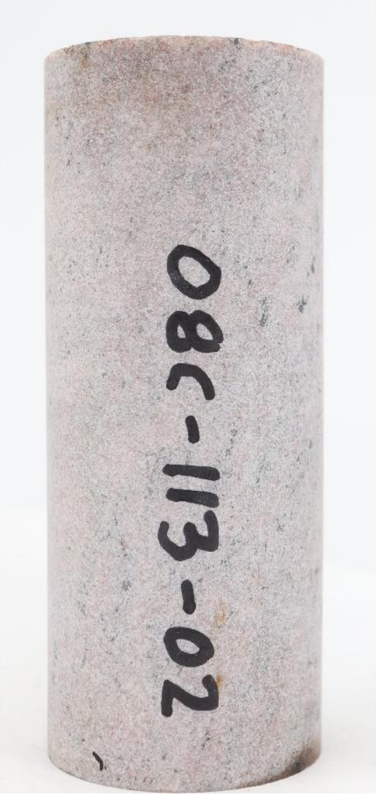			
Diameter (mm)	**Height (mm)**	**Density (kg/m^3)**	
50.6	126.1	2 639	
Comments:			

Specimen ID: KFM08C-113-02

Youngs Modulus (E):	82.8	[GPa]
Poisson Ratio (ν):	0.380	[-]
Axial peak stress (σ_c):	379.6	[MPa]

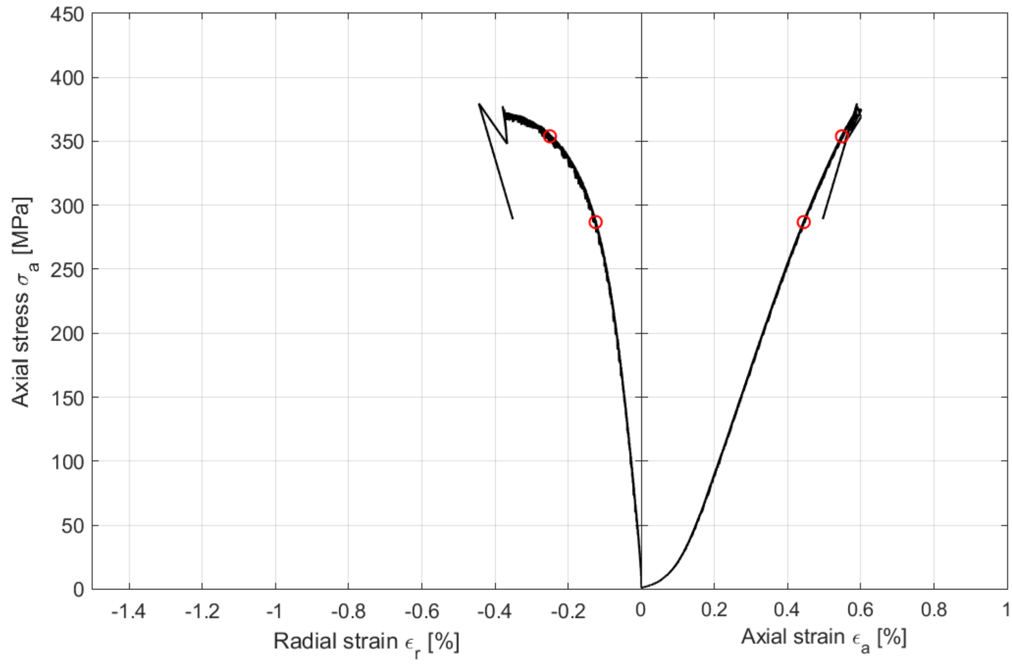

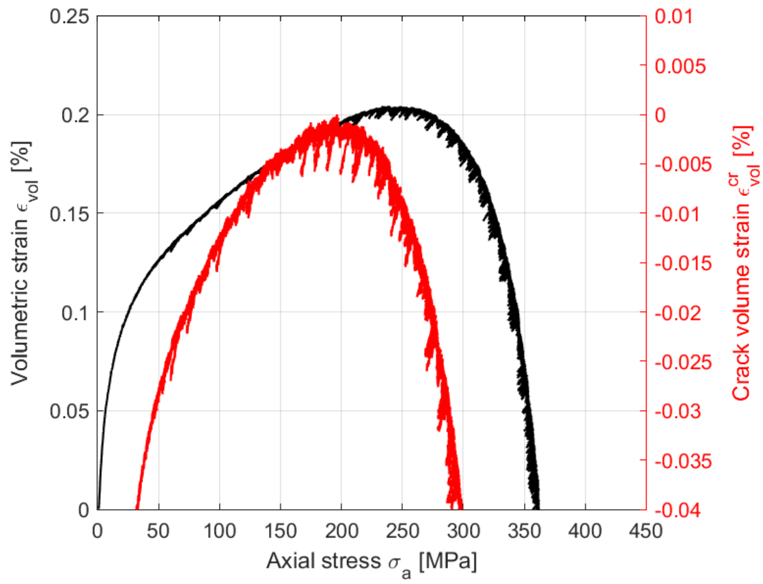

6.3.2 Results for the entire test series

A summary of the test results is shown in Table 6-2 and Table 6-3.

Table 6-3. Results from density measurements and uniaxial compression tests.

Identification	Density (kg/m^3)	Compressive strength (MPa)	Young's modulus (GPa)	Poisson ratio (-)
KFM06C-113-01	2 639	372.9	82.8	0.345
KFM06C-113-02	2 636	324.9	80.1	0.337
KFM06C-113-03	2 635	263.6	79.0	0.267
KFM06C-113-04	2 628	345.4	76.5	0.326
KFM06C-113-05	2 633	386.9	80.5	0.343
KFM06C-113-06	2 633	328.1	79.8	0.306
KFM06C-113-07	2 637	342.4	78.4	0.333
KFM06C-113-08	2 629	433.9	82.4	0.323
KFM06C-113-09R	2 633	371.2	77.1	0.365
KFM08C-113-01	2 640	330.5	84.2	0.366
KFM08C-113-02	2 639	379.6	82.8	0.380

Table 6-4. Calculated mean values and standard deviations.

Identification	Density (kg/m^3)	Compressive strength (MPa)	Young's modulus (GPa)	Poisson ratio (-)
Mean value	2 637	352	80.3	0.336
Std dev	6.0	43.8	2.5	0.031

6.4 Triaxial compression test

6.4.1 Results for each individual specimen

The cracking is shown in pictures taken on the specimens with comments on observations made during testing. The elasticity parameters have been evaluated by using the results from the local deformation measurements. Red rings are superposed on the graphs indicating every five minutes of the progress of testing. The results for the individual specimens are as follows:

Specimen ID: KFM06C-115-01			
Before mechanical test		After mechanical test	
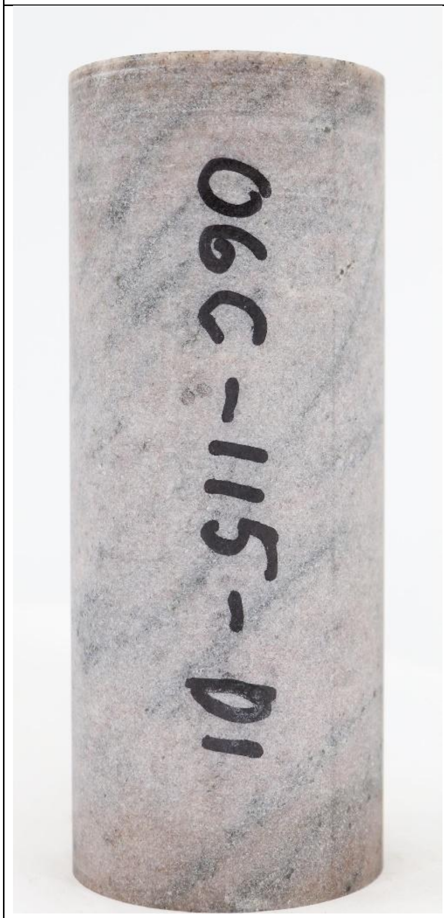			
Diameter (mm)	**Height (mm)**	**Density (kg/m^3)**	
50.6	126.5	2 649	
Comments:			

Specimen ID: KFM06C-115-01

Youngs Modulus (E): 83.2 [GPa]

Cell pressure: 5 [MPa]

Poisson Ratio (ν): 0.243 [-]

Axial peak stress (σ_c): 412.8 [MPa]

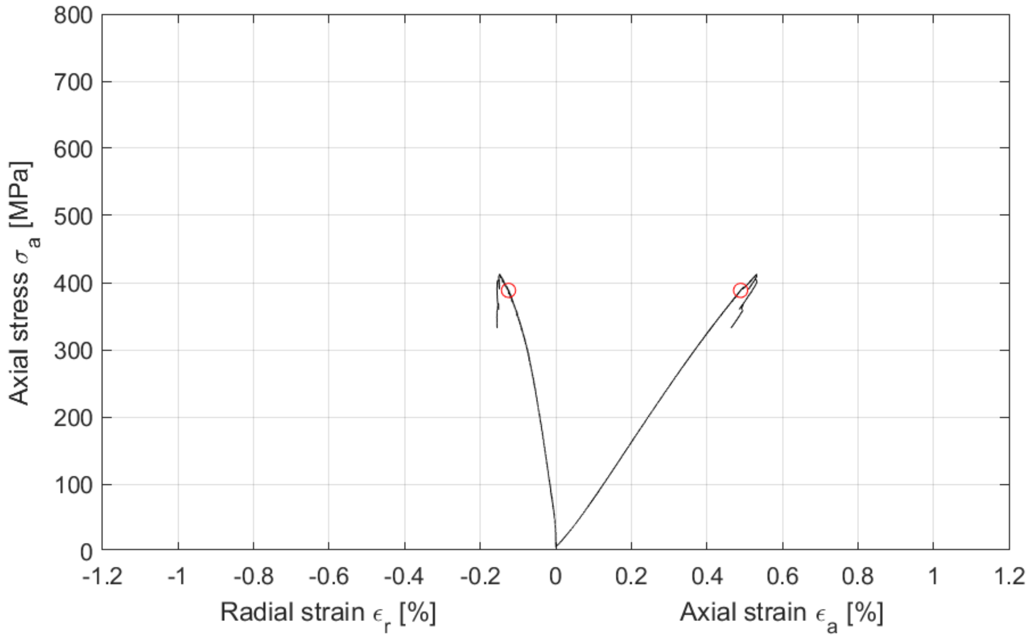

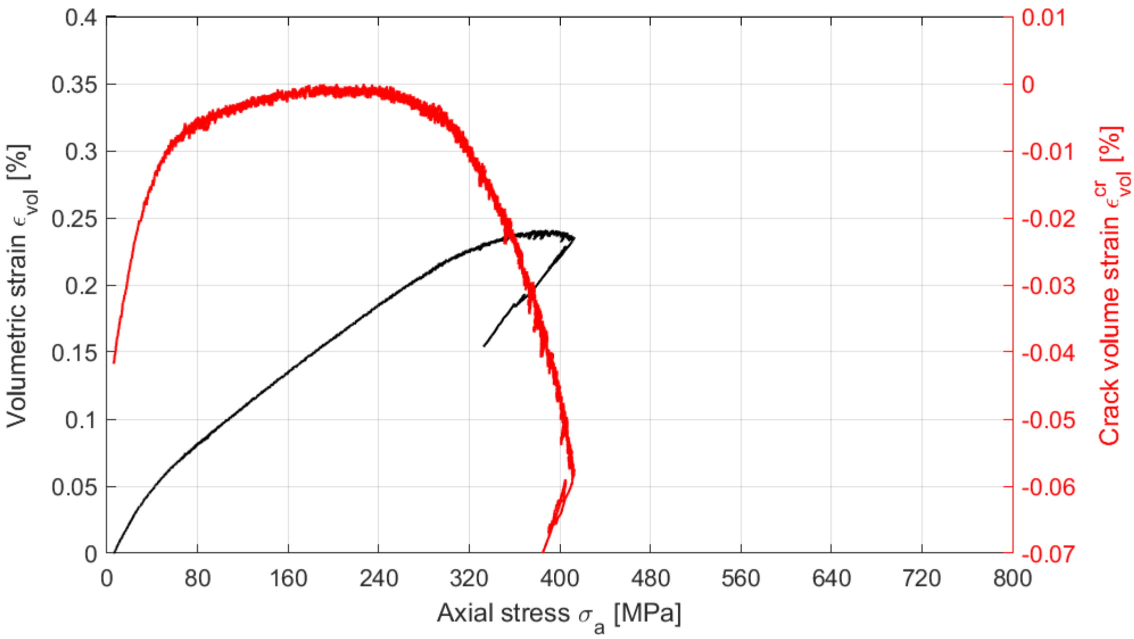

<table>
<tr><td colspan="2">Specimen ID: KFM06C-115-02</td><td colspan="2"></td></tr>
<tr><td colspan="2">Before mechanical test</td><td colspan="2">After mechanical test</td></tr>
<tr><td colspan="2">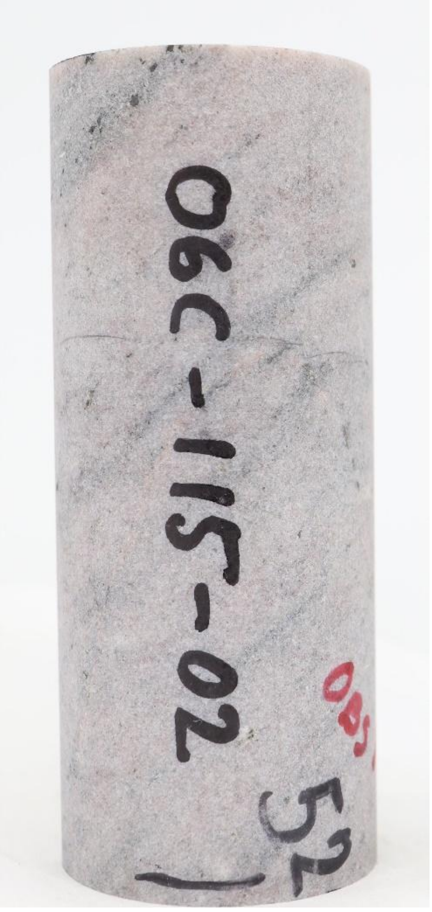</td><td>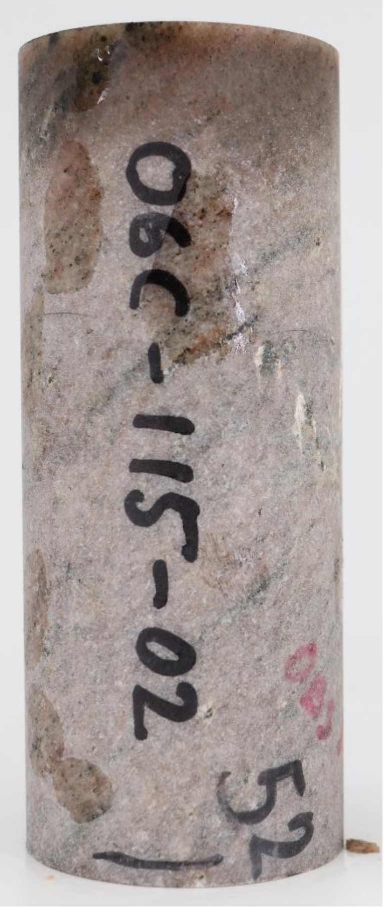</td><td></td></tr>
<tr><td>Diameter (mm)</td><td>Height (mm)</td><td>Density (kg/m³)</td><td></td></tr>
<tr><td>50.7</td><td>124.9</td><td>2 646</td><td></td></tr>
<tr><td>Comments:</td><td colspan="3"></td></tr>
</table>

Specimen ID: KFM06C-115-02

Youngs Modulus (E):	79.5 [GPa]	Cell pressure:	10 [MPa]
Poisson Ratio (ν):	0.325 [-]		
Axial peak stress (σ_c):	631.1 [MPa]		

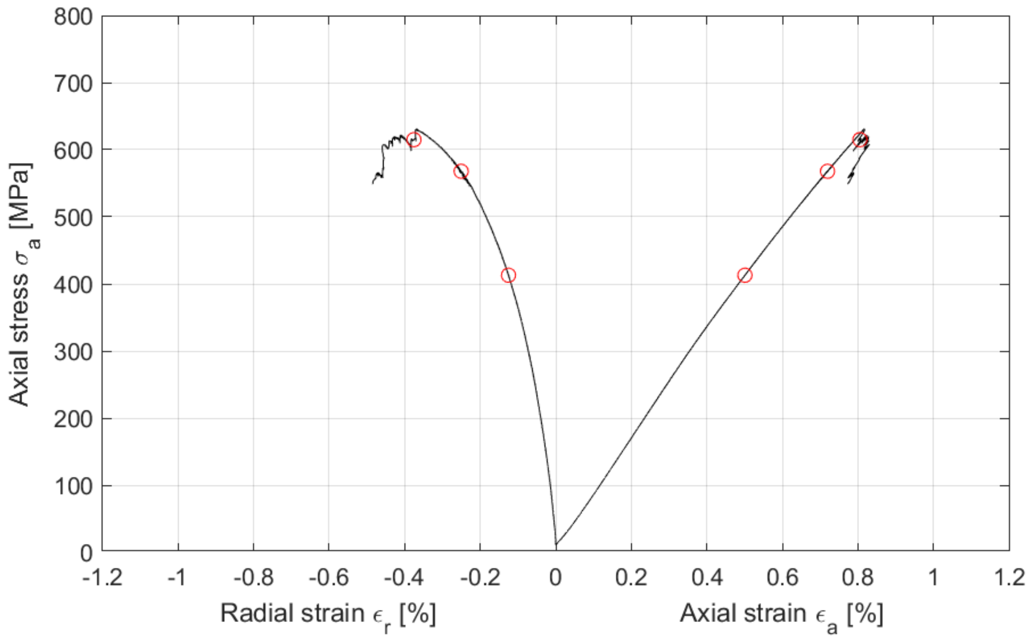

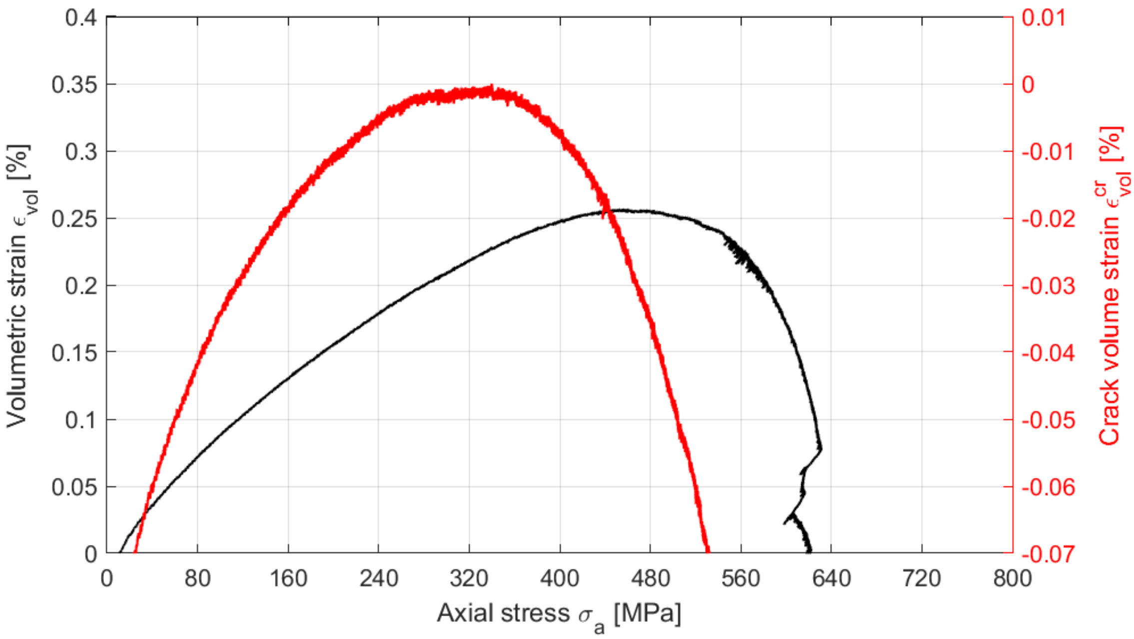

Specimen ID: KFM06C-115-03			
Before mechanical test		After mechanical test	
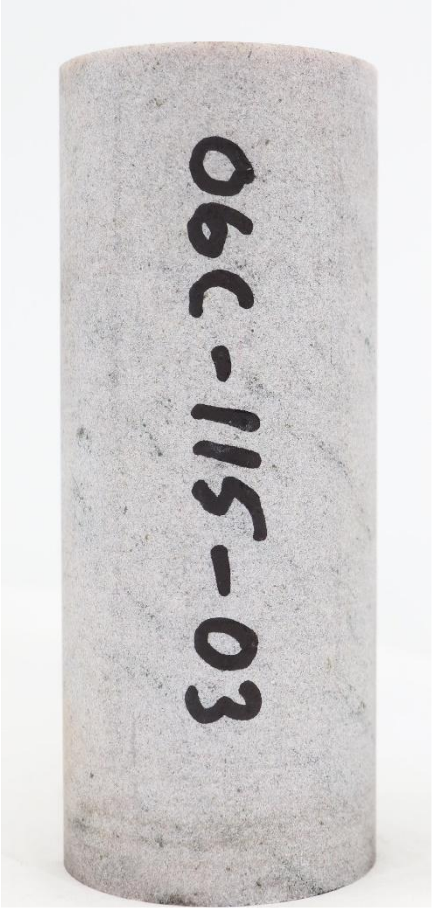			
Diameter (mm)	**Height (mm)**	**Density (kg/m³)**	
50.7	126.5	2 649	
Comments:	The specimen was loaded until the maximum force of the equipment was reached after approximately 15 minutes loading which yielded a stress of 738.1 MPa. This load was held constant until the specimen failed after 49 minutes yielding a creep failure.		

Specimen ID: KFM06C-115-03

Youngs Modulus (E):	77.0 [GPa]	Cell pressure:	20 [MPa]
Poisson Ratio (ν):	0.289 [-]		
Axial peak stress (σ_c):	738.1 [MPa]		

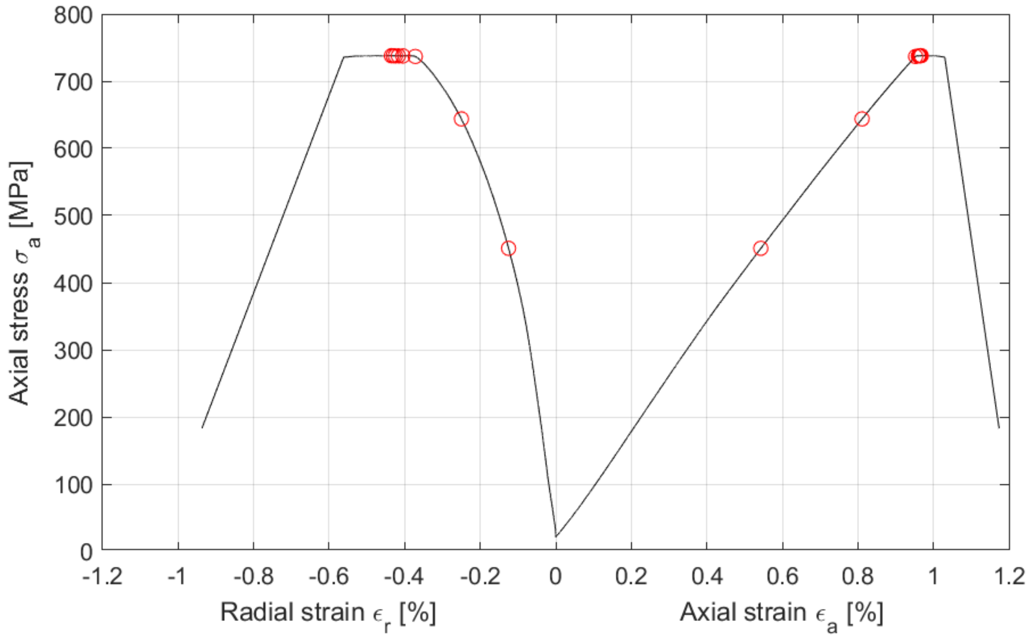

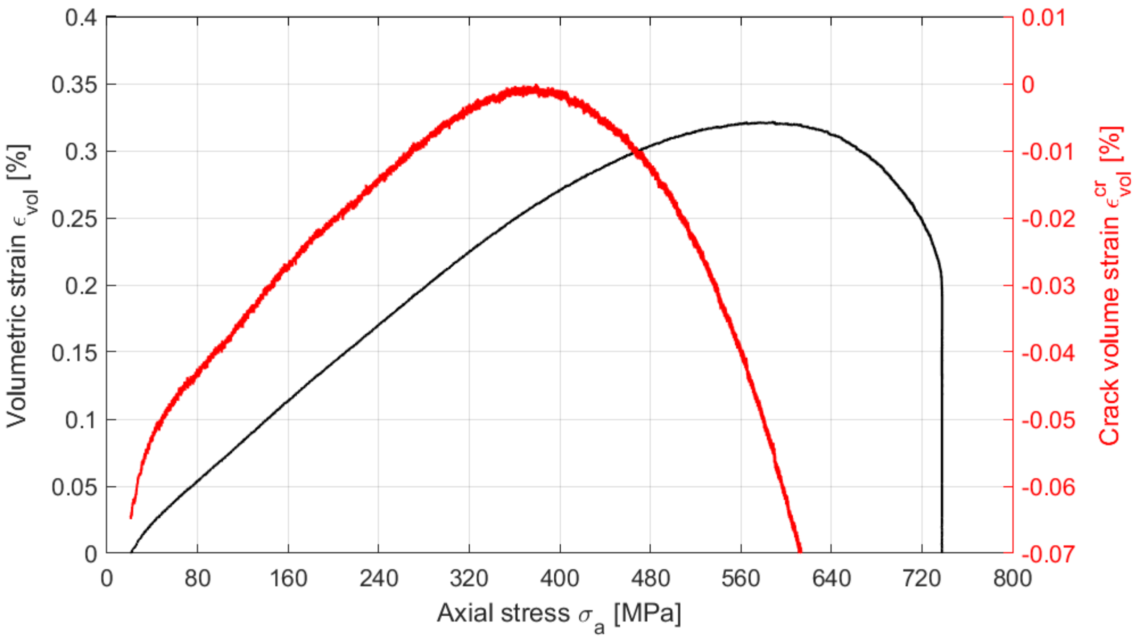

Specimen ID: KFM06C-115-04R			
Before mechanical test		After mechanical test	
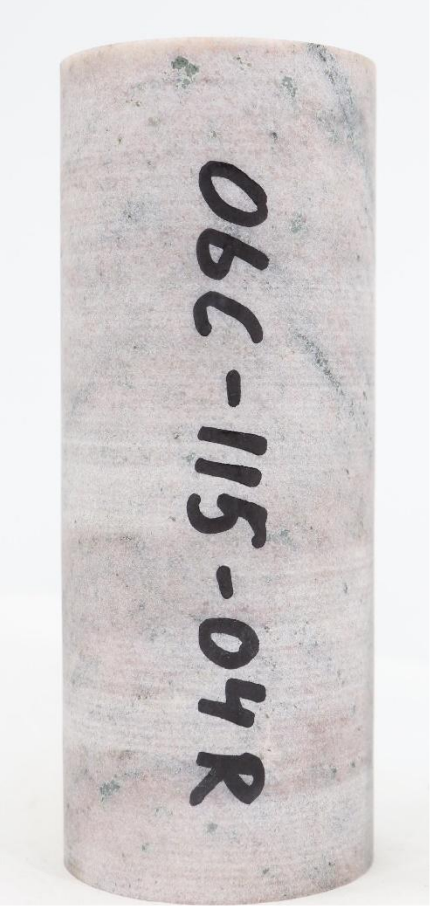 			
Diameter (mm)	**Height (mm)**	**Density (kg/m^3)**	
50.7	127.7	2 645	
Comments:			

Specimen ID: KFM06C-115-05			
Before mechanical test		After mechanical test	
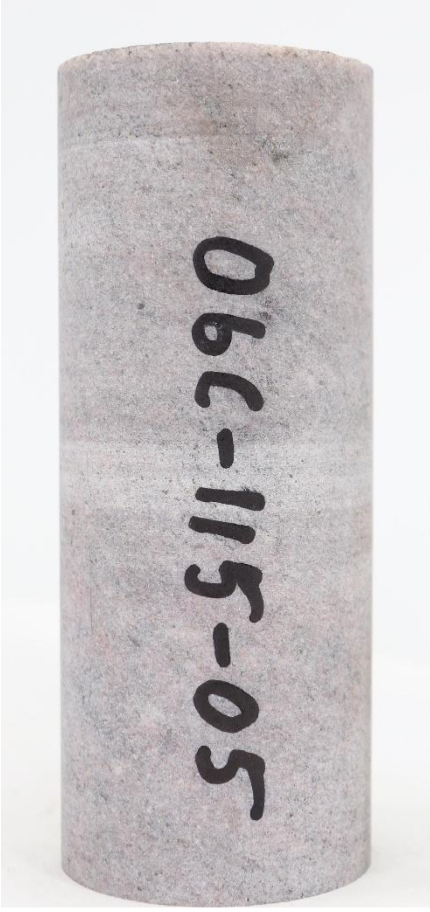			
Diameter (mm)	**Height (mm)**	**Density (kg/m^3)**	
50.7	127.7	2 646	
Comments:			

Specimen ID: KFM06C-115-05

Youngs Modulus (E): 81.9 [GPa]

Cell pressure: 15 [MPa]

Poisson Ratio (ν): 0.293 [-]

Axial peak stress (σ_c): 664.4 [MPa]

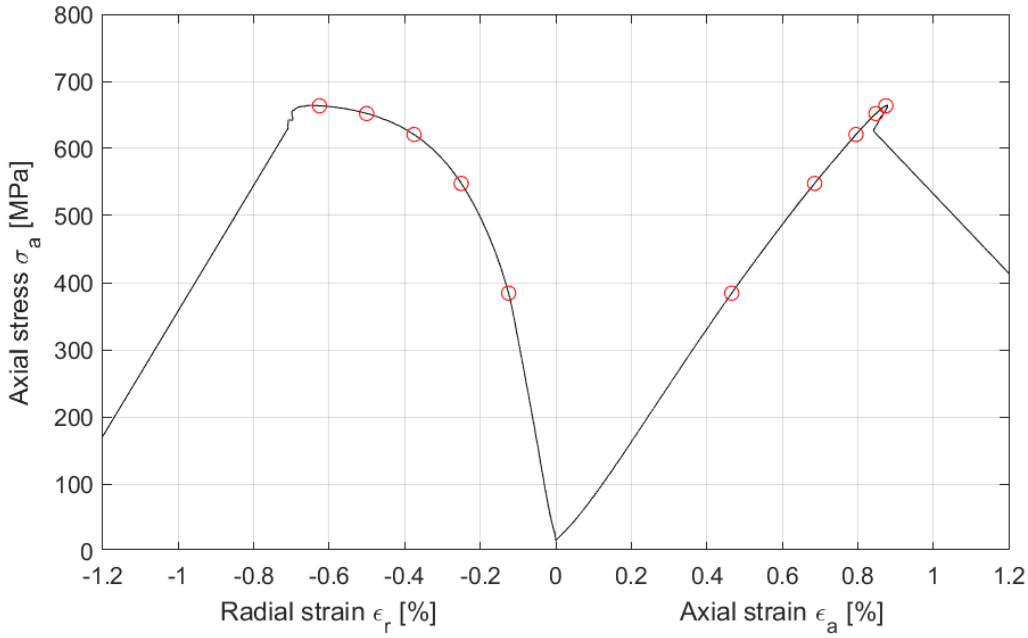

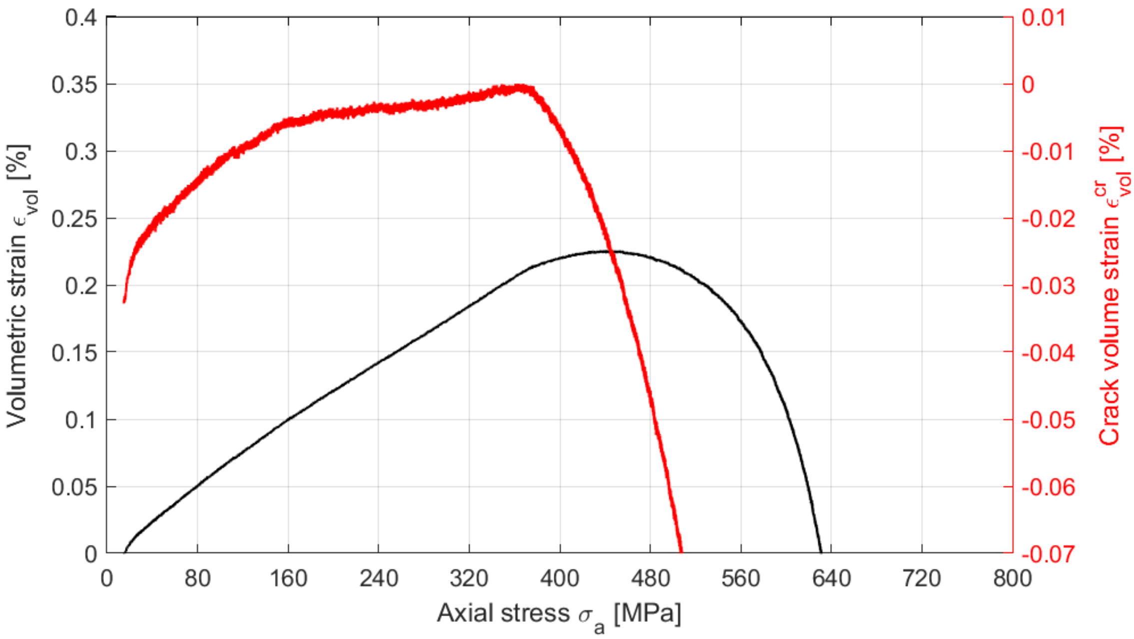

Specimen ID: KFM06C-115-06			
Before mechanical test		After mechanical test	
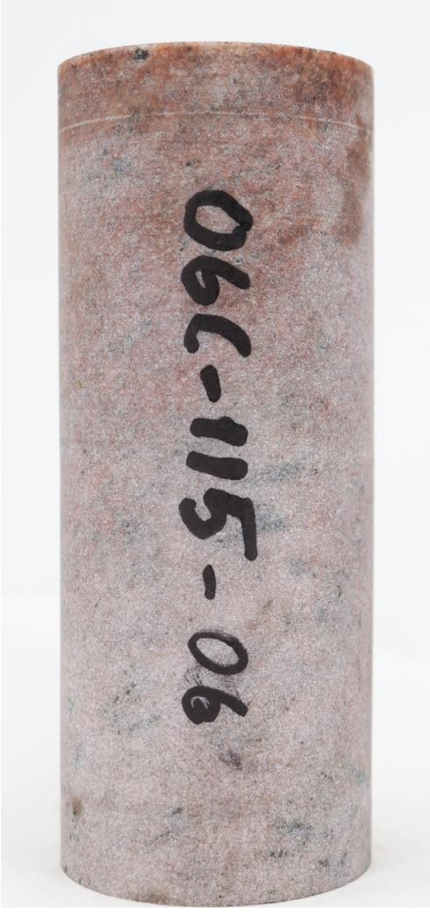		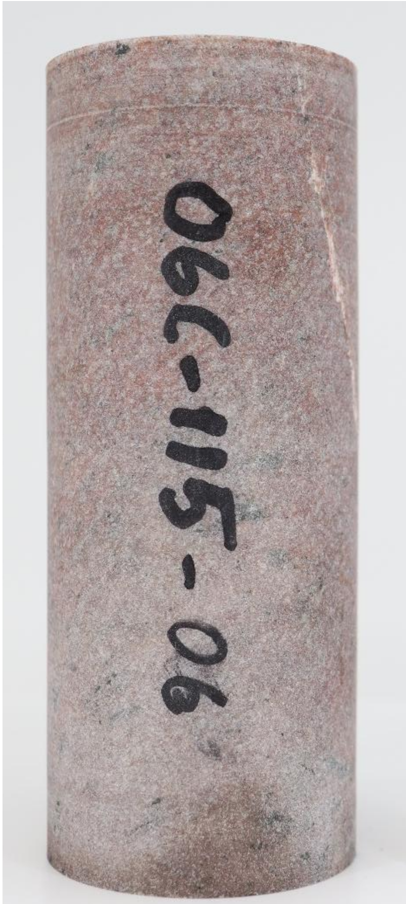	
Diameter (mm)	**Height (mm)**	**Density (kg/m^3)**	
50.9	127.8	2 634	
Comments:			

Specimen ID: KFM06C-115-06

Youngs Modulus (E): 83.1 [GPa]

Cell pressure: 5 [MPa]

Poisson Ratio (ν): 0.286 [-]

Axial peak stress (σ_c): 392.8 [MPa]

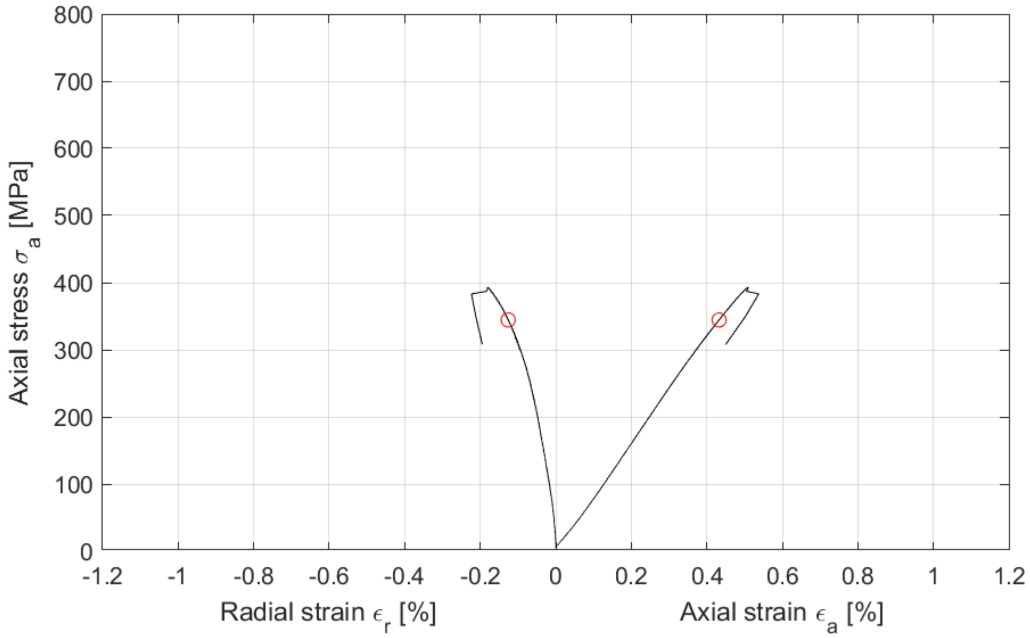

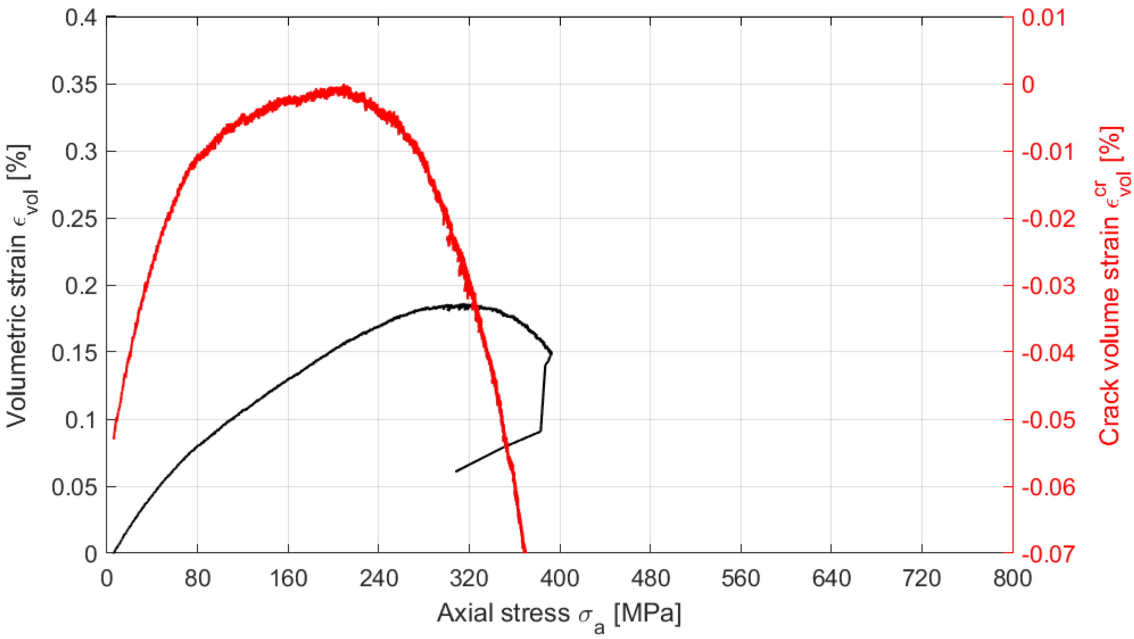

Specimen ID: KFM06C-115-07			
Before mechanical test		After mechanical test	
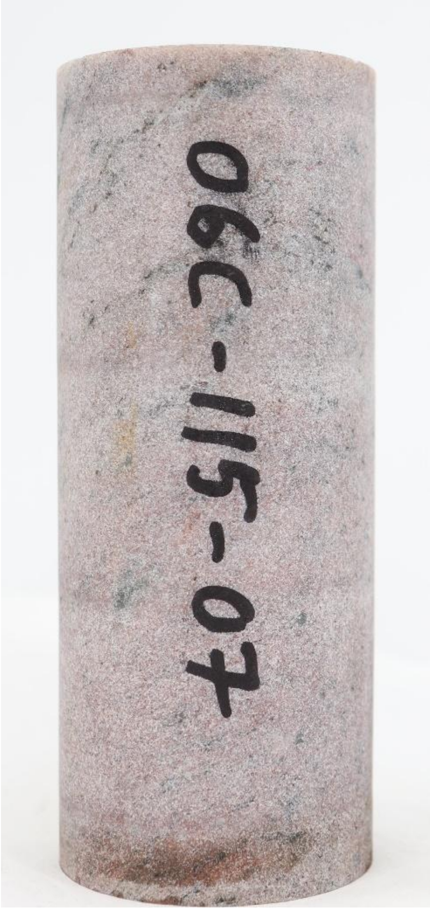			
Diameter (mm)	**Height (mm)**	**Density (kg/m³)**	
50.9	126.0	2 640	
Comments:			

Specimen ID: KFM06C-115-07

Youngs Modulus (E): 78.0 [GPa]

Cell pressure: 10 [MPa]

Poisson Ratio (ν): 0.299 [-]

Axial peak stress (σ_c): 545.8 [MPa]

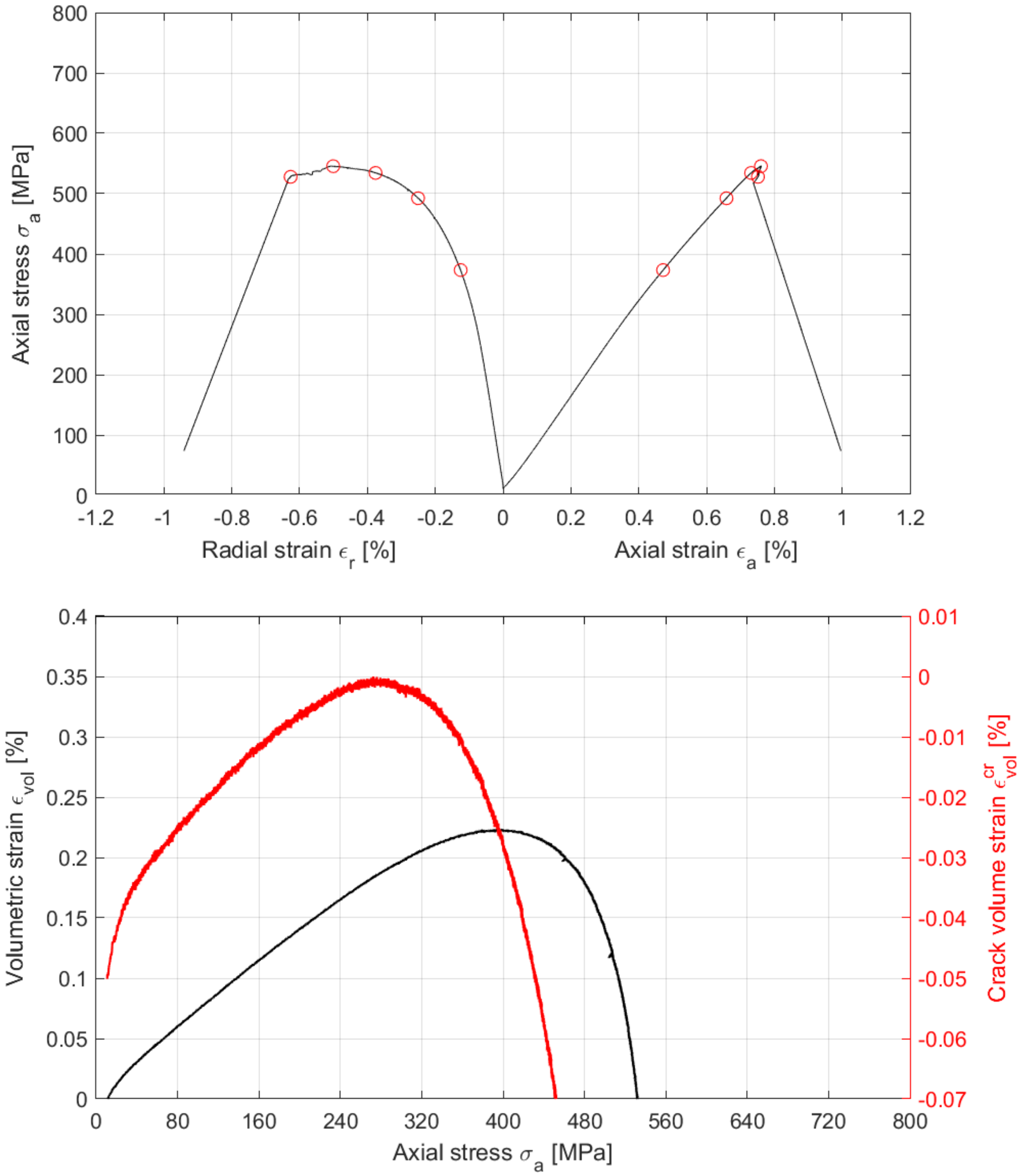

<table>
<tr><td colspan="2">Specimen ID: KFM06C-115-08</td><td colspan="2"></td></tr>
<tr><td colspan="2">Before mechanical test</td><td colspan="2">After mechanical test</td></tr>
<tr><td colspan="2">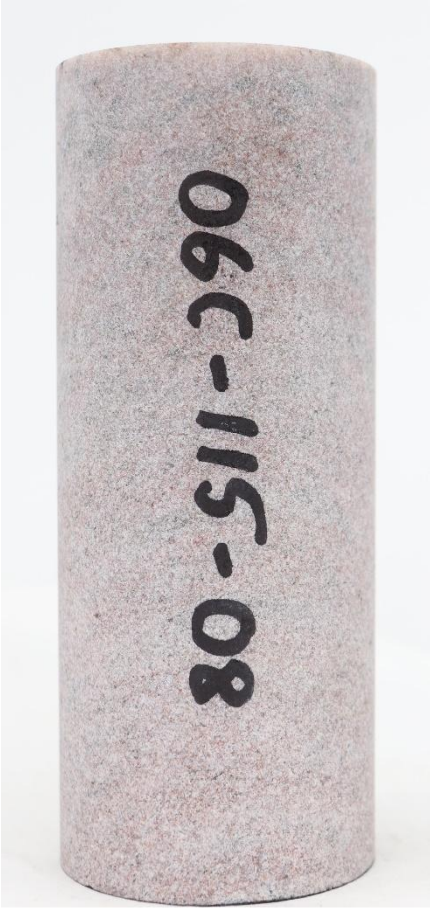</td><td></td><td></td></tr>
<tr><td>Diameter (mm)</td><td>Height (mm)</td><td>Density (kg/m³)</td><td></td></tr>
<tr><td>50.9</td><td>126.0</td><td>2 639</td><td></td></tr>
<tr><td>Comments:</td><td colspan="3"></td></tr>
</table>

Specimen ID: KFM06C-115-08

Youngs Modulus (E): 75.0 [GPa] Cell pressure: 15 [MPa]

Poisson Ratio (ν): 0.355 [-]

Axial peak stress (σ_c): 640.3 [MPa]

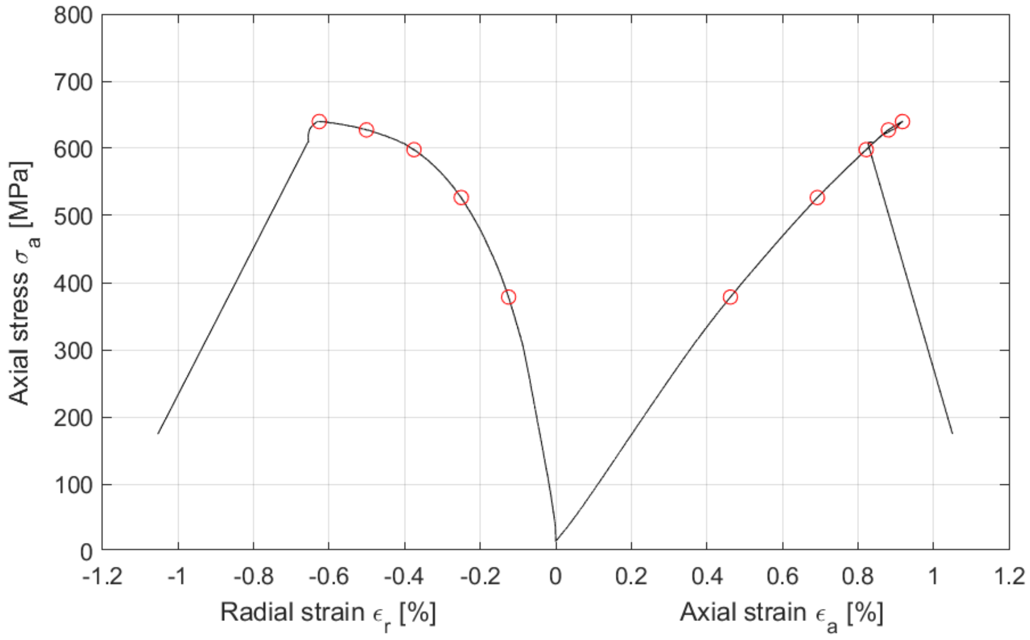

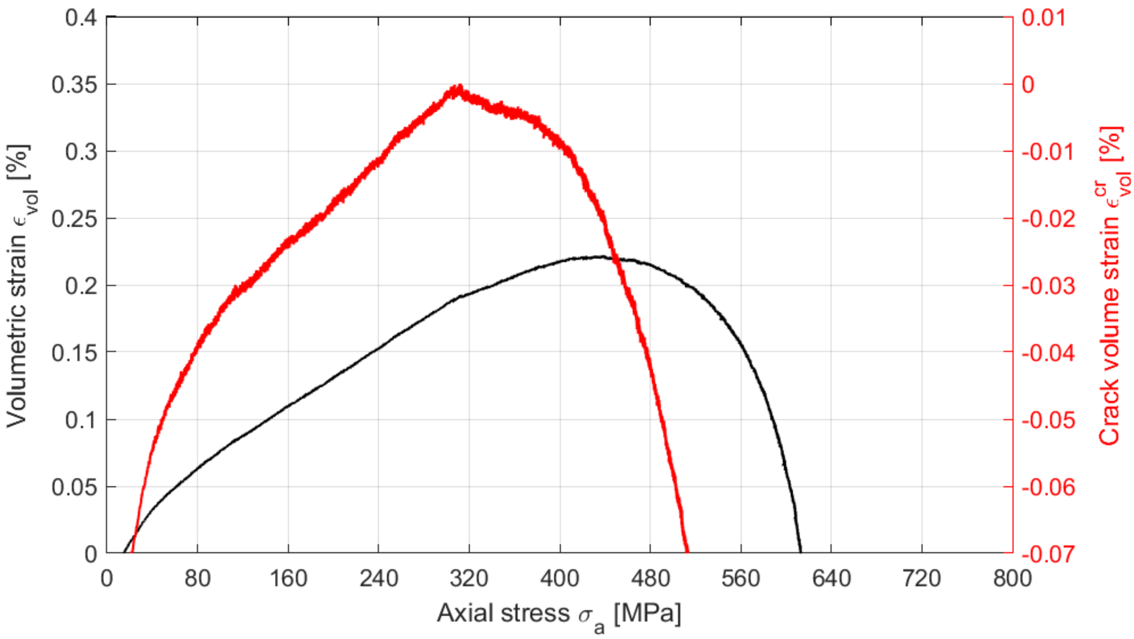

Specimen ID: KFM06C-115-09			
Before mechanical test		After mechanical test	
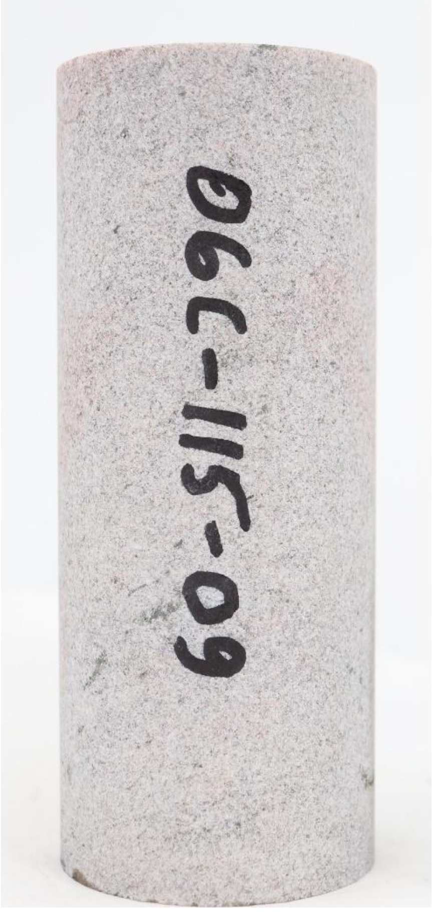			
Diameter (mm)	**Height (mm)**	**Density (kg/m³)**	
50.9	126.0	2 645	
Comments:			

Specimen ID: KFM06C-115-09

Youngs Modulus (E): 75.4 [GPa]   Cell pressure: 20 [MPa]

Poisson Ratio (ν): 0.306 [-]

Axial peak stress (σ_c): 674.6 [MPa]

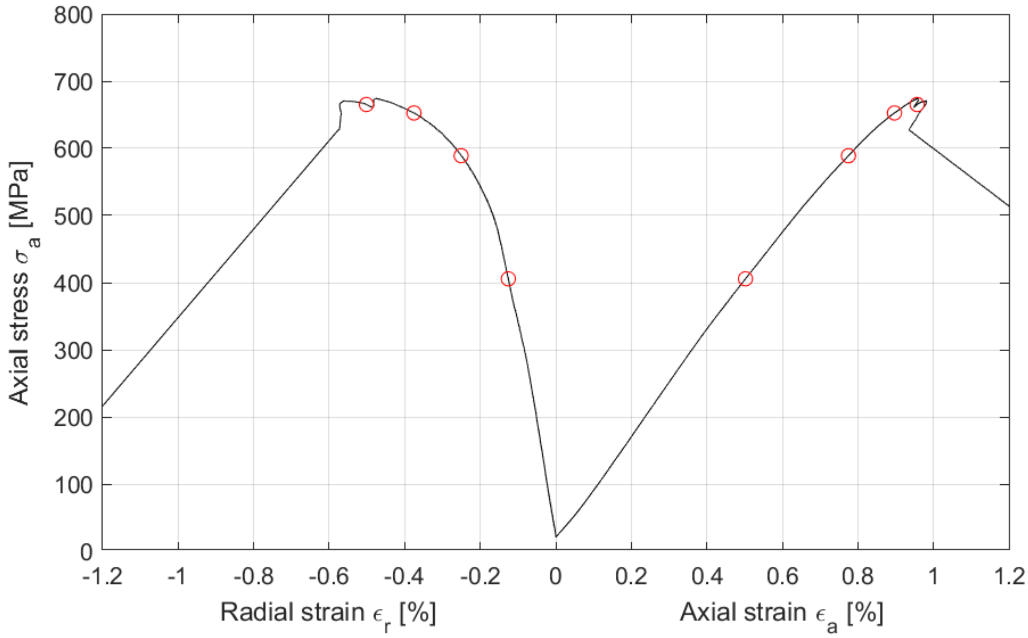

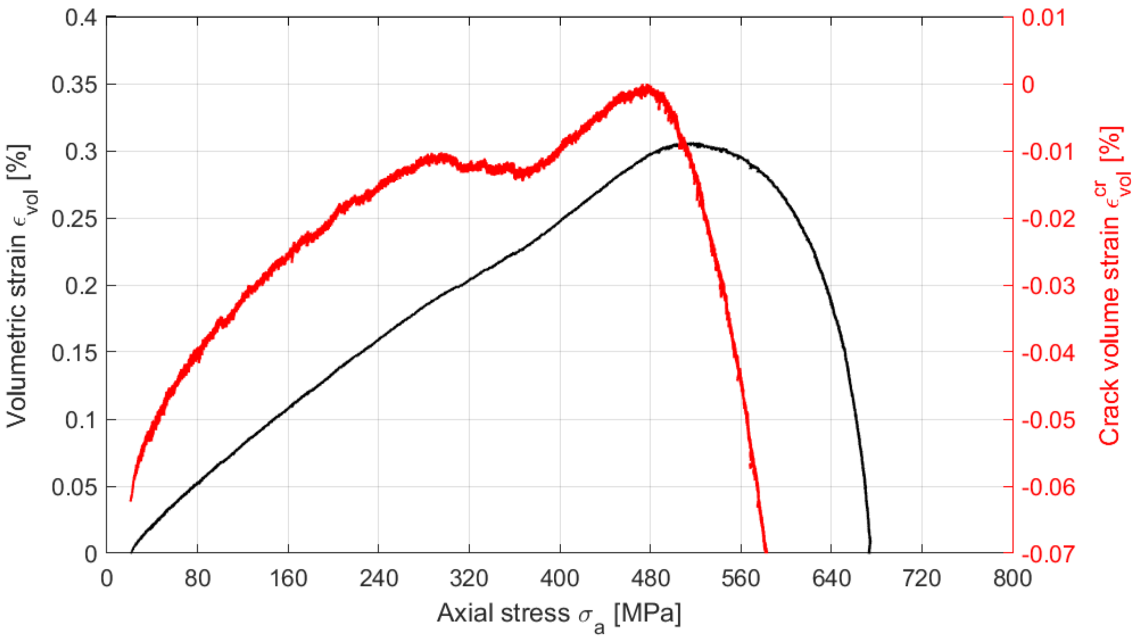

Specimen KFM06C-115-03 was loaded to the maximum load of the equipment and the load was held constant until failure. The strain and stress development with time are shown in Figure 6-3. The maximum stress was reached after approximately 922 s. The deformations continued after this as a creep process eventually leading to failure. In order to look more closely, new variables are introduced by zeroing the strains and stresses are done at t = 922 s, i.e.

$$\bar{\varepsilon}_i = \varepsilon_i - \varepsilon_{i,\mathrm{t922}} \text{ where } i = \mathrm{a,r,v}$$

$$\bar{\sigma}_\mathrm{a} = \sigma_\mathrm{a} - \sigma_{\mathrm{a,t922}}$$

The strain and stress values at t = 922 s are $\varepsilon_{\mathrm{a,t922}} = 0.955$, $\varepsilon_{\mathrm{r,t922}} = -0.377$, $\varepsilon_{\mathrm{v,t922}} = 0.208$ and $\sigma_{a,\mathrm{t922}} = 737.5$ MPa. A close-up of the strains and stress developments are shown in Figure 6-4. The black lines show a calculated average strain rate between t = 1 300 s and t = 2 500 s. The calculated average strain rates are $\dot{\varepsilon}_\mathrm{a} = 5.86 \cdot 10^{-8}$ s^{-1}, $\dot{\varepsilon}_\mathrm{r} = -2.13 \cdot 10^{-7}$ s^{-1} and $\dot{\varepsilon}_\mathrm{v} = -3.65 \cdot 10^{-7}$ s^{-1}.

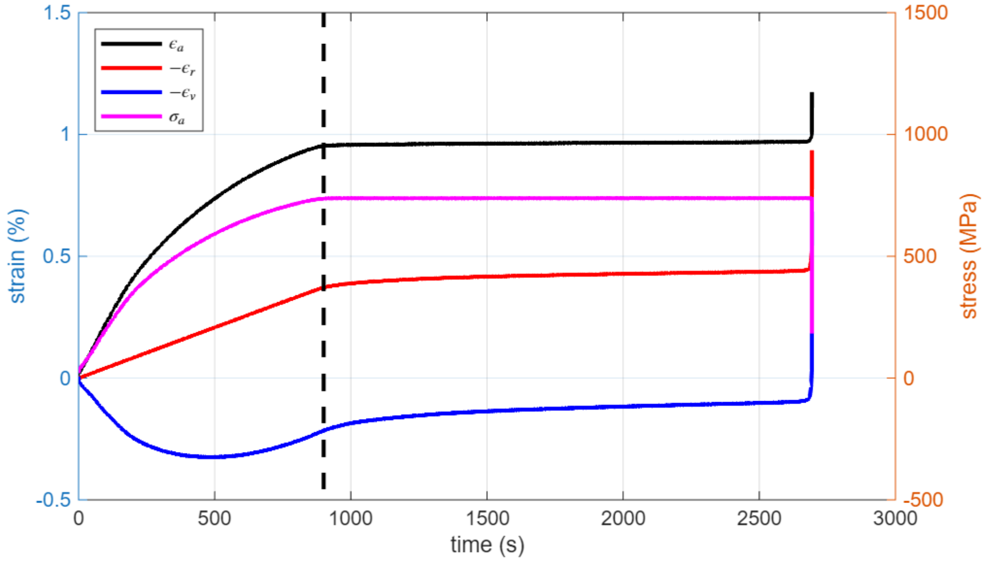

Figure 6-3. *Strains and stress as a function of time for the test of specimen KFM06C-115-03. The dashed line at t = 922 s indicates when maximum stress was reached.*

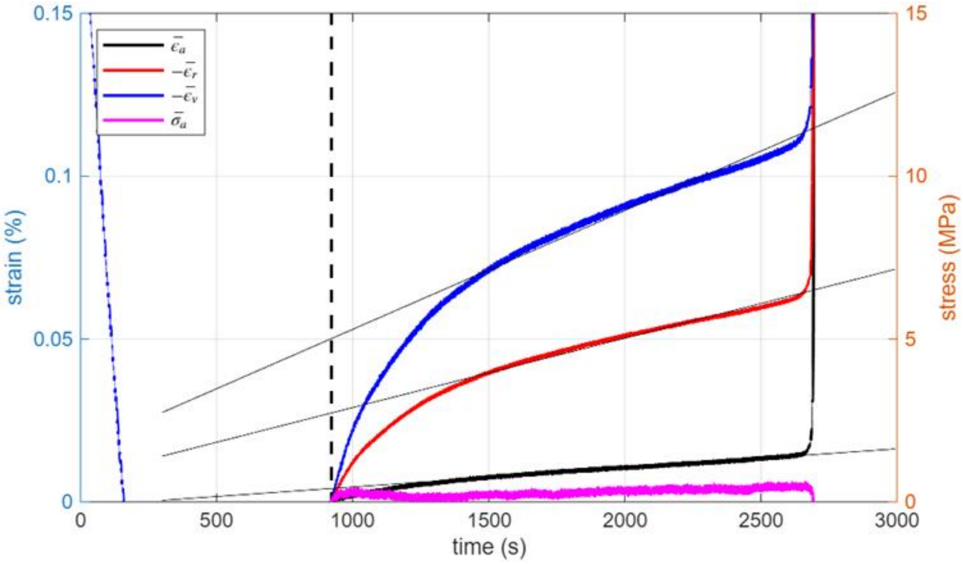

Figure 6-4. *Strains and stress as a function of time for the test of specimen KFM06C-115-03. The dashed line at t = 922 s indicates when maximum stress was reached.*

6.4.2 Results for the entire test series

A summary of the test results is shown in Table 6-5 and Table 6-6.

Table 6-5. Results from density measurements and triaxial compression tests.

Identification	Conf press (MPa)	Density (kg/m^3)	Compressive strength (MPa)	Young's modulus (GPa)	Poisson ratio (-)
KFM06C-115-01	5	2 649	412.8	83.2	0.243
KFM06C-115-02	10	2 646	631.1	79.5	0.325
KFM06C-115-03	20	2 649	738.1 (*)	77.0	0.289
KFM06C-115-05	15	2 646	664.4	81.9	0.293
KFM06C-115-06	5	2 634	392.8	83.1	0.286
KFM06C-115-07	10	2 640	545.8	78.0	0.299
KFM06C-115-08	15	2 639	640.3	75.0	0.355
KFM06C-115-09	20	2 645	674.6	75.4	0.306

(*) Loaded to maximal stress and held constant with a delayed failure.

Table 6-6. Calculated mean values and standard deviations.

Identification	Density (kg/m^3)	Young's modulus (GPa)	Poisson ratio (-)
Mean value	2 643	71.1	0.300
Std dev	4.9	3.3	0.032

6.5 Results overview of all compression tests

The triaxial compressive strength, the tangent Young's modulus and the tangent Poisson ratio versus borehole length (secup) for all compression tests, are presented in Figure 6-5 and Figure 6-7. Figure 6-8 shows compressive strength versus confining pressure for all compression tests.

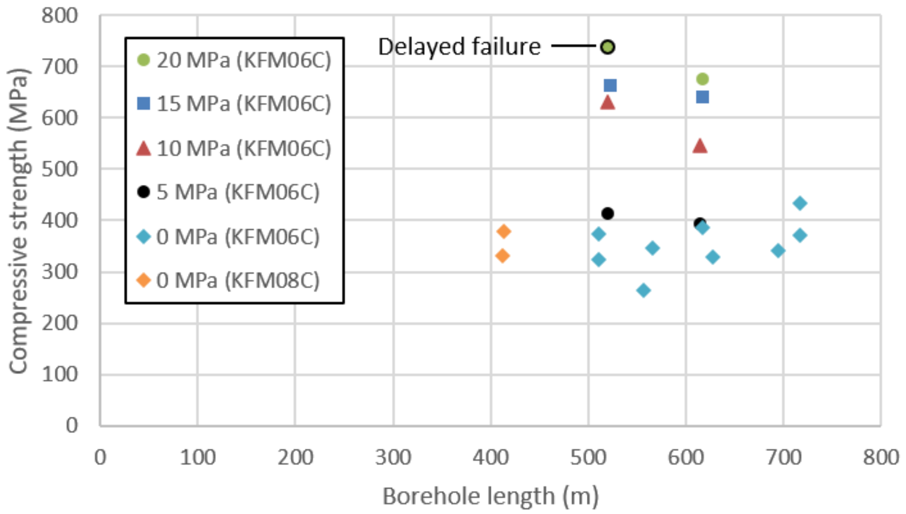

__Figure 6-5.__ Compressive strength as a function of borehole length for all the compression tests. The delayed failure was due to the maximum force of the test equipment was reached after 15 minutes and the load was kept constant until a creep failure occurred after 49 minutes.

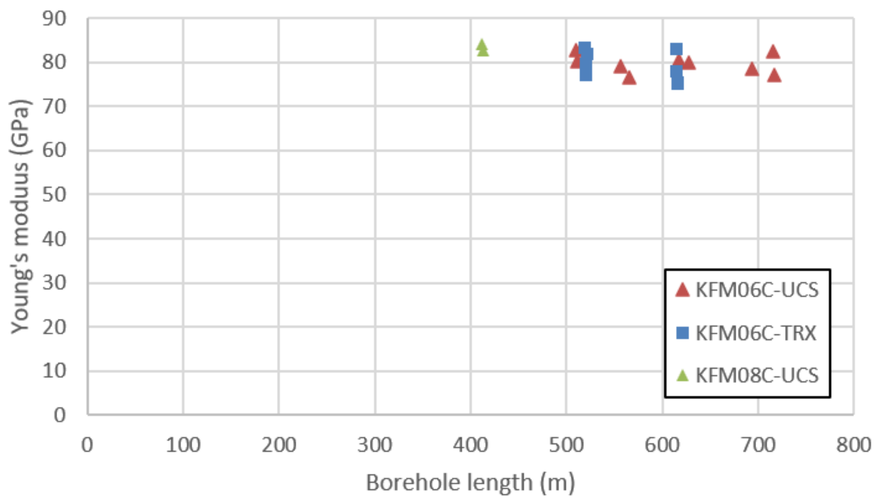

Figure 6-6. *Young's modulus as a function of borehole length for all compression tests.*

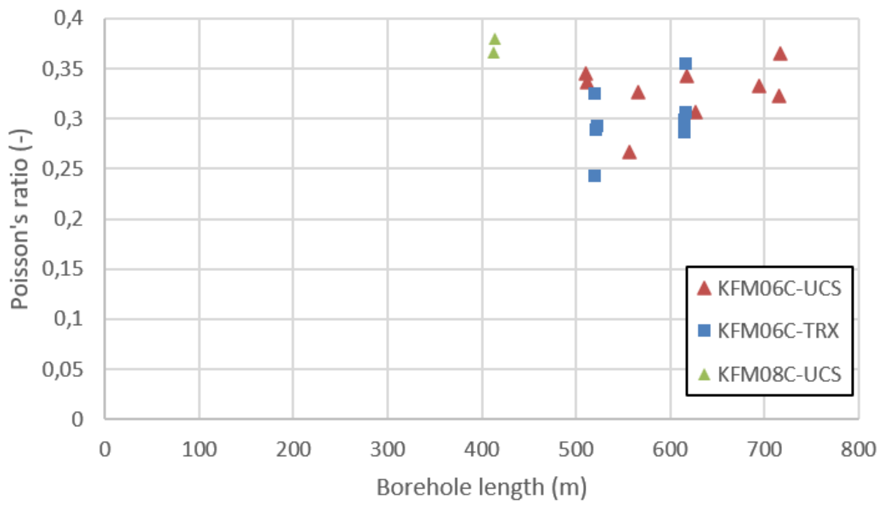

Figure 6-7. *Poisson's ratio as a function of borehole length for all compression tests.*

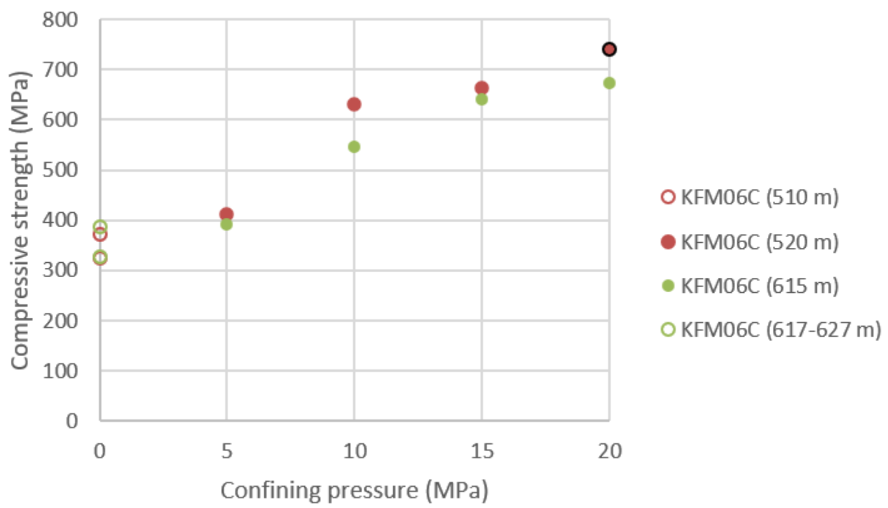

Figure 6-8. *Compressive strength as a function of confining pressure for all compression tests. The solid red marker with a black ring denotes the specimen with a delayed failure (KFM06C-115-03).*

7 References

SKB's (Svensk Kärnbränslehantering AB) publications can be found at www.skb.com/publications. SKBdoc documents will be submitted upon request to document@skb.se.

ASTM, 2001. ASTM 4543-01, Standard practice for preparing rock core specimens and determining dimensional and shape tolerance, ASTM International, West Conshohocken, PA, USA.

CEN, 2008. EN 13755:2008. Natural stone test methods - Determination of water absorption at atmospheric pressure, CEN.

Eberhardt E, Stead D, Stimpson B, Read R S, 1998. Identifying crack initiation and propagation thresholds in brittle rock. Can. Geotech. J. 35, pp. 222–233.

Ghazvinian E, Diederichs M, Martin D, Christiansson R, Hakala M, Gorski B, Perras M, Jacobsson L, 2012. Prediction thresholds for crack initiation and propagation in crystalline rocks. ISRM Commission on Spall Prediction Report on Testing Procedures, ISRM.

ISRM, 1979. Suggested method for determining water content, porosity, density, absorption and related properties and swelling and slake-durability index properties. Int. J. Rock. Mech. Min. Sci. & Geomech. Abstr, 16(2), pp. 141–156.

ISRM, 1999. Draft ISRM suggested method for the complete stress-strain curve for intact rock in uniaxial compression. Int. J. Rock. Mech. Min. Sci. 36(3), pp. 279–289.

Jacobsson L, Sandström J, Flansbjer M, Sjögren T, Brander L, 2016. ONKALO POSE experiment – Laboratory determination of density, porosity and mechanical anisotropy of gneiss and granite, Posiva Working Report 2016-31, Posiva OY Finland.

Martin C D, Chandler N A, 1994. The progressive fracture of Lac du Bonnet granite. Int. J. Rock. Mech. Min. Sci. & Geomech. Abstr. 31(6), pp. 643–659.

Mathworks, 2025. MATLAB Release 25.1.0.2943329 (R2025a), The MathWorks, Inc., Natick, Massachusetts, USA.

Petersson J, Skogsmo G, Berglund J, von Dalwigk I, Wängnerud A, Danielsson P, Stråhle A, 2006a. Boremap mapping of telescopic drilled borehole KFM06C. Forsmark site investigation. SKB P-06-79. Svensk Kärnbränslehantering AB.

Petersson J, Wängnerud A, von Dalwigk I, Berglund J, Andersson U B, 2006b. Boremap mapping of telescopic drilled borehole KFM08C. Forsmark site investigation. SKB P-06-203. Svensk Kärnbränslehantering AB.

Stråhle A, 2001. Definition och beskrivning av parametrar för geologisk, geofysisk och bergmekanisk kartering av berg, SKB-R-01-19. Svensk kärnbränslehantering AB. In Swedish.

Appendix A: Core mapping diagrams

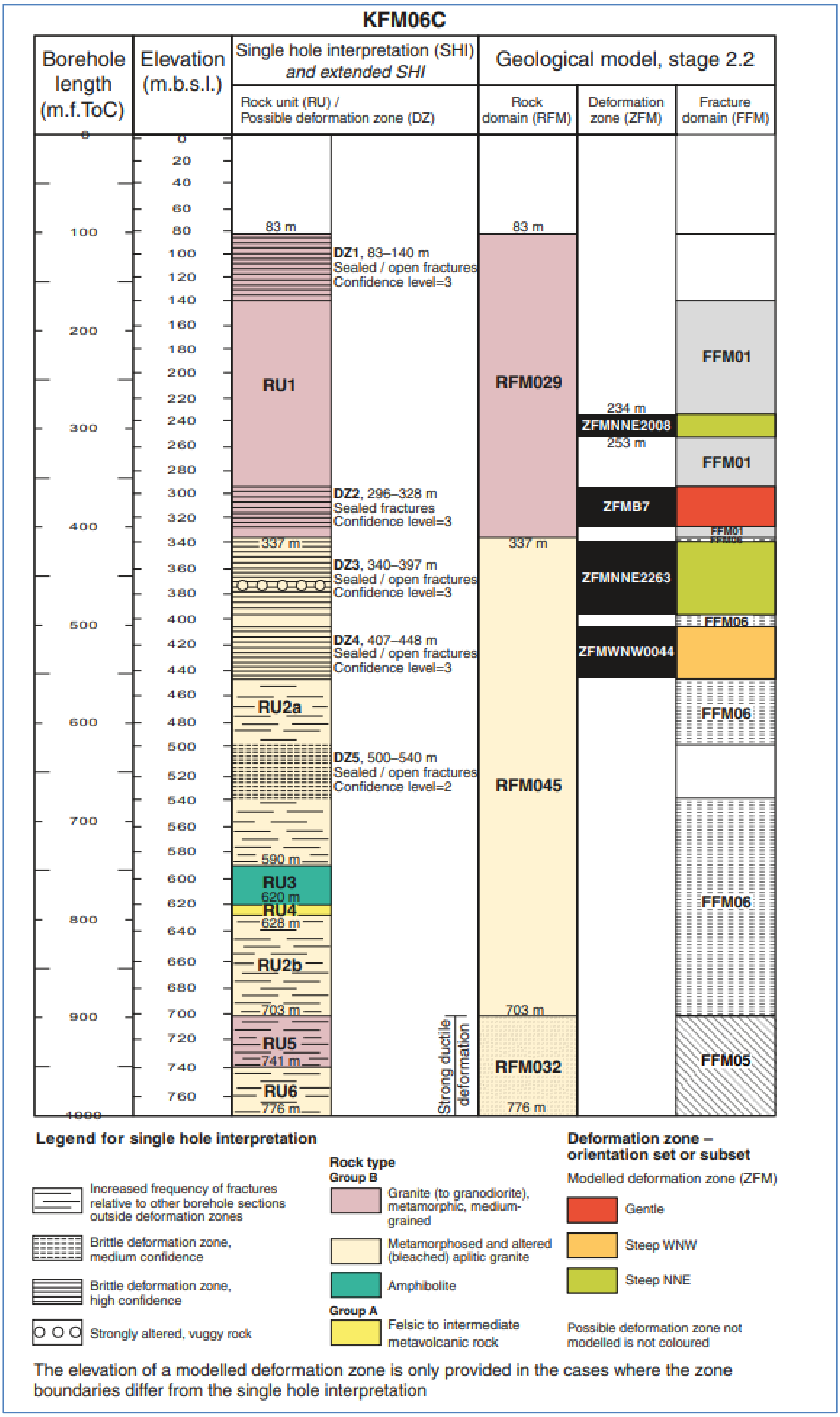

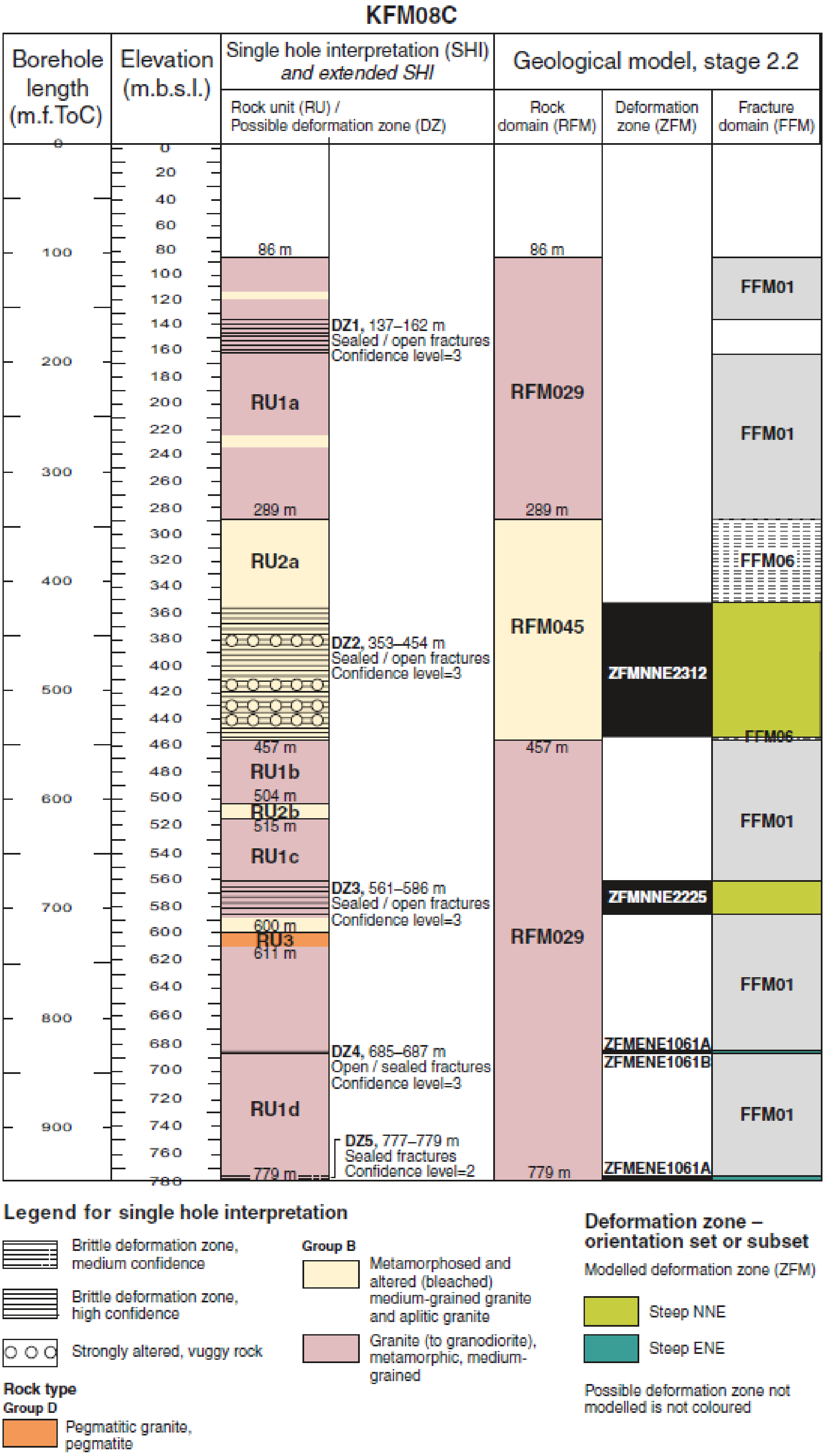
KFM08C
Borehole length (m.f.ToC)
Elevation (m.b.s.l.)
Single hole interpretation (SHI) and extended SHI
Rock unit (RU) / Possible deformation zone (DZ)
Geological model, stage 2.2
Rock domain (RFM)
Deformation zone (ZFM)
Fracture domain (FFM)
86 m
RU1a
DZ1, 137–162 m
Sealed / open fractures
Confidence level=3
289 m
RU2a
DZ2, 353–454 m
Sealed / open fractures
Confidence level=3
457 m
RU1b
504 m
RU2b
515 m
RU1c
DZ3, 561–586 m
Sealed / open fractures
Confidence level=3
600 m
RU3
611 m
DZ4, 685–687 m
Open / sealed fractures
Confidence level=3
RU1d
DZ5, 777–779 m
Sealed fractures
Confidence level=2
779 m
RFM029
RFM045
ZFMNNE2312
ZFMNNE2225
ZFMENE1061A
ZFMENE1061B
FFM01
FFM06
Legend for single hole interpretation
Brittle deformation zone, medium confidence
Brittle deformation zone, high confidence
Strongly altered, vuggy rock
Rock type
Group D
Pegmatitic granite, pegmatite
Group B
Metamorphosed and altered (bleached) medium-grained granite and aplitic granite
Granite (to granodiorite), metamorphic, medium-grained
Deformation zone – orientation set or subset
Modelled deformation zone (ZFM)
Steep NNE
Steep ENE
Possible deformation zone not modelled is not coloured

Appendix B: Circumferential strain calculation

The following equations describe the correct calculation of radial strains when using a circumferential deformation device, see Figure B-1.

$$\varepsilon_{\mathrm{r}} = \frac{\Delta C}{C_{\mathrm{i}}}$$

where

$$C_{\mathrm{i}} = 2\pi R_{\mathrm{i}} = \text{initial specimen circumference}$$

$$\Delta C = \text{change in specimen circumference} = \frac{\pi \cdot \Delta X}{\sin\left(\frac{\theta_{\mathrm{i}}}{2}\right) + \left(\pi - \frac{\theta_{\mathrm{i}}}{2}\right)\cos\left(\frac{\theta_{\mathrm{i}}}{2}\right)}$$

and

$$\Delta X = \text{change in LVDT reading} = X_{\mathrm{i}} - X_{\mathrm{f}}$$

$$X_{\mathrm{i}} = \text{initial chain gap;}\ X_{\mathrm{f}} = \text{current chain gap}$$

$$\theta_{\mathrm{i}} = \text{initial chord angle} = 2\pi - \frac{L_{\mathrm{c}}}{R_{\mathrm{i}} - r}$$

$$L_{\mathrm{c}} = \text{chain length (measured from center of one end roller to center of the other end roller)}$$

$$r = \text{roller radius}$$

$$R_{\mathrm{i}} = \text{initial specimen radius}$$

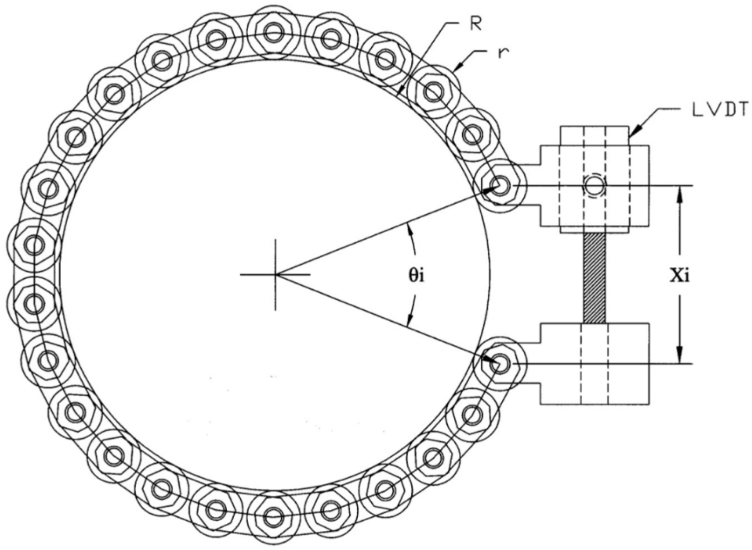

Figure B-1. *Chain for radial deformation measurement.*

Appendix C: Diagrams from uniaxial compression tests

Specimen ID: KFM06C-113-01

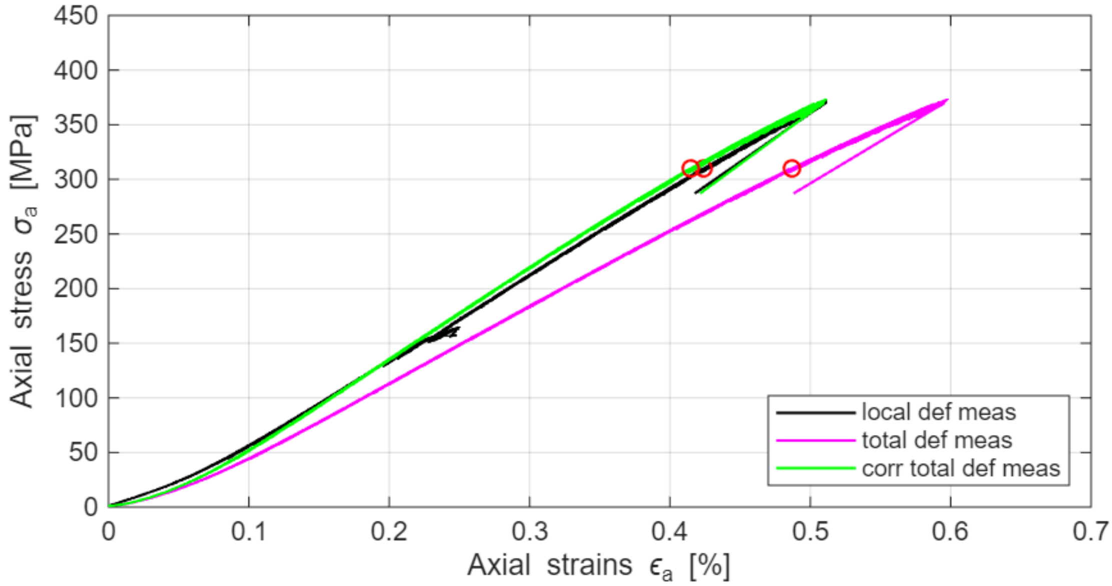

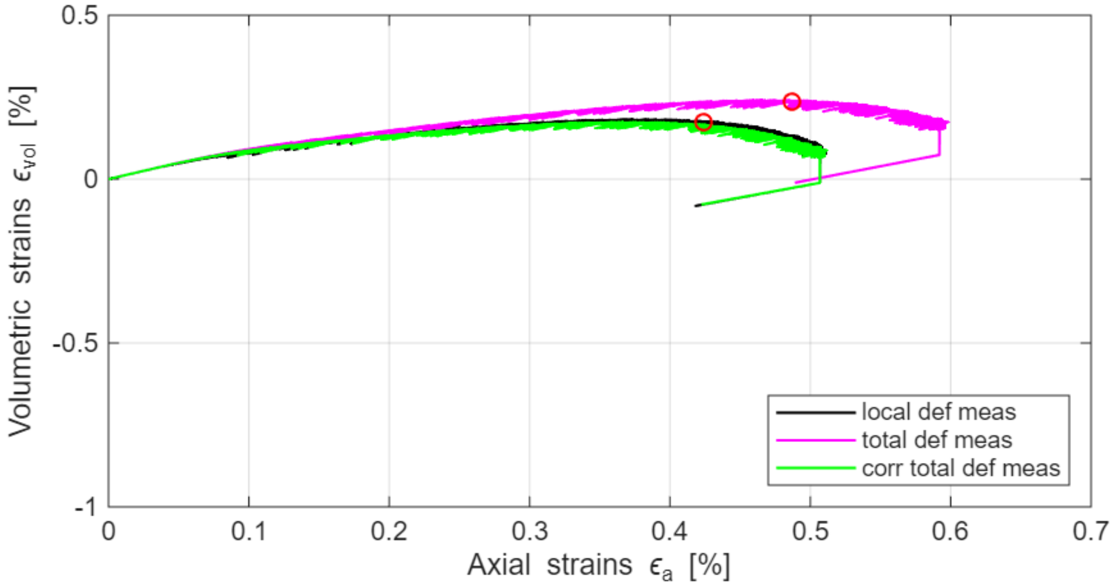

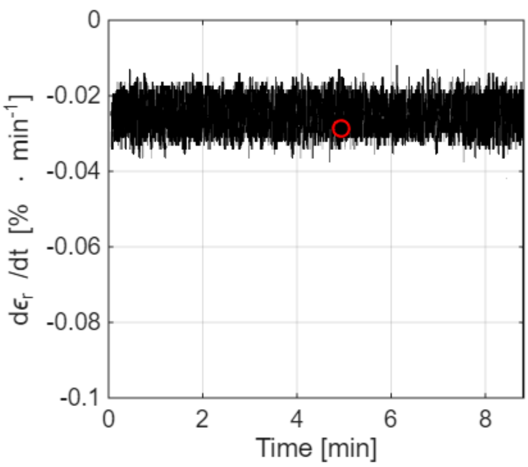

Explanation to curves above:

Based on local deformation (black)

Based on total deformation (magenta)

Based on corrected deformation (green)

Calculated system stiffness:

K_{system} = 6.8 [GN/m]

Specimen ID: KFM06C-113-02

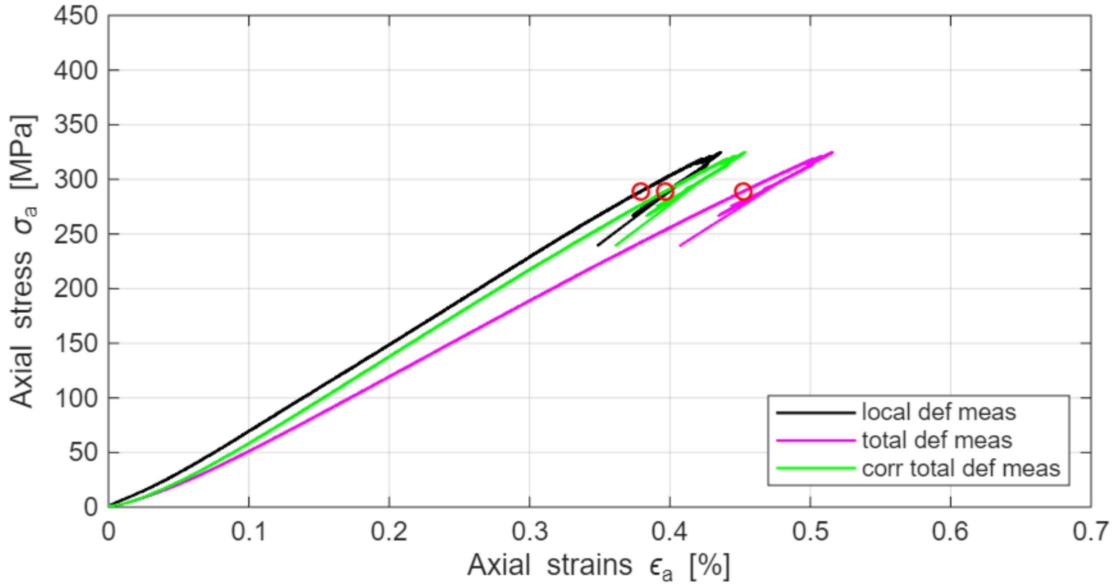

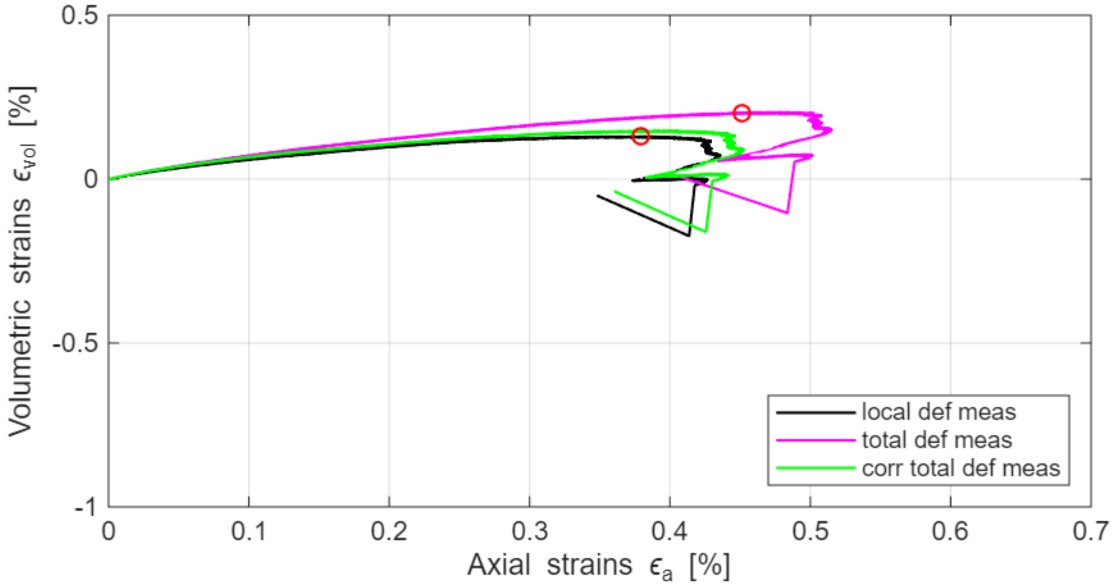

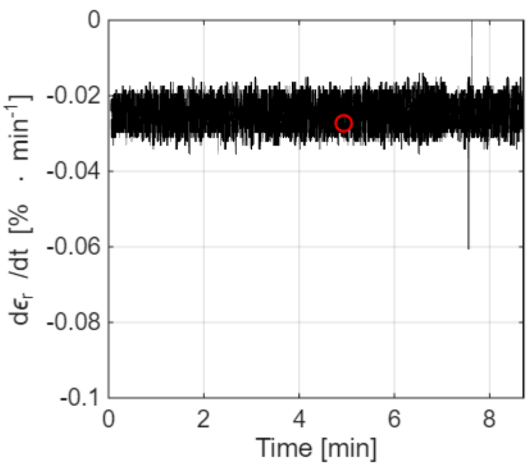

Explanation to curves above:

Based on local deformation (black)

Based on total deformation (magenta)

Based on corrected deformation (green)

Calculated system stiffness:

K_{system} = 8.2 [GN/m]

Specimen ID: KFM06C-113-03

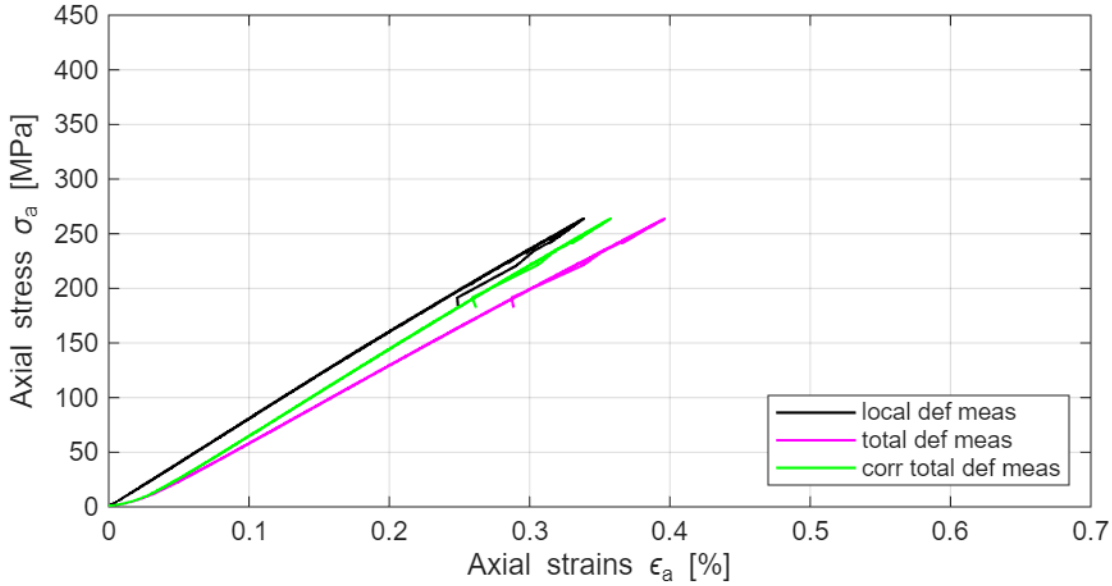

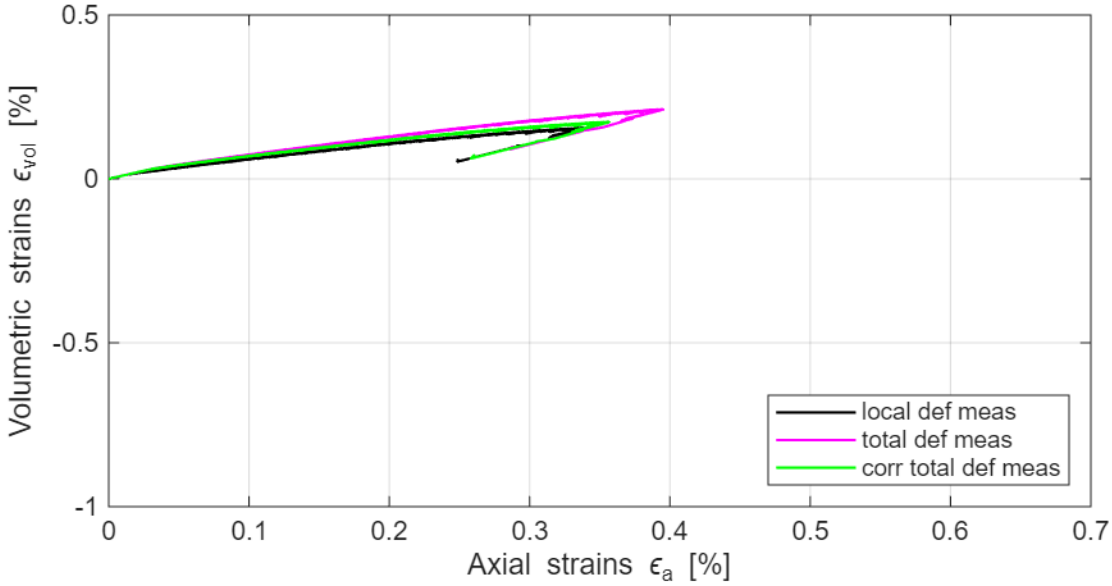

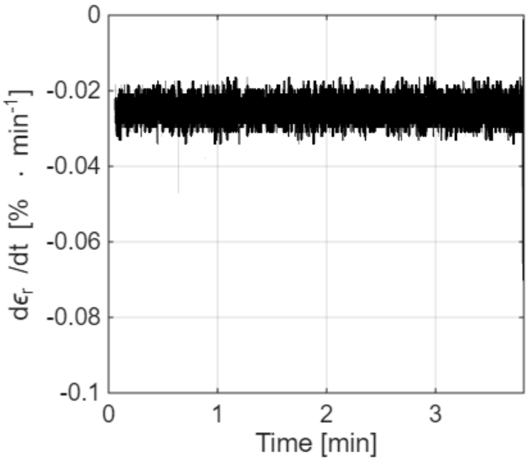

Explanation to curves above:

Based on local deformation (black)

Based on total deformation (magenta)

Based on corrected deformation (green)

Calculated system stiffness:

K_{system} = 10.8 [GN/m]

Specimen ID: KFM06C-113-04

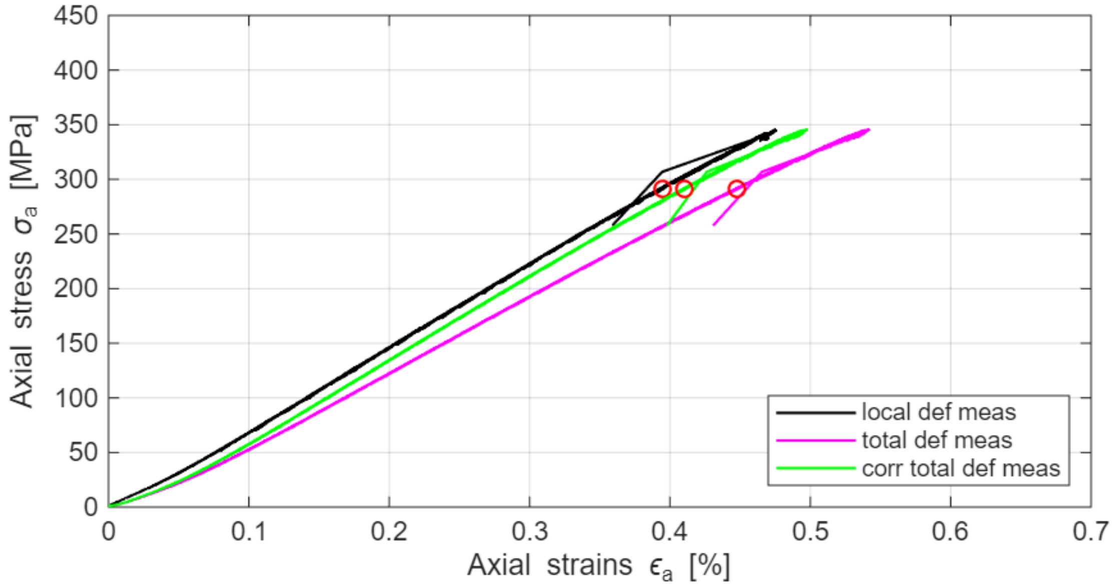

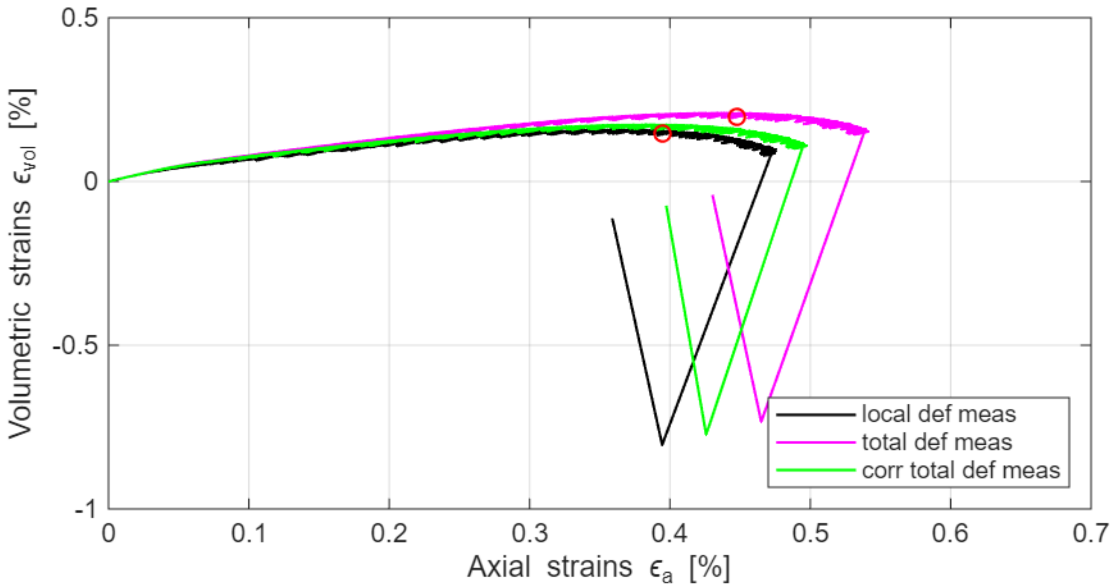

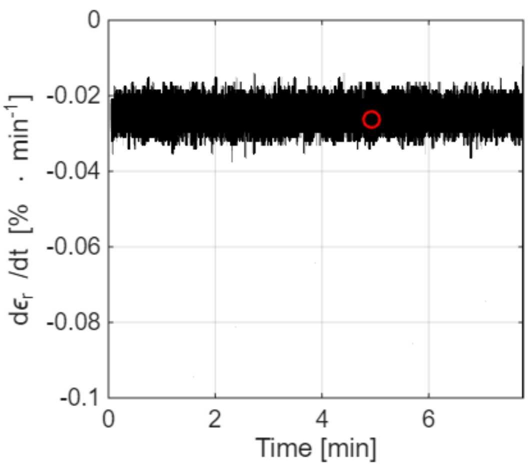

Explanation to curves above:

Based on local deformation (black)

Based on total deformation (magenta)

Based on corrected deformation (green)

Calculated system stiffness:

K_{system} = 12.6 [GN/m]

Specimen ID: KFM06C-113-05

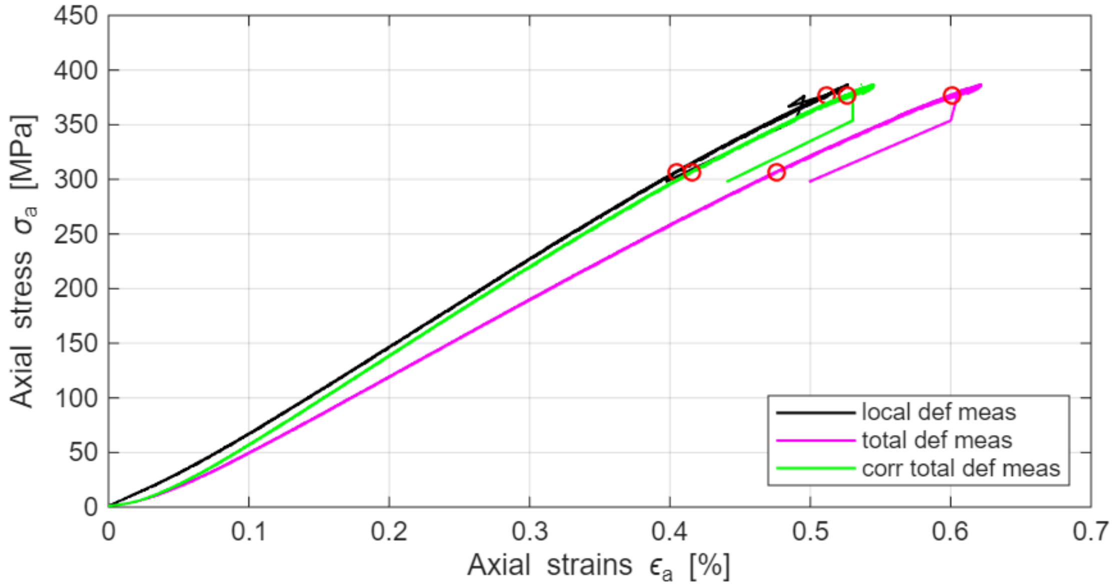

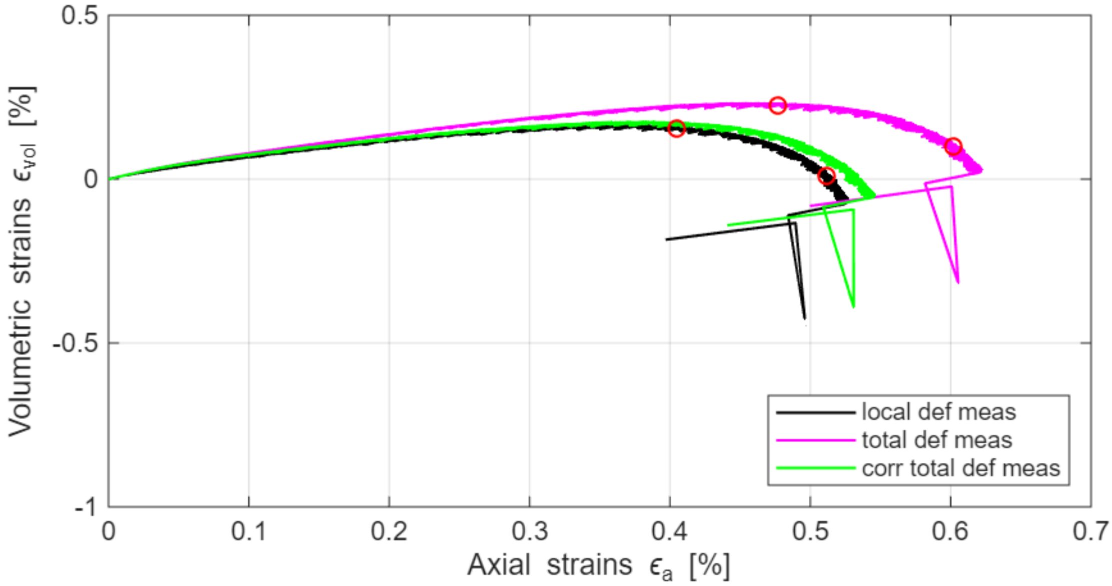

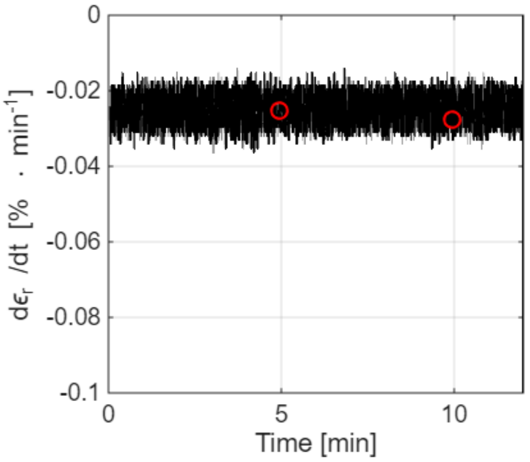

Explanation to curves above:

Based on local deformation (black)

Based on total deformation (magenta)

Based on corrected deformation (green)

Calculated system stiffness:

K_{system} = 8.1 [GN/m]

Specimen ID: KFM06C-113-06

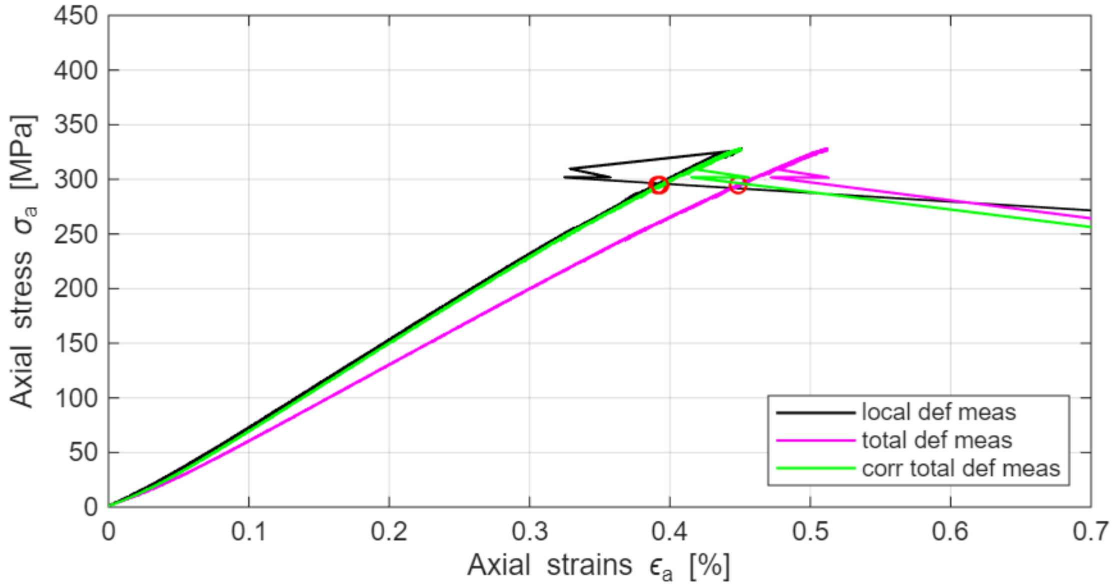

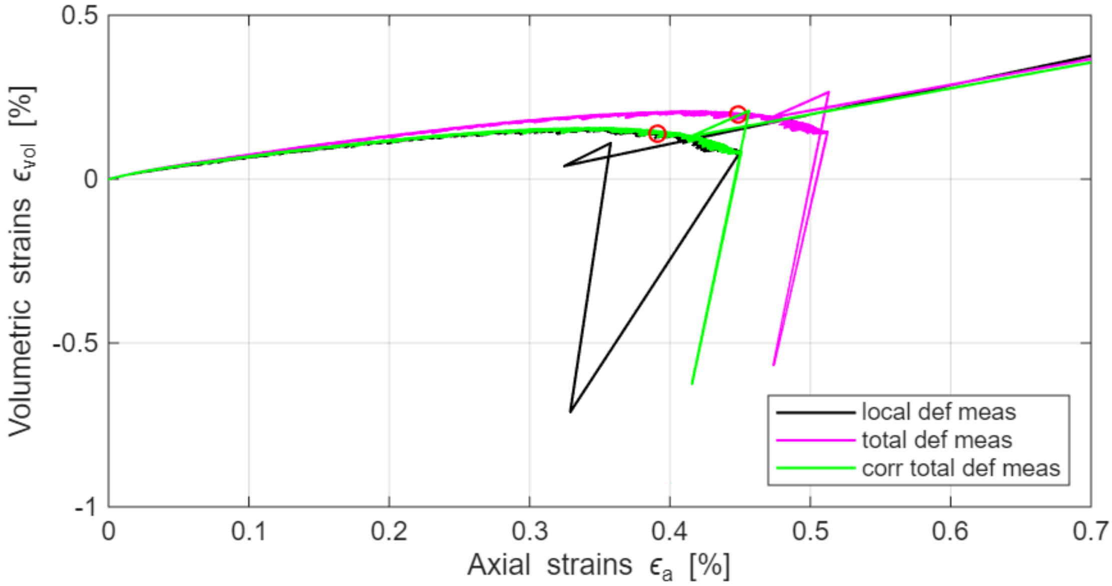

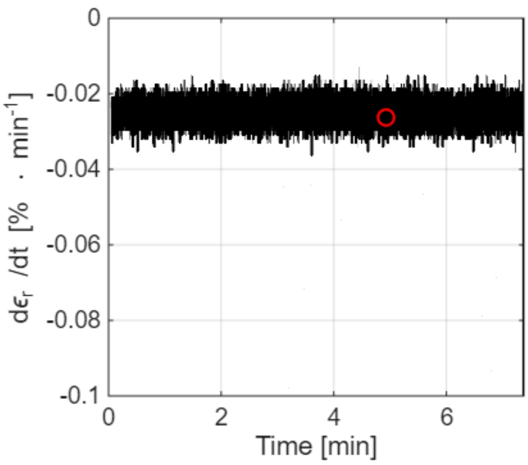

Explanation to curves above:

Based on local deformation (black)

Based on total deformation (magenta)

Based on corrected deformation (green)

Calculated system stiffness:

K_{system} = 8.3 [GN/m]

Specimen ID: KFM06C-113-07

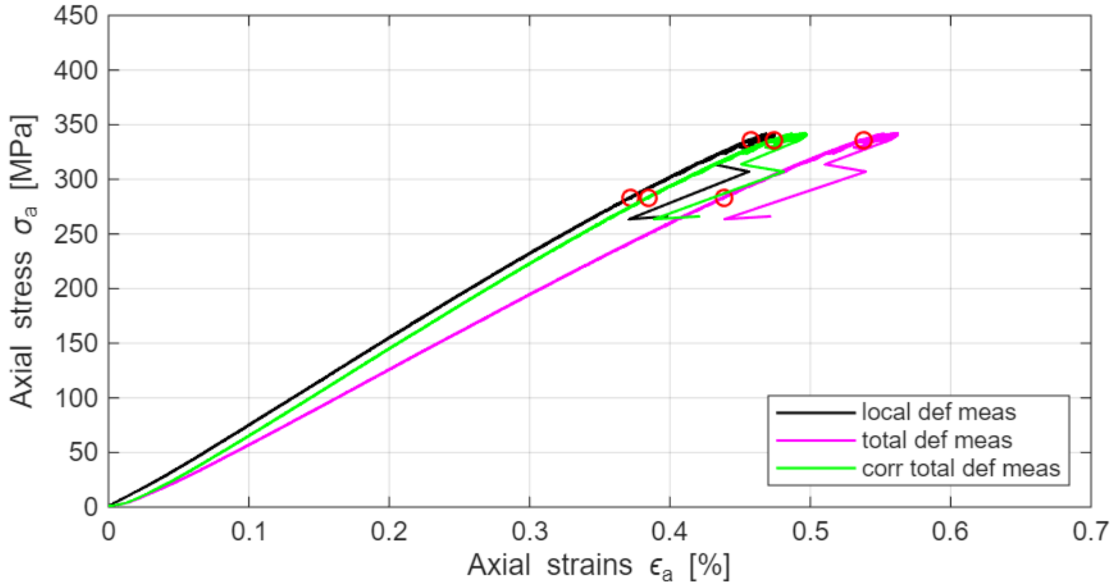

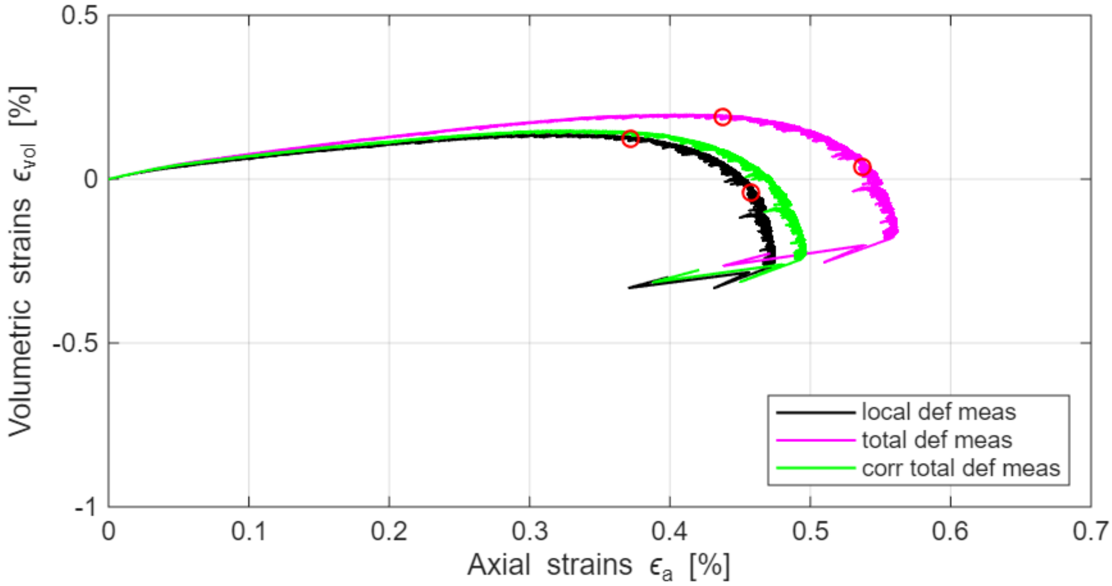

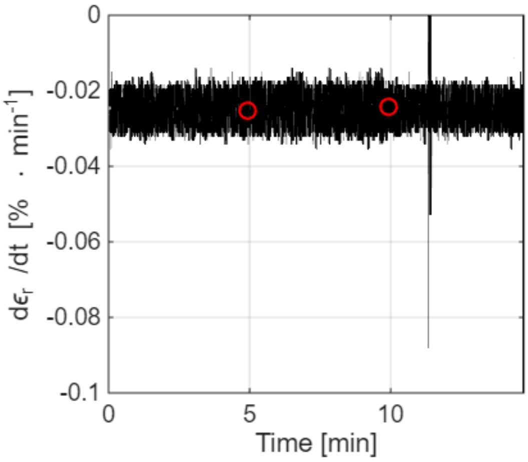

Explanation to curves above:

Based on local deformation (black)

Based on total deformation (magenta)

Based on corrected deformation (green)

Calculated system stiffness:

K_{system} = 8.3 [GN/m]

Specimen ID: KFM06C-113-08

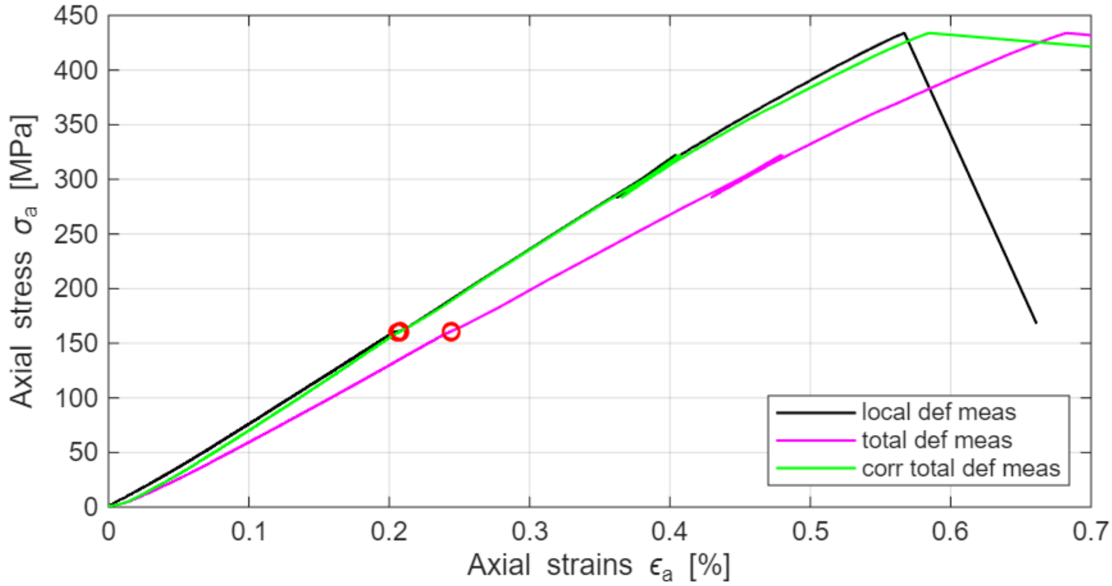

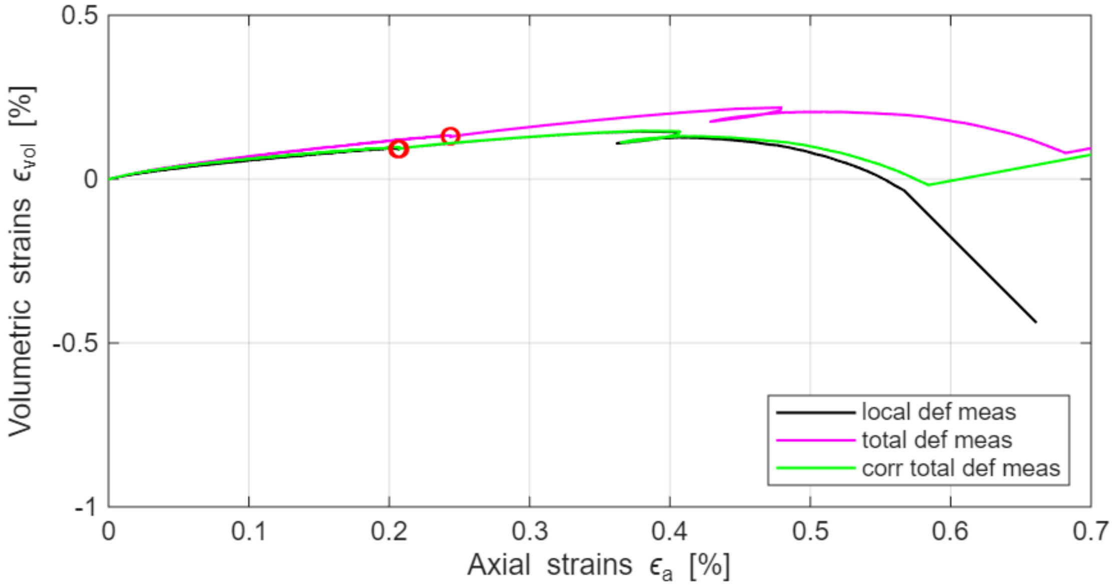

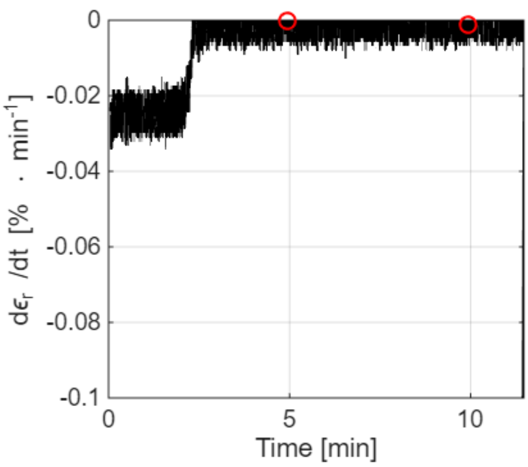

Explanation to curves above:

Based on local deformation (black)

Based on total deformation (magenta)

Based on corrected deformation (green)

Calculated system stiffness:

K_{system} = 7 [GN/m]

Specimen ID: KFM06C-113-09R

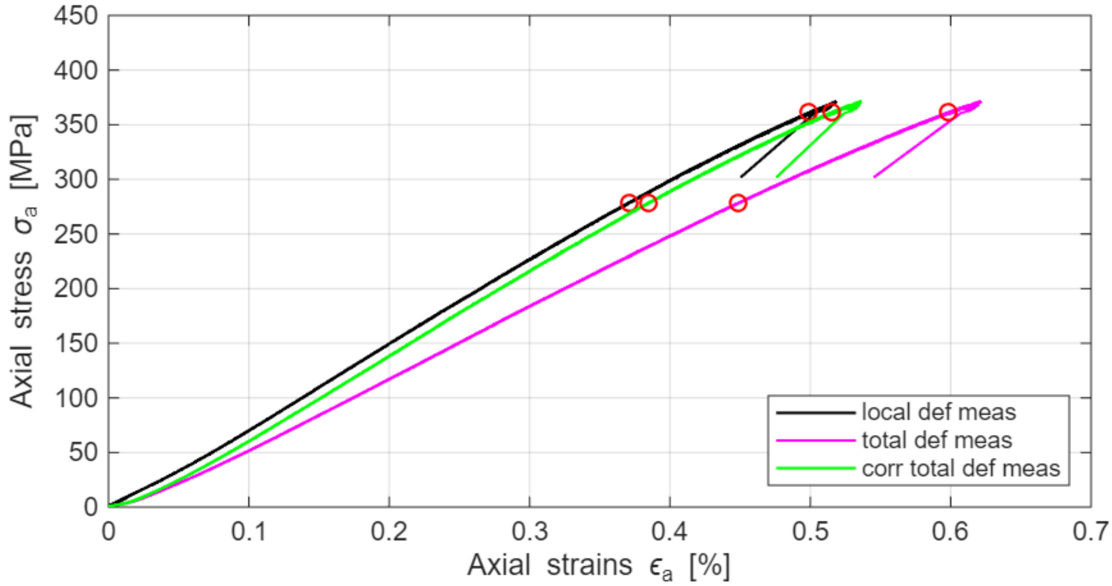

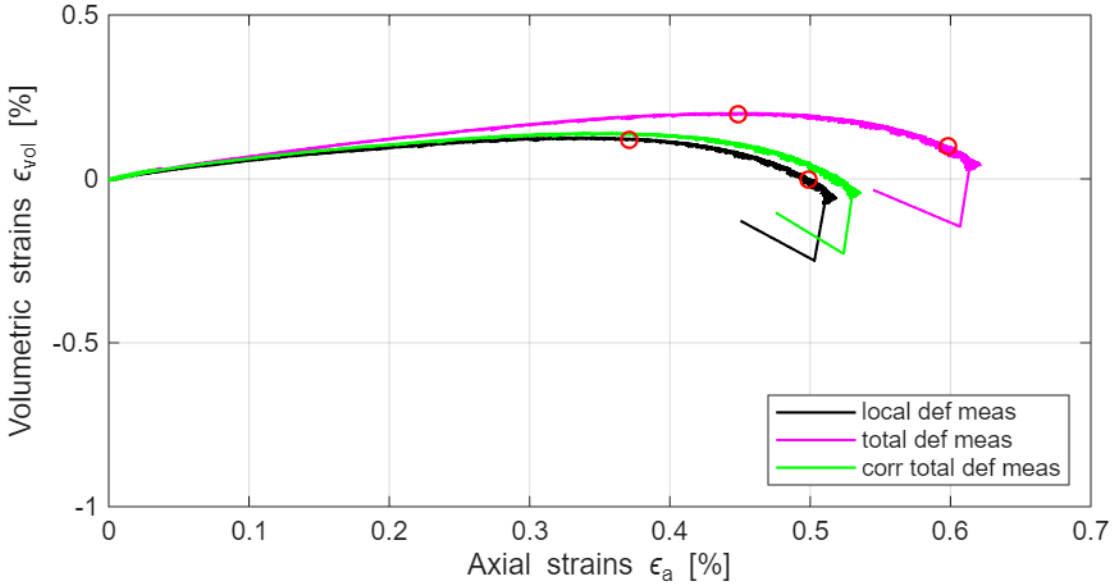

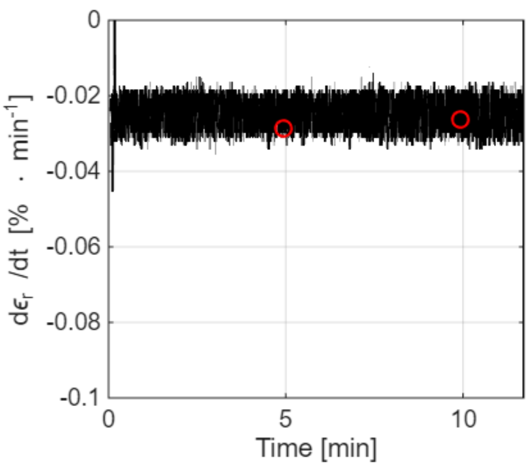

Explanation to curves above:

Based on local deformation (black)

Based on total deformation (magenta)

Based on corrected deformation (green)

Calculated system stiffness:

K_{system} = 6.9 [GN/m]

Specimen ID: KFM08C-113-01

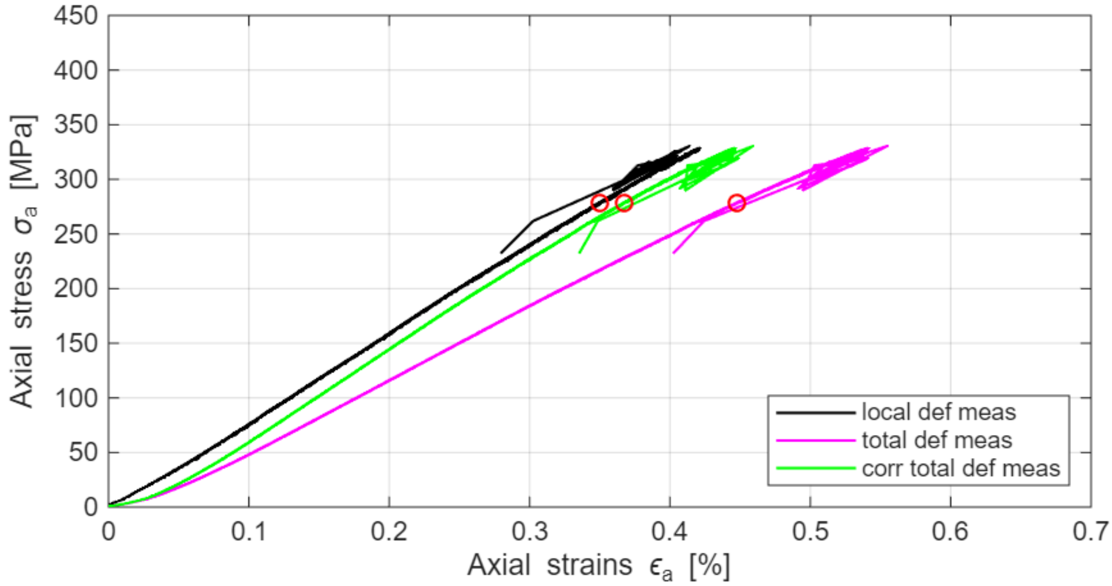

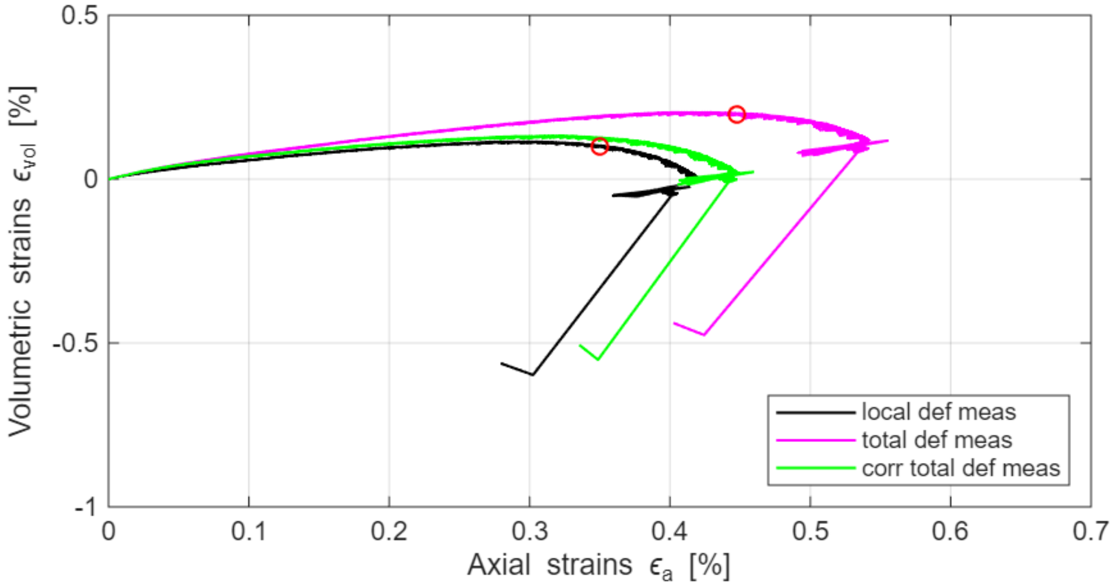

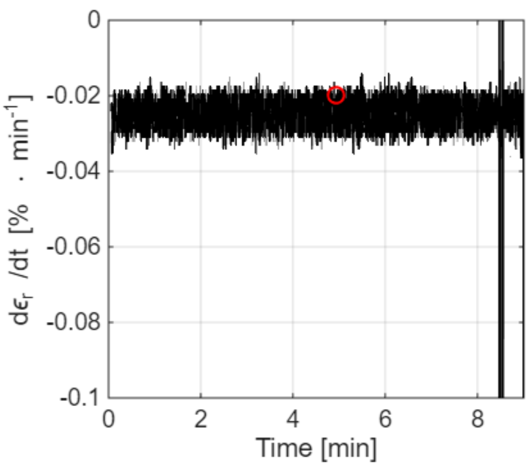

Explanation to curves above:

Based on local deformation (black)

Based on total deformation (magenta)

Based on corrected deformation (green)

Calculated system stiffness:

K_{system} = 5.6 [GN/m]

Specimen ID: KFM08C-113-02

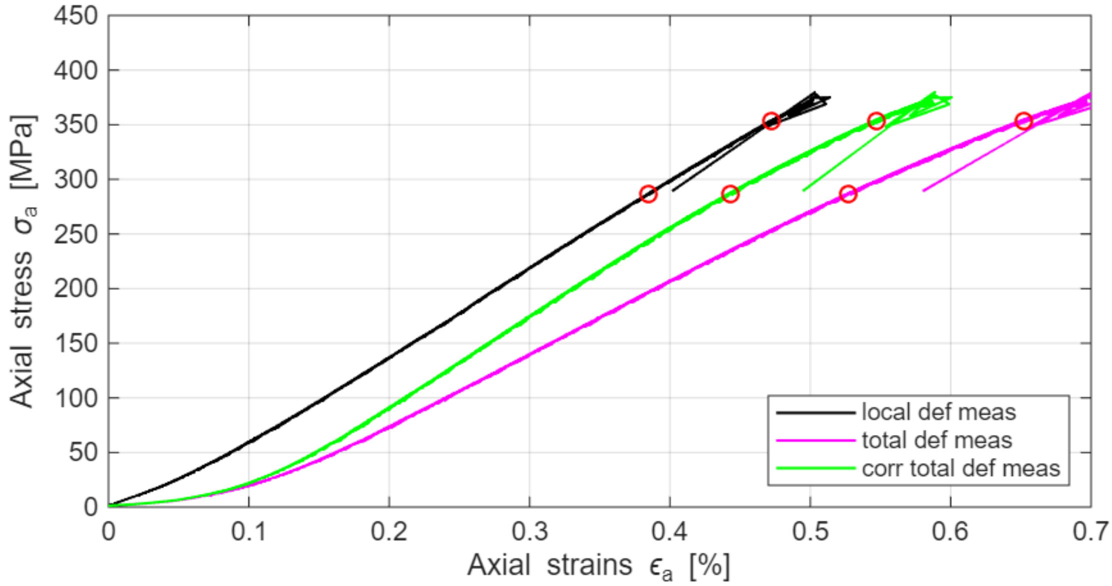

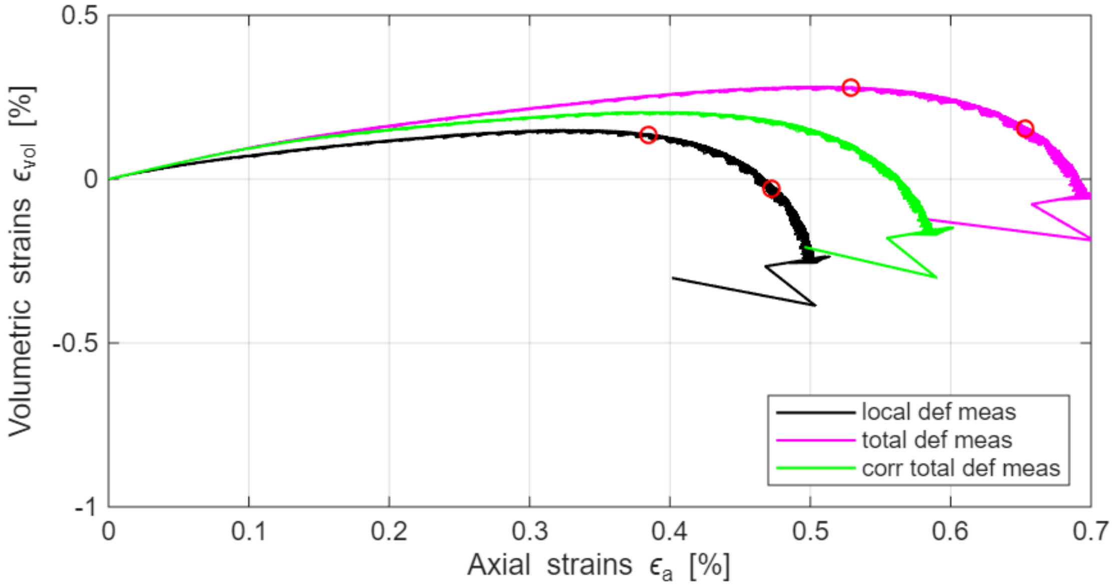

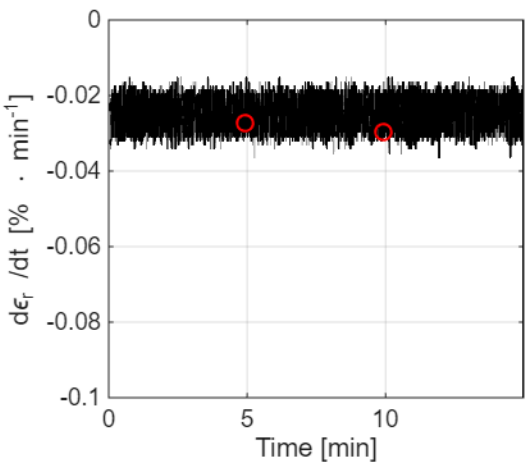

Explanation to curves above:

Based on local deformation (black)

Based on total deformation (magenta)

Based on corrected deformation (green)

Calculated system stiffness:

K_{system} = 5.4 [GN/m]